

Aus dem Helmholtz Zentrum München
Deutsches Forschungszentrum für Gesundheit (GmbH)
Abteilung: Genvektoren
Vorstand: Prof. Dr. Wolfgang Hammerschmidt

Evolution of pre-germinal center B cell lymphoma



Dissertation
zum Erwerb des Doktorgrades der Naturwissenschaften
an der Medizinischen Fakultät der
Ludwig-Maximilians-Universität München

vorgelegt von

Laura Bernhardine Kuhn

aus

München

Jahr

2021

Mit Genehmigung der Medizinischen Fakultät
der Universität München

Betreuer(in):

PD Dr. Ursula Zimmer-Strobl

Zweitgutachter(in):

Prof. Dr. Aloys Schepers

Dekan:

Prof. Dr. med. Thomas Gudermann

Tag der mündlichen Prüfung:

17.12.2021

I. Content

Evolution of pre-germinal center B cell lymphoma		
I.	Content	III
II.	List of figures	VI
III.	List of tables	VII
IV.	Acronyms	VIII
V.	Abstract	X
VI.	Zusammenfassung	XII
1.	Introduction	1
1.1.	General B lymphocyte development	1
1.2.	Immune response of B lymphocytes	3
1.3.	CD40 signaling	4
1.3.1.	Activation of NF- κ B signaling	5
1.3.2.	The role of NF- κ B signaling in B cell lymphoma	7
1.3.3.	Mouse models involved in non-canonical NF- κ B signaling and CD40-induced lymphomagenesis	8
1.4.	B cell lymphoma and different subgroups	9
1.5.	Transposable elements	13
1.5.1.	Transposable elements as a tool to discover new oncogenes	14
1.5.2.	The PB mouse model	15
2.	Aims of thesis	16
3.	Results	18
3.1.	Contribution of non-canonical NF- κ B signaling on CD40-induced B cell lymphoma development	18
3.1.1.	Impact of non-canonical NF- κ B signaling on B cells of young LC40 mice	19
3.1.1.1.	Identifying new RELB-dependent targets in constitutive CD40-activated B cells	21
3.1.1.2.	CD40-induced upregulation of CD85k is dependent on RELB	23
3.1.1.3.	CD40-induced IL9R upregulation is dependent on RELB and induces in vitro cell proliferation upon IL-9 stimulation	24
3.1.1.4.	T helper cells act as a potential IL9 source	27
3.1.2.	IL9R and CD85k upregulation in human primary B cells after CD40 stimulation	28
3.1.3.	Lymphoma incidence is significantly reduced by RelBKO in LMP1/CD40 mice	30
3.1.4.	Identification of the B cell population inducing lymphoma in LMP1/CD40 mice	33

3.2.	CycD1//LC40 mice as MCL model	38
3.2.1.	CYCD1 overexpression does not affect the phenotype of young LC40 mice	38
3.2.2.	Lymphoma development in cycD1//LC40 mice	40
3.2.3.	The impact of C57BL/6 and BALB/c background on lymphoma development in LC40 mice	44
3.3.	PiggyBac transposon screen for identification of new cancer genes	45
3.3.1.	Lymphoma development of PB mice	46
3.3.2.	Identification of new driver genes	50
4.	Discussion	62
4.1.	Role of non-canonical NF- κ B signaling to B cell lymphoma	62
4.2.	CycD1//LC40 mice as a Mantle Cell Lymphoma (MCL) model	68
4.3.	Influence of strain background on lymphoma development in LC40 mice	70
4.4.	New drivers of B cell lymphoma development	71
5.	Material and Methods	75
5.1.	Mouse strains	75
5.2.	Molecular biology	76
5.2.1.	Mouse genotyping	76
5.2.2.	RNA extraction, cDNA synthesis and qPCR	78
5.2.3.	Southern Blot	79
5.2.4.	BCR and TRADIS Sequencing	81
5.2.5.	RNA Sequencing	82
5.3.	Mouse related assays	82
5.3.1.	Preparation of murine lymphocytes	82
5.3.2.	Isolation of B cells and T cells	82
5.3.3.	Transplantation experiments	83
5.4.	Flow cytometry	83
5.4.1.	Surface staining	83
5.4.2.	Detection of IL-9 by intracellular FACS	84
5.5.	Cell culture	84
5.5.1.	Cultivation and stimulation of murine B cells	84
5.5.2.	Cell proliferation assay	85
5.5.3.	Establishment of the LMP1/CD40 cell line	85
5.5.4.	Cultivation of feeder layer cell	85
5.5.5.	Cultivation and stimulation of primary human B cells	86
5.6.	Immunohistochemistry	86

5.7.	Western Blot and WES simple protein	86
5.8.	Statistics and data analysis	88
6.	References	89
7.	Appendix	100
7.1.	Supplement data	100
7.2.	Curriculum Vitae	101
7.3.	Eidesstattliche Erklärung	102
7.4.	Erklärung	102
7.5.	Danksagung	103

II. List of figures

Figure 1 Scheme of the CD40 receptor stimulation	5
Figure 2 Scheme of the NF- κ B pathway	7
Figure 3 Scheme of the LMP1/CD40 and RelBKO transgenic mice	9
Figure 4 Scheme of the PB transposon mouse model	15
Figure 5 Determination of the expression of the non-canonical NF- κ B pathway components	18
Figure 6 RELB-dependent upregulation of activation markers on B cells	20
Figure 7 The top differentially expressed genes comparing B cells of LC40 and RelBKO//LC40 mice	21
Figure 8 Validation of differentially expressed genes by qPCR	22
Figure 9 CD85k expression level of B cells	24
Figure 10 IL9R expression level of B cells	25
Figure 11 The division rate of splenic B cells isolated from LC40 and RelBKO/LC40 mice	26
Figure 12 The division rate of splenic B cells isolated from control and RelBKO mice	27
Figure 13 IL9 expression of ex vivo short-term stimulated Th cells	28
Figure 14 The protein levels of RELB and p52 in primary human B cells after CD40 stimulation	29
Figure 15. IL9R and CD85k expression on primary human B cell	30
Figure 16 Representative FACS dot plots of the CD21/CD23 immunophenotype of the old LC40, RelBKO//LC40 and control mice	31
Figure 17 Determination of clonal B cell expansions in aged LC40, RelBKO//LC40, and control mice	32
Figure 18 Immunohistochemistry of spleen tissue from aged LC40 and the RelBKO//LC40 mice	32
Figure 19 FACS gating strategy to sort B cells of LC40 donor mice for transplantation experiments	34
Figure 20 Detection of B cells in blood of NSG mice after transplantation	35
Figure 21 Detection of B cell in the spleen of NSG mice after transplantation	35
Figure 22 Re-transplantation of the AB14 B cell population	36
Figure 23 The immunophenotype of the murine LC40 cell line compared to primary murine B cells	37
Figure 24 Determination of Cdc25A mRNA levels	38
Figure 25 Splenic weight and B cell numbers of young cdc25A//LC40, LC40, cdc25A and control mice	39
Figure 26 The immunophenotype of young cdc25A//LC40, LC40, cdc25A and control mice	40
Figure 27 Clonal B cell expansion, splenic weight, and B cell numbers of aged cdc25A//LC40 and LC40 mice.	41
Figure 28 The CD21/CD23 immunophenotype of aged cdc25A//LC40, LC40 and control mice	42
Figure 29 The B220/CD5 immunophenotype of aged cdc25A//LC40, LC40 and control mice	43
Figure 30 Age-related splenomegaly of LC40 mice depends on their genetic background	44
Figure 31 Scheme of cdc25A//PB and LC40//PB mouse model	45
Figure 32 Splenic weight, survival, and development of a clonal B cell expansion of aged PB mice	46
Figure 33 Example FACS blots of PB mice for the stainings CD23/CD21	48
Figure 34 Example FACS blots of PB mice for the stainings B220/CD5	49
Figure 35 Example FACS plots of PB mice for the stainings IgM/IgD	50
Figure 36 Overview of the ATP2 insertions in a karyoplot	51
Figure 37 Numbers of common insertion site (CIS) for each splenic sample	53
Figure 39 Heatmaps of top hits for control//PB, cdc25A//PB and LC40//PB mice	54
Figure 39 Normalized read coverage of all LC40//PB samples	55
Figure 40 Normalized read coverage of all cdc25A//PB samples	56
Figure 41 Normalized read coverage of all control//PB samples	57
Figure 42 Venn diagram displaying the intersection between different transposon screens	58
Figure 43 The general molecular function of all top hit depicted in the heatmaps of Figure 32	59
Figure 44 Transposon insertion patterns for selected genes	61

III. List of tables

Table 1 Summary of LC40//PB, cycD1//PB and control//PB mice used to identify new driver genes in lymphoma.	47
Table 2 The primer sequences for each PCR	77
Table 3 The master mix recipe for each PCR	78
Table 4 The time and temperature settings for each step of each PCR program	78
Table 5 List of primers and Roche probe number used for qPCR	79
Table 6 Table of FACS antibodies	84
Table 7 Antibodies used for Western Blot or WES protein simple	87
Table 8 List of samples derived from aged LC40, RelBKO//LC40 and control mice	100

IV. Acronyms

ABC-DLBCL	Activated B cell – diffuse large B cell lymphoma subtype
ATM	Ataxia-Telangiectasia mutated
BAFF	B cell activating factor
BAFFR	B cell activating factor receptor
BCR	B cell receptor
BL	Burkitt lymphoma
BTK	Bruton's tyrosine kinase
CAR	Chimeric antigen receptor
CBM complex	CARD11, BCL10 and MALT1 complex
CCDC148	Coiled-coil domain containing protein 148
CD40L	CD40 ligand
CDR3	Complementarity-determining region 3
CIS	Common insertion site
CLL	Chronic lymphocytic leukemia
CNR1	Cannabinoid receptor 1
CXCR	CXC-motif-chemokine receptor
CYCD1	Cyclin D1
DLBCL	Diffuse large B cell lymphoma
DNA	Deoxyribonucleotide acid
DZ	Dark zone
EBV	Epstein-Barr virus
FACS	Fluorescence associated cell sorting
FCS	Fetal calves' serum
FDA	U.S. Food and Drug Administration
FL	Follicular lymphoma
FoB	Follicular B cell
GC	Germinal center
GCB	Germinal center B cell
IC	Intracellular
ICAM	Intercellular adhesion molecule
ICOS-L	Inducible T cell co-stimulator ligand
ID	Identification number
IgH	Immunoglobulin heavy chain
IL	Interleukin
IL9R	Interleukin 9 receptor
ITR	Inverted terminal repeats
JAK	Janus kinase
LC40	LMP1/CD40
LINE	Long interspersed nuclear elements
LMP1	Latent membrane protein 1
LTR	Long terminal repeat
LZ	Light zone
MALT	Mucosa-associated lymphoid tissue
MAP	Mitogen-activated protein
MCL	Mantle cell lymphoma
MFI	Median fluorescence intensity
MHC	Major histocompatibility complex
MSCV	Murine stem cell virus
MZB	Marginal zone B cell
MZL	Marginal zone lymphoma

NA	Not available
NF- κ B	Nuclear factor κ -light-chain-enhancer of activated B-cells
NIK	NF- κ B inducing kinase
NSG	NOD scid gamma
pA	polyA site
PB	PiggyBac
PCR	Polymerase chain reaction
PI3K	Phosphoinositide 3-kinase
R-CHOP	Rituximab/Cyclophosphamid/Doxorubicin/Vincristin/Prednison
RelBKO	RELB knock-out
RHBDF1	Rhomboid 5 homolog 1
RNA	Ribonucleotide acid
RT	Room temperature
RUNX1	Runt-related transcription factor 1
SA	Splice acceptor
SB	Sleeping beauty
SD	Splice donor
Seq	Sequencing
SHM	Somatic hypermutation
SINE	Short interspersed nuclear elements
SLL	Small lymphocytic leukemia
SOX	SRY (Sex Determining Region Y)-Box
SP	Spleen
STAT	Signal transducer and activator of transcription
TAB2	TAK1-Binding Protein 2
TAPDANCE	Transposon annotation Poisson distribution association network connectivity environment
TCR	T cell receptor
TD	T dependent
TE	Transposable element
Th cells	T helper cell
TI	T independent
TLR	Toll like receptor
TNFR	Tumor necrosis factor receptor
TRAF	Tumor necrosis receptor associated factors
TrisE	Tris EDTA
TSO	Template switch oligonucleotide
UV	Ultraviolet
WHO	World health organization

V. Abstract

Pre-germinal center B cells lymphoma originate from mature B cells bypassing the germinal center. In recent years, LMP1/CD40 (LC40) mice became a useful model to study pre-germinal center lymphoma as they do not form germinal centers in their spleen and develop lymphoma in aged mice as a result of a chronic CD40 activation of their B cells. Transplantation experiments performed here, confirmed that the tumor population originates from a CD23⁻/CD21⁻ premalignant, aberrant B cell population.

To understand the contribution of non-canonical NF- κ B signaling to lymphomagenesis in LC40 mice, LC40 mice deficient in RELB - a transcription factor involved at non-canonical NF- κ B signaling - (RelBKO//LC40) were utilized. Inactivation of RELB reduced lymphoma burden and diminished the outgrowth of the aberrant CD21⁻/CD23⁻ B cell population in LC40 mice. Moreover, a comparative study of young RelBKO//LC40 and LC40 mice showed that constitutive activation of non-canonical NF- κ B signaling led to an elevated expression of genes potentially involved in lymphomagenesis. One of these RELB-dependent genes is the IL9 receptor (IL9R). Due to its dependency on functional RELB, only B cells derived from LC40 RELB-proficient mice proliferated after IL9 stimulation. In addition, Th cells, a major source of IL9, were found in greater numbers in LC40 mice compared to RelBKO//LC40 mice; hinting to a positive feedback loop that leads to increased IL9R stimulation and proliferation of B cells, which may drive mice towards lymphoma development. Cumulatively, this research indicates that constitutive activation of the non-canonical NF- κ B pathway has a deleterious role in tumor development.

Furthermore, CD40 stimulation favors the progression of Mantle cell lymphoma (MCL), which is characterized by a cyclinD1 (cycD1) overexpression. Currently, no suitable mouse model that mimics the impact of CD40 on MCL is available. Thus, LC40 mice were crossed with cycD1 mice, to generate mice bearing the CYCD1 overexpression and the constitutive CD40 activation (cycD1//LC40 mice). Analysis of aged mice showed that CYCD1 overexpression accelerated the lymphomagenesis of LC40 mice, but the immune phenotype remained the same in both young and aged mice. The tumor population of both transgenic mice was CD21⁻, CD23⁻, B220^{low}, IgM⁺ and tendentially CD5⁺, and therefore similar to the MCL phenotype.

For another project, the tumor evolution of CD40-induced B cell lymphoma or B cell lymphoma with CYCD1 overexpression was investigated. To enable a transposon-based, random

mutagenesis screen for driver mutations, the PiggyBac system was combined with LC40 or cycD1 mice. After sample collection and sequencing, bioinformatic analysis could identify genes which were frequently affected by the transposon-based mutagenesis. Thus, new genes could be discovered which might harbor roles in B cell lymphoma initiation and/or progression in a constitutive CD40 signaling or an CYCD1 overexpression dependent manner.

VI. Zusammenfassung

Präkeimzentrums B-Zelllymphome bilden sich aus reifen B-Zellen, bevor sie eine Keimzentrumsreaktion durchlaufen. Um die Entstehung dieser B-Zelllymphome zu untersuchen, wurden in dieser Arbeit LMP1/CD40 (LC40) Mäuse als zentrales Tumormodell verwendet, da diese Mäuse keine Keimzentren in der Milz ausbilden und durch die konstitutive CD40 Aktivierung im fortgeschrittenen Alter B-Zelllymphome entwickeln. Durch Transplantationsexperimente konnte nachgewiesen werden, dass die Tumoren auf eine prä maligne, aberrante CD21⁻/CD23⁻ B-Zellpopulation zurückzuführen sind.

Des Weiteren konnte durch die Analyse von RELB defizienten LC40 Mäusen (RelBKO//LC40) festgestellt werden, dass die Tumorinzidenz durch die Inaktivierung des alternativen NF- κ B Signalweges von LC40 Mäusen deutlich reduziert wird. Zusätzlich verringerte die Inaktivierung von RELB die B-Zellexpansion der aberranten Population. Außerdem zeigten die Untersuchungen von jungen LC40 Mäusen im Vergleich zu RelBKO//LC40 Mäusen, dass die Aktivierung des alternativen NF- κ B Signalweges bereits in jungem Alter zu einer erhöhten Expression von Genen führt, welche potenziell die Tumorentstehung fördern. Eines dieser RELB abhängig exprimierten Gene ist der IL9 Rezeptor (IL9R). Daher regt eine IL9 Stimulation B-Zellen von LC40 Mäusen zur verstärkten Proliferation an. Als Quelle von IL9 konnten Helfer T-Zellen identifiziert werden. Interessanterweise hatten LC40 Mäuse mehr IL9 produzierende Helfer T-Zellen im Vergleich zu RelBKO//LC40 Mäusen. Dies könnte darauf hinweisen, dass sich in LC40 Mäusen eine positive Rückkopplung entwickelt, welche zu einer erhöhten IL9R Stimulation der LC40 exprimierenden B-Zellen führt. Die Rückkopplung scheint von der konstitutiven Aktivierung des nicht-kanonischen Signalweges in B-Zellen abhängig zu sein und könnte dazu beitragen, dass RelBKO//LC40 eine geringere B-Zellexpansion und Tumorinzidenz aufweisen als LC40 Tiere.

Interessanterweise fördert eine CD40 Stimulation auch die Progression von Mantelzell-Lymphomen (MCL), welches durch eine initiale CyclinD1 (cycD1) Überexpression charakterisiert ist. Momentan gibt es noch keine geeigneten Mausmodelle für diesen Verlauf der Krankheit, daher ist die Entwicklung eines Modells von großem Interesse. Um ein solches Modell zu generieren, wurden LC40 Mäuse mit cycD1 Mäusen gekreuzt (cycD1//LC40). Die B-Zellen dieser Mäuse weisen die für MCL charakteristische CYCD1 Überexpression sowie ein chronisches CD40 Signal auf. Analysen von gealterten cycD1//LC40 Tieren zeigten, dass die

Entwicklung von Lymphomen in LC40 Mäusen durch die CYCD1 Überexpression etwas beschleunigt wird. Der Immunphänotyp von B-Zellen aus LC40 Tieren wurde durch die CYCD1 Überexpression weder in jungen noch alten Mäusen verändert. Der Immunphänotyp der Tumorphpopulation ist CD21⁻, CD23⁻, B220^{low}, IgM⁺ und tendenziell CD5⁺ und ähnelt dem Immunphänotyp von Mantelzell-Lymphomen.

Ein weiteres Projekt befasst sich mit der Tumorevolution von B-Zelllymphomen, die durch ein konstitutives CD40 Signal oder eine CYCD1 Überexpression beeinflusst werden. Hierzu wurde unter Verwendung des konditionellen PiggyBac (PB) Systems eine Transposon basierte, randomisierte Mutagenese in *cycD1* und LC40 Mäusen induziert. Nach vollständiger Probenkollektion konnten durch Sequenzierung von Tumorproben und bioinformatische Auswertung Gene identifiziert werden, die besonders häufig von der Transposon induzierten Mutagenese betroffen waren. Somit konnten erfolgreich neue Gene entdeckt werden, die für die Entwicklung bzw. Progression von Lymphomen mit entweder konstitutivem CD40 Signal oder mit einer CYCD1 Überexpression verantwortlich sind.

1. Introduction

In the 1960s, B lymphocytes and T lymphocytes were discovered as two interacting parts of the adaptive immune system in chicken by distinguishing the organs where they develop. Cells that were dependent on the thymus got the name T cells, while cells derived from the chicken bursa were named B cells (Cooper *et al.*, 1966). In mammals, the bursa is absent and B cells develop in the bone marrow. B cells are responsible for the expression of antibodies, which are specific, clonally diverse cell surface immunoglobulin receptors recognizing epitopes.

1.1. General B lymphocyte development

Like all blood cell types, B cells originate from multipotent hematopoietic stem cells in the bone marrow. By inducing the expression of the tyrosine kinase FLT3, the multipotent hematopoietic stem cells lose their long-term self-renewal and develop into oligopotent progenitors (Adolfsson *et al.*, 2001). The multipotent progenitors commit to either the myeloid or the lymphoid lineage. The common lymphoid progenitors give rise to T, B, natural killer or some dendritic cells. Several transcription factors (e.g. PU.1) and stimuli (e.g. IL7) direct the differentiation into the early pro-B cell stage, which is characterized by the expression of PAX5, EBF-1 and E2A. If it has not started yet, the V(D)J recombination of the immunoglobulin heavy chain (IgH) locus is induced by E2A and EBF at this cell stage. After the D-J_H locus is successfully rearranged, the V(D)J recombination is completed in the late pro-B cell stage by recombining a V_H gene segment to the D-J_H segment. The transcription factor PAX5 is required to progress B cell development beyond the pro-B cell stage. If PAX5 is lacking, cells continue differentiating into T cells rather than B cells (Busslinger, 2004). The successful V(D)J recombination of the *igh* gene and expression of the surrogate light chain results in expression of the pre-B cell receptor (pre-BCR) at the cell surface which marks the entrance into the large pre-B cell stage. At this stage, cells proliferate to increase the population size, before entering the resting small pre-B cell stage, where the rearrangement of the immunoglobulin light chain locus takes place. Since the D segment is absent in the light chain gene, the rearrangement happens by joining V_L to J_L segments. In case the recombination of the first light chain locus fails, pre-B cells get another chance to produce a functional B cell receptor (BCR) by rearranging the second light chain locus. In humans and mice, the κ light chain locus tends to be arranged first and the λ light chain locus second. A cell that can produce a functional, intact BCR is classified as immature B cell. To provide central tolerance, immature

B cells are tested for autoreactivity and recognition of self-antigen. Every immature B cell not passing this test is eliminated or undergoes further modification. Cells surviving this safety mechanism leave the bone marrow towards the spleen (Murphy, 2012). Immature B cells enter the spleen via the blood stream and undergo transitional stages to mature into follicular B cells (FoB) and marginal zone B cells (MZB). In their immature and transitional state, B cells are positive for AA4.1, unable to proliferate upon BCR stimulation and have a high turnover rate (Allman *et al.*, 2001). The survival of peripheral, immature B cells is highly dependent on stimulation provided in B cell follicles of the spleen. An essential pro-survival cytokine is the B cell activating factor (BAFF) which is secreted by dendritic follicular cells and some other cell types. B cells express three kinds of BAFF-receptors which are BAFFR, TACI and BCMA and all three belong to the tumor necrosis factor receptor (TNFR) family. The most important one for the survival of immature B cells is BAFFR, since BAFFR-deficient mice have less mature B cells due to a developmental block at the transitional B cell stages (Sasaki *et al.*, 2004). Classically, transitional B cells receiving a stronger BCR signaling together with a BAFF stimulation develop into FoBs, expressing CD23⁺, IgD^{high}, IgM^{low}, CD21^{mid} (Pillai and Cariappa, 2009). Recent studies also revealed that the induction of a metabolic quiescence favors the developmental progression into the FoB cell fate (Farmer *et al.*, 2019). For B cells developing into MZB cells a reduced BCR signaling but increased NF- κ B signaling is necessary. They locate in the marginal zone between the B cell follicle and the red pulp of the spleen. Further, they are IgM^{high}, IgD^{low}, CD21⁺ and CD23^{low} and play a major role in the primary immune response (Pillai and Cariappa, 2009). Moreover, NOTCH2 signaling is crucial for MZB development, as Notch2 knock out mice show a defect in MZB development and constitutive NOTCH2 signaling leads to enhanced MZB development (Saito *et al.*, 2003; Hampel *et al.*, 2011). In addition mice lacking TAOK3, a mitogen-activated protein (MAP) kinase essential to transmit NOTCH signaling, miss MZBs (Hammad *et al.*, 2017). Mature B cells can be classed into two major groups: B1 and B2 cells. While B2 cells are MZBs and FoBs and constitute the more conventional type that makes up the majority of B cell in the spleen and develops as described above, B1 cells are mainly produced in the embryo's yolk sack and in the pre-natal fetal liver. The B1 cell development in the bone marrow after birth is less efficient (Montecino-Rodriguez and Dorshkind, 2012). Furthermore, B1 cells can be distinguished into CD5^{high} B1a and CD5^{low} B1b cells. The surface glycoprotein CD5 is also expressed on T cells and lowers the threshold of BCR / T cell receptor (TCR) mediated activation after antigen recognition (Dalloul, 2009). B1 cells are the major B

cell subset in the peritoneal cavity, but they are also found in the spleen and in the bone marrow. Alike MZBs, B1 cells are involved in primary immune responses and are less dependent on T cell help than FoB cells.

1.2. Immune response of B lymphocytes

Depending on the antigen type, B cell activation happens in a thymus/T cell independent (TI) or thymus/T cell dependent (TD) manner. In both cases, the BCR must detect the antigen and initiates a B cell activating signaling cascade. The TI immune response can be triggered by B cell mitogens e.g. lipopolysaccharides and leads to a polyclonal activation and proliferation via toll-like receptors. Antigens inducing this kind of TI response are referred as TI-1 antigens. The TI-2 antigens contain a repetitive structure and originate from microbes. These antigens themselves are able to induce an immune response by crosslinking the BCR. The TI immune response is mainly performed by MZBs and B1 cells and is essential for a rapid and initial adaptive immune response. After the BCR is triggered by a TD protein antigen, B cells migrate to the interface of the B cell follicle and the T cell zone. Further, antigens bound by the BCR are internalized, processed and presented on the major histocompatibility complex class (MHC) II, ready to be recognized by a T cell receptor (TCR) (Murphy, 2012). At the T cell/B cell border, a long-lasting collaboration between T and B cells is formed and needs several factors to ensure a stable connection. For example the SLAM family receptor interaction and the TCR interaction with the peptide-loaded MHCII molecule of B cells (Biram, Davidzohn and Shulman, 2019). Moreover, integrin interactions e.g. LFA-1 on T cells engaging with intercellular adhesion molecules (ICAM) on B cells enhance a stable connection and provide a competitive advantage in polyclonal immune responses (Zaretsky *et al.*, 2017). Furthermore, the co-stimulatory membrane receptors CD80 and CD86 on B cells influence helper T cells (Th cells) by increasing their proliferative potential (Liebert *et al.*, 2002). At the T cell/B cell interface, FoBs form peri-follicular germinal center (GC) precursors which express intermediate levels of BCL6 and co-express the transcription factors RELB and IRF4. The expression of RELB is essential to initiate GC formation. To transition into GC B cells, BCL6 gets up-regulated and the stimulation received by T cells e.g. CD40 signaling must cease to progress the GC B cell development (Zhang *et al.*, 2017). CD40 is a TNFR, which is expressed on B cells, and the stimulation is mediated by activated T cell, which express its interaction partner CD40L. CD40 stimulation upregulates the inducible T cell co-stimulator ligand (ICOS-L) on B cells, which contributes to an entangled interaction between B and T cells (Liu *et al.*, 2015).

The importance of CD40 signaling is even enhanced, considering that RELB and also NFKB2 - members of the non-canonical NF- κ B pathway induced by CD40 - are required to form functional GCs (De Silva *et al.*, 2016). Part of the GC reaction is the activation-induced cytidine deaminase driven somatic hypermutation (SHM) of the antigen-binding variable regions of immunoglobulin genes to further improve their affinity (Mesin, Ersching and Victora, 2016). Additionally, isotype switching happens during the GC reaction, but is not restricted to this developmental stage (Gatto and Brink, 2010). The GC is parted into a light zone (LZ) and dark zone (DZ), which allows compartmentation of the molecular processes of the GC reaction. In the DZ, SHM and cell proliferation is performed, while in the LZ the BCR affinity is tested. Therefore, follicular dendritic cells present antigen to the B cells, and B cells compete for limited Th cell stimulation. Only B cells with a non-autoreactive BCR can re-enter the DZ for further modification or leave the GC as high affinity plasma cells or memory B cells (Mesin, Jonatan and Victora, 2016). Further, B cell with a higher BCR affinity are preferentially selected and during this positive selection the activation of the NF- κ B signaling pathway is essential, which is provided by T cell dependent CD40 stimulation (Nowosad, Spillane and Tolar, 2016). For plasma cell differentiation a higher affinity BCR and the upregulation of BLMIP1 via IRF4 is required. Plasma cells upregulate the CXC-motif-chemokine receptor (CXCR) 4 and exit the GC at the DZ side (Suan, Sundling and Brink, 2017). B cells with a functional, but lower affinity BCR and an upregulation of ABF-1 develop into memory B cells. For the upregulation of ABF-1 anti-CD40 stimulation by T cells is required (Chiu *et al.*, 2014).

1.3. CD40 signaling

In general, the TNFR CD40 is a transmembrane glycoprotein and is expressed by dendritic cells, monocytes, epithelial cells, and B cells. Since the cytoplasmic part of CD40 has no intrinsic catalytic activity, the initial signal transduction is dependent on tumor necrosis receptor associated factors (TRAF) (Harnett, 2004). Upon TRAF signal transduction CD40 signaling is able to activate various pathways e.g. MAP kinase pathways like ERK1/2, JNK1/2 and p38, phosphoinositide 3-kinase (PI3K) and NF- κ B signaling (Dadgostar *et al.*, 2002) (Figure 1). Moreover, the intracellular domain of CD40 interacts with the Janus kinase 3 (JAK3), which leads to activation of signal transducer and activator of transcription (STAT) 3, 6 and 5a (Chatzigeorgiou *et al.*, 2009). Generally, CD40 stimulation activates B cells, induces proliferation, and is involved in different stages of B cell activation (Bishop and Hostager, 2003). Further, the quantity of the CD40 signaling influences the development of memory B

cells. This signal quantity relies on the B cell/T cell interaction since Th cells provide the CD40 ligand (CD40L). The CD40 signal mediated by Th cells is stronger, if B cell have a high affinity BCR or a high amount of antigen is available. It is weaker, if the BCR has a low affinity or little antigen is present. B cells receiving a strong CD40 signal preferentially develop into CD80^{high} memory B cells and tend to differentiate into plasma blasts. Whereas B cells getting a weaker CD40 stimulation commit towards CD80^{low} memory B cells and are more prone to develop into GC B cells and memory B cells (Koike *et al.*, 2019). Besides, the CD40 signal transduction via TRAF2, the NF- κ B pathway has to be intact for optimal isotype switching during the GC reaction (Woolaver *et al.*, 2018). In the following chapters the activation of the NF- κ B pathway is further described.

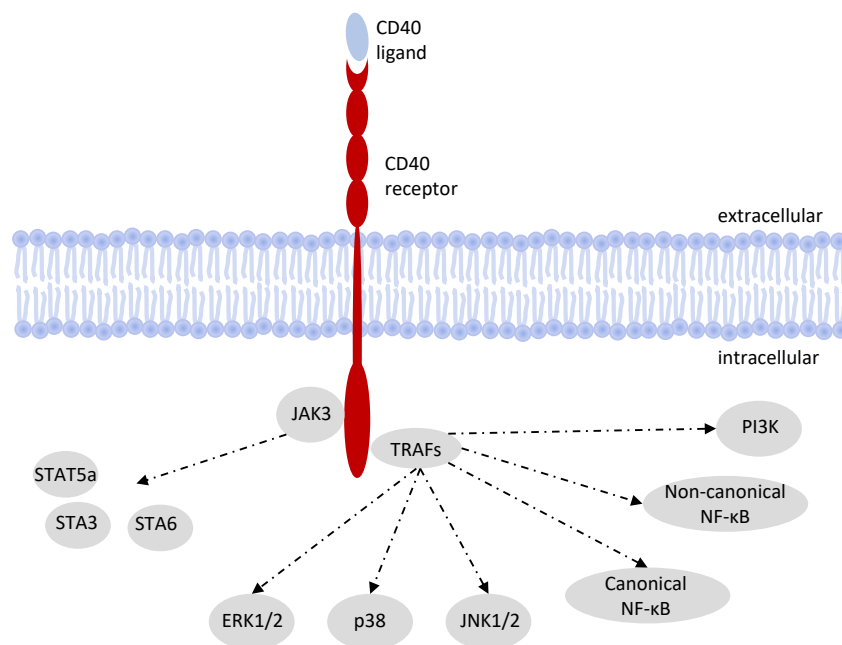


Figure 1 The CD40 receptor is stimulated by the CD40 ligand. For CD40 signaling TRAFs or JAK3 interact with the intracellular domain of CD40 and induce NF- κ B pathways, PI3K signaling, the MAP kinase signaling e.g. ERK1/2, JNK1/2 and p38, and STAT3,6,5a signaling. The graphic is based on Chatzigeorgiou, 2009.

1.3.1. Activation of NF- κ B signaling

Nuclear factor binding near the κ -light-chain gene in B cells, or short NF- κ B consists of five transcription factors forming homo- and heterodimers translocating into the nucleus to induce inflammation, proliferation, and further cellular processes. While the factors p50 and p52 arise from post-translational cleavage of their precursor proteins p105 (NFKB1) and p100 (NFKB2), the family members RELA, RELB and c-REL are translated as mature proteins including their transcription transactivation domain (Zhang, Lenardo and Baltimore, 2017). NF- κ B signaling involves two major pathways, which are the canonical and the non-canonical

or alternative NF- κ B pathway (Fig. 2). The canonical NF- κ B pathway is induced by pattern-recognition receptors such as toll-like receptors (TLRs), tumor necrosis superfamily receptors (TNFRs), and T cell receptor and B cell receptor signaling as well as cytokine receptors. The BCR activates the NF- κ B pathway via the Brutons tyrosine kinase (BTK), which further downstream phosphorylates CARD11. After its phosphorylation, CARD11 forms a complex with MATL1 and BCL10 (CBM complex) and has the potential to activate the IKK complex (Roué and Sola, 2020). TNFRs and TLRs transmit their signaling via TRAF2, 5 or 6 to the kinase TAK1, which activates the IKK complex containing IKK α , IKK β and IKK γ (Zhijian J, 2005). After phosphorylation of the IKK complex, phosphorylation of the inhibitory molecule I κ B α leads to its degradation and the transcription factor complexes p50/RELA and p50/c-REL translocate to the nucleus (Pires *et al.*, 2018). In contrast, the non-canonical NF- κ B signaling is more selectively activated by a subset of TNFR members as LT β R, BAFFR, CD40 and RANK. An essential protein for the signal transduction of this pathway is the NF- κ B inducing kinase (NIK), which is constitutively degraded in resting cells, and has to be stabilized for signal transmission. TRAF2 and TRAF3 are cooperatively involved in degradation of NIK and inhibitors of the non-canonical NF- κ B signaling. After TNFR stimulation, TRAF2 and TRAF3 are recruited to the receptor followed by their degradation, which allows NIK to get stabilized and accumulate (Razani, Reichardt and Cheng, 2011). The activation of NIK leads to a phosphorylation of the homodimer IKK α . The homodimer transfers the phosphate to the C-residue of p100, which leads to its ubiquitination and procession to p52 and the heterodimer p52/RelB translocates into the nucleus to induce gene transcription (Pires *et al.*, 2018).

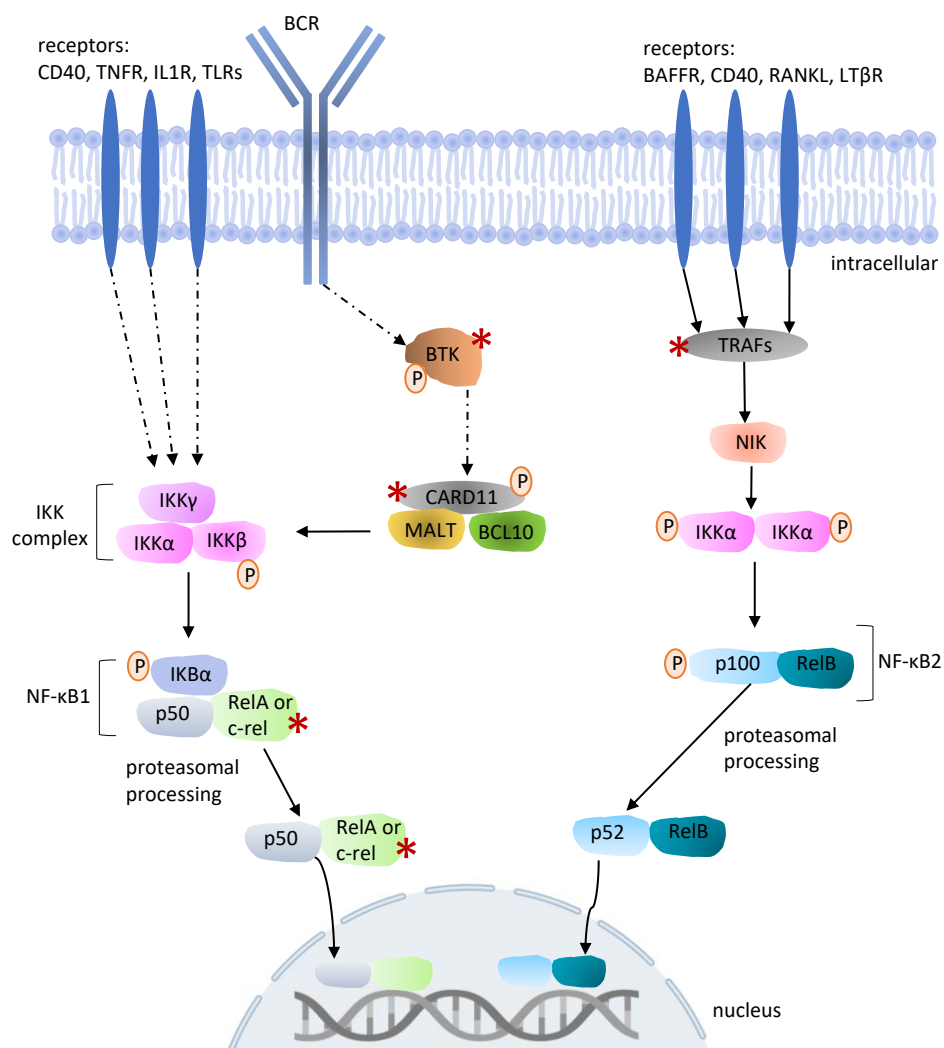


Figure 2 The canonical NF- κ B pathway is induced by TNFRs, CD40, TLRs and cytokine receptors like IL1R, which activate the IKK complex by phosphorylation of IKK β . Subsequently, I κ B α of NF- κ B1 complex is phosphorylated and processed. This releases the transcription factor complex RelA/p50 or c-Rel/p50, which translocates into the nucleus. The non-canonical NF- κ B pathway is activated by BAFFR, CD40, RANKL or LT β R. The signal is transduced by NIK to IKK α and p100. After p100 is processed into p52, the transcription factors p52/RelB translocate into the nucleus. The BCR is able to activate the canonical NF- κ B pathway via burtons tyrosine kinase (BTK) and the CBM complex consisting of MALT, BCL10 and CARD11. Red stars indicate genes that can be mutated in B cell lymphoma and P indicates a phosphorylation site. Dotted arrows indicate a signal transduction which includes steps not depicted here. The graphic is based on Roué and Sola 2020.

1.3.2. The role of NF- κ B signaling in B cell lymphoma

Oncogenic activation of the NF- κ B pathway is observed in several B cell lymphomas e.g. in the ABC- subtype of DLBCL (Lenz *et al.*, 2008; Cai *et al.*, 2017), splenic MZL (D. Rossi *et al.*, 2011) and MCL (Saba *et al.*, 2016). Of special note is the role that non-canonical NF- κ B signaling plays in refractory and relapsed MCL patients. As its activation via CD40 provides chemoresistance to BTK inhibitor agents like ibrutinib (Rauert-Wunderlich *et al.*, 2018b), these MCL patients are particularly difficult to cure and no satisfying treatment is available yet. Unfortunately, clinical trials including bortezomib – an inhibitor of the proteasomal degradation of p100 and I κ B α –

did not result in an improved outcome for patients (Leonard *et al.*, 2017; Davies *et al.*, 2019). An explanation might be provided in the complexity of NF- κ B and its different functions in different cell types, as NF- κ B signaling is also essential for the anti-tumor immune response of T cells and NK cells. Thus, the success of a therapy targeting a general NF- κ B inhibitor is highly dependent on the tumor microenvironment (Pires *et al.*, 2018). Further research is required to pinpoint malignant effector proteins more downstream of NF- κ B signaling and to receive a better understanding of the tumor environment to be able to cure these chemo resistant diseases.

1.3.3. Mouse models employed in the study of non-canonical NF- κ B signaling and CD40-induced lymphomagenesis

Since the NF- κ B signaling cascade involves many proteins, several mouse models exist to study its impact on lymphomagenesis. For example, transgenic mice bearing a B cell specific NIK overexpression or a B cell specific TRAF3 knock-out obtain B cell lymphoma due to an overactivation of the non-canonical NF- κ B signaling (Sasaki *et al.*, 2008; Moore *et al.*, 2012). As CD40 signaling also activates the canonical and non-canonical NF- κ B signaling, the Zimmer-Strobl laboratory designed the LMP1/CD40 (LC40) mouse model to study constitutive CD40 activation in B cells (Hömig-Hölzel *et al.*, 2008; Hojer *et al.*, 2014). The chimeric fusion protein LC40 consists of the intracellular signaling domain of CD40 and the transmembrane domain of the EBV latent membrane protein 1 (LMP1). While the CD40 domain ensures the same biological signaling transduction as the natural TNFR CD40, the LMP1 part enables a ligand-independent constitutive activation by inducing self-aggregation in the plasma membrane. To receive a B cell exclusive induction, transgenic mice bearing this chimeric construct combined with a lox-P stop cassette in their *rosa26* gene locus were crossed with CD19-Cre mice. Since CD19 is a co-receptor of the BCR, LC40 is exclusively expressed in B cells. The constitutive CD40 signaling leads to an elevated number of B and T cells, a splenomegaly, and an upregulation of various adhesion and activation related surface proteins. Furthermore, B cells of LC40 mice are trapped in splenic and lymph node follicles, though show a declined germinal centers formation. Additionally, it activates MAP kinase signaling and the non-canonical NF- κ B pathway. Moreover, LC40 supports B cell proliferation and *in vitro* survival. Of special note is the increased B cell lymphoma burden observed in aged LC40 mice compared to controls (Hömig-Hölzel *et al.*, 2008; Zapf, 2017). Further studies revealed, that these indolent tumors can be transformed into an aggressive state, if the immune surveillance of T cells is suppressed

(Vincent-Fabert *et al.*, 2018). Previous colleagues, Kristina Stojanovic and Stefanie Zapf, could show, that the tumor development correlates with the outgrowth of an aberrant B cell population with the immunophenotype of B220^{low}, CD19⁺, CD23⁻, CD21⁻. Furthermore, this outgrowth seems to be partially dependent on the non-canonical NF- κ B signaling as RELB-deficient LC40 mice have a declined number of B cells and particularly a decreased outgrowth of this population. This also aligns with the diminished BAFF-mediated survival and B cell development of RELB and c-REL double knock out mice (Almaden *et al.*, 2016). Considering these preliminary data of the LC40 mouse model and oncogenic power of the NF- κ B pathway, it is of high interest to further investigate the impact of the non-canonical NF- κ B to the lymphomagenesis in LC40 mice.

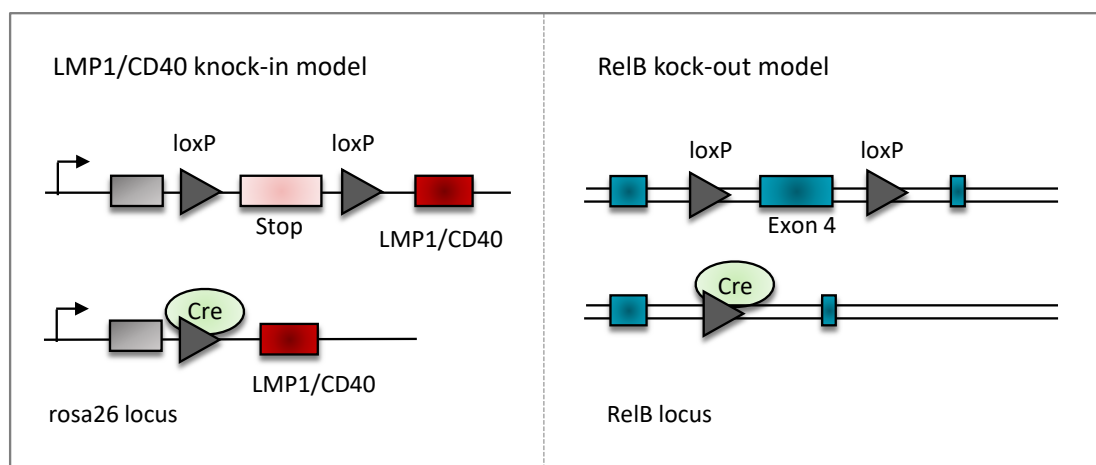


Figure 3 A scheme of the LMP1/CD40 transgenic cassette and the RelB knock-out model are depicted. The LC40 transgene is inserted into the rosa26 locus. The RelB knock-out is induced by cutting out exon 4.

1.4. B cell lymphoma and different subgroups

According to the 2016 revised World Health Organization (WHO) classification of lymphoid neoplasms, B cell lymphoma is the most prevalent lymphoma type and encompasses the largest number of distinct diagnostic entities (Swerdlow *et al.*, 2016).

The goal of classification is to identify homogenous groups of distinct entities to facilitate treatment strategies and to recognize uncommon diseases which need further investigation (Campo *et al.*, 2011). A very clear classifications of neoplasms derived from B cells is the one into Hodgkin and Non-Hodgkin lymphoma. A characteristic of Hodgkin lymphoma are Hodgkin and Reed-Sternberg tumor cells which usually derive from mature post-germinal center B cells but lost their B cell phenotype and identity (Mathas, Hartmann and Küppers, 2016). Thanks to chemotherapy and radiation, classical Hodgkin lymphoma is a highly curable neoplasm and

most patients are cured by first line therapy. The five-year relative survival of those patients is between 89.8% and 96.4% depending on their age (Shanbhag and Ambinder, 2019). Non-Hodgkin B cell lymphomas are highly diverse, and their classification is based on morphology, cell of origin and genetic variation. Some of these subgroups are: Small lymphocytic lymphoma/chronic lymphocytic leukemia (SLL/CLL), Burkitt lymphoma (BL), diffuse large B cell lymphoma (DLBCL), marginal zone lymphoma (MZL), follicular lymphoma (FL) and mantle cell lymphoma (MCL).

For SLL and CLL the malignant cells are small, mature B lymphocytes occasionally admixed with larger or atypical lymphocytes. Both entities are considered as the same indolent disease with a different manifestation, as SLL is predominantly located in the spleen and lymph nodes, while CLL also occurs in the blood and bone marrow (Zelenetz *et al.*, 2015). Monoclonal B-cell lymphocytosis is considered as the precursor for both (Swerdlow *et al.*, 2016).

A highly aggressive, rapidly growing B cell lymphoma derived from germinal center B cells is Burkitt lymphoma. This disease features a deregulation of *c-myc* by its t(8;14)(q24;q32) translocation. Endemic BL is associated with Epstein-Barr virus (EBV) and occasionally it is also associated with human immunodeficiency virus (HIV) (Kalisz *et al.*, 2019). Currently, the most common treatment approach of this highly chemo-sensitive lymphoma is an intensified combination chemotherapy including the anti-CD20 directed rituximab, which yields in an overall survival rate of 75-85%. Central nervous system involvement and increased age are poor prognostic factors related to a higher mortality risk. The ideal treatment of patients suffering of a relapse of BL is still an unmet medical challenge (J. Crombie, 2020).

Worldwide, diffuse large B cell lymphoma (DLBCL) accounts for up to 35% of non-Hodgkin lymphoma, making it the most common entity of lymphoid malignancies in adults (Chapuy *et al.*, 2018). As the name already indicates, DLBCL is a neoplasm consisting of abnormally large B cells arranged in a diffuse pattern, so normal follicular structures are disturbed. Morphologically, in most cases of DLBCL a heterogenous number of reactive small T cells and histiocytes mingle in the background of the tumorous cells (Li, Young and Medeiros, 2018). According to the in 2016 updated WHO classification of lymphoid neoplasms, DLBCL have been grouped into two subgroups depending on their cell of origin. One subgroup is derived from GC B cells (GC-DLBCL), and the other from activated B cells (ABC-DLBCL). Genome studies of DLBCL patients revealed that mutations in the PI3K/AKT/mTOR and JAK/STAT pathway and

the concurrent mutation of the epigenetic regulatory genes histone-lysine N-methyltransferase KMT2D and the histone-lysine N-methyltransferase EZH2 or transcriptional coactivator CREBBP occur more often in GCB-DLBCL. In ABC-DLBCL altered BCR-signaling and Toll-like receptor signaling via mutations in CD79B and MYD88 is frequently observed. Additionally, gene aberrations in tumor suppressor genes TP53 and CDKN2A are more likely to be manifested in ABC-DLBCL than in GCB-DLBCL (Karube et al. 2018, Chapuy et al. 2018). The same study also discovered that genetic alterations in the NOTCH signaling pathway impart a poor prognostic factor independent of the subgroup. Additionally, in both DLBCL subtypes members of NF- κ B signaling cascade are upregulated, thus NF- κ B signaling is an oncogenic driver independent of the DLBCL subtype (Odqvist *et al.*, 2014). At present, the standard first line therapy remains chemotherapy with R-CHOP-21, which leads to a cure of 60% of patients. Since 10-15% of patients suffer of a primary refractory disease and 20-30% of patients relapse, further therapeutic approaches are needed (G. Swennen, et al. 2020). The novel technology of chimeric antigen receptor (CAR) T cell therapy might be an option and is FDA approved for DLBCL patients relapsing after two prior lines of therapy. CAR T cell therapy involves genetic modification of a patient's autologous T cell to express a TCR directed against a tumor antigen, the T cells *in vitro* cell expansion, and re-transplantation into the patient (Miliotou and Papadopoulou, 2018). For B cell lymphoma the TCR of CAR T cells is usually directed against the B cell marker CD19. A recent study compared patients treated with commercial CAR T cell therapy and alternate therapies and reports an improved outcome for patients administered the CAR T therapy (Sermer *et al.*, 2020). Admittedly, the authors also disclose, that after adjustment for baseline unfavorable lymphoma biology, the superiority of CAR T therapy is a bit unsettled. Thus, further medical advances are demanded for this disease.

Self-explanatorily, marginal zone lymphoma (MZL) derives from MZBs. This indolent tumor is subclassified into extra-nodal MZL of mucosa-associated lymphoid tissue (MALT), splenic MZL and nodal MZL. All three subtypes frequently share certain genetic abnormalities e.g. trisomy of chromosome 3 and 18 and ~50% of MZL tumors contain mutations, which activate the NF- κ B pathway (Zucca, Bertoni and Rossi, 2018). A marker set to distinguish splenic MZL from the other two subtypes is EME2, ERCC5, SETBP1, USP24, and ZBTB32 (Robinson *et al.*, 2020) and nodular MZL can be differed from splenic MZL by a PTPRD lesion (Spina *et al.*, 2016). In MALT lymphoma, BCL10, MALT1 and BIRC3 are involved in the most frequent chromosomal translocations leading to an activation of the NF- κ B signaling pathway (Zucca, Bertoni and

Rossi, 2018). General forms of MALT lymphoma should be treated with a combinatory chemotherapy e.g. R-CHOP. For splenic MZL rituximab alone is recommended and in selected cases or inefficiency of rituximab a splenectomy can be advised. The current standard treatment for nodal MZL follows the treatment recommendations of follicular lymphoma and is a combinatory chemotherapy (Zucca *et al.*, 2020).

Generally, follicular lymphoma (FL) is considered an indolent lymphoma and is the malignant counterpart of healthy germinal center B cells. About 85% of FLs contain a translocation of BCL2 placing it under control of the immunoglobulin heavy chain promoter on chromosome 14. This aberration on its own does not lead to FL, but further mutations are required to develop the disease (Freedman and Jacobsen, 2020). The higher the total number of genetic aberrations and genetic complexity, the lower the overall survival of patients. Especially deletions of TP53 and CREBBP hint to a shortened patient survival (Qu *et al.*, 2019). Moreover, the patients' survival also decreases with age. Noteworthy, the tumor microenvironment - consisting of T cells, macrophages, and dendritic cells - impacts FL progression in two dimensions. While cytokines like IL4 and IL21 support the tumor growth, factors such as enriched regulatory T cells benefit the anti-tumoral immune response (Sugimoto and Watanabe, 2016). The tight biological interplay of the environment and the lymphoma cells might also influence the transformation into an aggressive lymphoma. If FL is diagnosed at an early stage, the preferred initial treatment is radiation therapy, although most patients are diagnosed when the disease is at an advanced stage. Patients with a low tumor burden are simply observed, as median follow-up studies after 16 years did not show significant differences between initially treated and untreated patients. In case of a refractory or relapsed tumor, patients receive different options of chemotherapy. In selected patients a CAR T cell therapy is chosen as the third line therapy (Dada, 2019; Freedman and Jacobsen, 2020).

Mantle cell lymphoma (MCL) is a highly diverse lymphoma derived from naive B cells localized in the mantle zone, and to date remains incurable. Classic MCL tumor cells did not enter the germinal center, often express SOX11 and involve lymph nodes and extra nodal sites. Another type of MCL is the leukemic non-nodal variant, which develops from B cells passing the germinal center and thus bears IGHV-mutations and is SOX11⁻. Initially this variant is frequently indolent, but can transform into an aggressive disease, if secondary abnormalities such as TP53 mutations occur (Swerdlow *et al.*, 2016). A genetic hallmark of MCL is the

overexpression of CYCLIN D1 (CYCD1) due to the translocation t(11;14)(q13;q23) that juxtaposes *cycD1* to the immunoglobulin (Ig) gene promoter. In a small subset of MCL CYCD2 or CYCD3 is overexpressed instead of CYCD1 (Martín-García *et al.*, 2019). Nevertheless, CYCD overexpression on its own does not lead to a neoplasm and additional mutations are required as healthy humans also carry this translocation and single CYCD1 overexpression in transgenic mice rarely develop lymphoma (Smith *et al.*, 2006). To induce lymphoma in CYCD1 overexpression mice, these mice are combined with other transgenic mutations e.g. a BIM- or Ataxia-Telangiectasia mutated (ATM)-deficiency (Katz *et al.*, 2014; Yamamoto *et al.*, 2015). Frequently, these additional alterations happen to be in genes related to DNA repair, cell cycle control or cell survival pathways (Jares, Colomer and Campo, 2007). As diverse as the cancer itself are the treatment options. Depending on the patients age and relapse and refractory status, stem cell transplantation and/or a suitable chemotherapy are the best choice. Relapsed patients often get treated with second generation Bruton kinase (BTK) inhibitor agents as Acalabrutinib, mTOR inhibitors and in selected cases cellular therapies (e.g. CAR T cell therapy). Problematic are the high chemotherapy-associated toxicity, infection-associated mortality and therapy-related myelodysplasia and development of second cancers in the mainly elderly patients. To improve the patient's life quality, the treatment choices are more and more shifting towards chemotherapy-free options and cellular therapies, which are currently being tested (Jain and Wang, 2019; Ladha *et al.*, 2019; Witzig and Inwards, 2019). As this cancer remains incurable, a more in depth understanding of the disease biology is required to find the ideal therapy. Since further investigations are necessary to unravel new oncogenes, which can be targeted in cancer therapy, transposon-based cancer screens are a good tool to achieve this goal.

1.5. Transposable elements

Transposable elements (TEs) comprise up to two thirds of the human genome and are defined as repetitive mobile DNA elements. Given their sheer numbers and unknown function, they are often referred to as “the dark matter” of the human genome (de Koning *et al.*, 2011). Depending on their transposition mechanism, they are classified into DNA transposons - which are mobilized directly as DNA molecules to their target site - and retrotransposons, which jump through an RNA intermediate. Retrotransposons can be further subdivided into endogenous retroviruses or long terminal repeats (LTR), and non-LTR including the two most common TEs in human: long interspersed nuclear elements (LINE) and short interspersed

nuclear elements (SINE). While most retrotransposons - especially LTRs - lost their ability to jump, some non-LTRs retain their ability as mobile elements, but are usually inactive (Anwar, Wulaningsih and Lehmann, 2017). Interestingly, recent research observes a boost of TE transcription occurring during mammalian preimplantation development, which might be involved in regulating toti- and pluripotency (Rodriguez-Terrones and Torres-Padilla, 2018). Moreover, LINE-1 hypomethylations and reactivation often leads to genomic instability, transcriptional deregulation and oncogenic activation which in general promotes cancer (Anwar, Wulaningsih and Lehmann, 2017; Burns, 2017). Recently, a study detected hypomethylation of LINE-1 in gamma herpesvirus associated primary effusion lymphoma, a subset of DLBCL. The hypomethylation might be initiated by the viral infection and accumulate over time (Ahuja *et al.*, 2020), therefore slowly facilitating oncogenic alterations. Apart from their natural alterations in cancer, TEs provide a suitable transgenic tool to induce mutagenesis in model organisms to identify new oncogenic driver genes.

1.5.1. Transposable elements as a tool to discover new oncogenes

Generally, DNA transposons are still encoded in mammalian DNA, but all lost their transposable ability in all mammalian species except in bats (Jebb *et al.*, 2020). Engineered DNA transposons still contain the inverted terminal repeats (ITR) which provide the binding sites for the transposase. Naturally, the transposase is part of the transposon, though to increase flexibility and simplicity the transposase and the engineered transposon vector are frequently used in a trans-complementary system. For the function of the transposon system the design of the mutagenic cassette in the transposon is key and different approaches exist. To inactivate tumor suppressor genes one option is an oncogene trap containing splice acceptors (SA) and pA signals in both orientations to endogenously obstruct gene transcription. Furthermore, these cassettes often comprise a splice donor (SD) and a promoter/enhancer to induce transcription of oncogenes. The Sleeping Beauty (SB) system, a cut and paste DNA transposon originating from fish, was the first transposable system available for vertebrate models. Another transposon system frequently used in mice is the PiggyBac (PB) transposon derived from the cabbage looper moth. Besides a sufficient transpositional activity, the target site selection property is essential for a transposon to be suitable for model organism. While SB shows a close to random integration profile with a slight preference to integrate in e.g. protein-induced deformed DNA structures, PB favors open chromatin and targets the sequence TTAA (Kawakami, Largaespada and Ivics, 2017). An

advantage of the PB transposon is the seamless excision leaving no footprints or damages at previous integration sites (Chen *et al.*, 2020), thus mutations are only induced at the present insertion site.

1.5.2. The PB mouse model

The PiggyBac (PB) transposon mouse model designed by Roland Rad has already been used in several transposon screens to unravel new oncogenic driver genes (Rad *et al.*, 2010, 2015). The PB mouse model consists of a CRE inducible *PB transposase* inserted in the *rosa26* locus and bifunctional activating and inactivating *atp2* transposons integrated in the donor locus at chromosome 2.

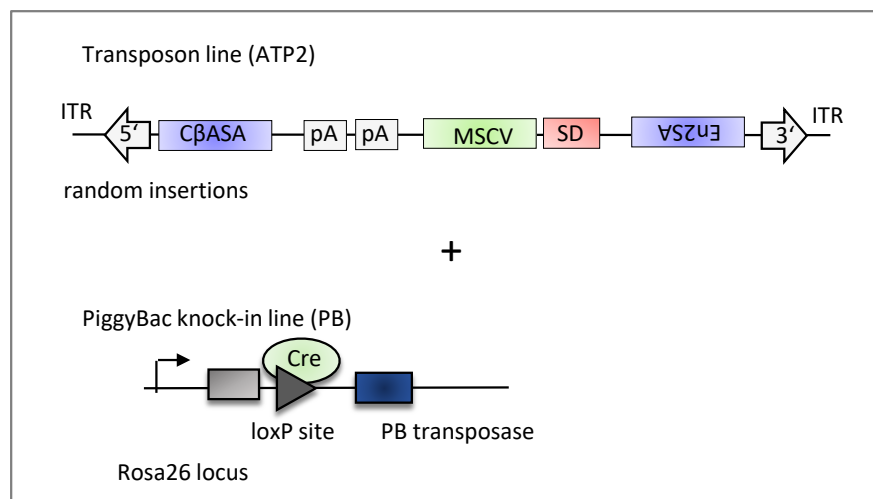


Figure 4 Scheme of the PB transposon mouse model. The ATP2 cassette is depicted in the upper part. It contains two splice acceptors (CβASA, En2SA), polyA sites (PA), the promoter MSCV and a splice donor (SD). PiggyBac transposase is inserted into the *rosa26* locus and under control of the CRE-recombinase.

The ATP2 transposon was chosen due to its murine stem cell virus (MSCV) promoter, which had proven to initiate lymphoma and leukemia. In order to receive gain of function mutations a transposon must jump in sense orientation upstream of a start codon and to create a loss of function mutation the pattern is more randomly spread out and in sense as well as anti-sense orientation (Rad *et al.*, 2010). To induce the mobilization of the transposons only in B cells, the PB system is combined with CD19-Cre mice. Since CD19 is a co-receptor of the BCR and only expressed in B cell, the CRE-recombinase is heterogeneously inserted into the CD19 gene locus to create a B cell specific model. Thus, the stop cassette upstream of the transposase is specifically exercised in B cells and transposons induced mutagenesis appears only in B cells.

2. Aims of thesis

Any B cell lymphoma, whose cell of origin is a mature B cell and has not entered a germinal center can be described as pre-germinal center lymphoma. Thus, most cases of MCL, and partially B-CLL, MZL and some cases of DLBCL fit into this category. The general goal of this scientific work was to investigate which genetic drivers initiate this disease and to develop models to simplify future basic research on pre-germinal center B cell lymphoma.

2.1. Influence of non-canonical NF- κ B pathway on lymphoma development in LC40 mice

As described before (1.3.3), LMP1/CD40 (LC40) mice develop lymphoma and lack germinal centers, thus are a good model to study the development of pre-germinal center B cell lymphoma. Inactivation of RELB in LC40 mice showed that activated non-canonical NF- κ B signaling contributes to the B cell expansion in young LC40 mice. Therefore, it was of high interest to investigate the influence of the non-canonical NF- κ B pathway to development of pre-GC B cell lymphomas. My aim was to compare the lymphoma incidences of RelBKO//LC40 and LC40 mice. Moreover, differential gene and protein expression in B cells from these two mouse models should be studied. Furthermore, the hypothesis whether these lymphomas derive from CD23⁻/CD21⁻ B cells should be tested, by transplanting different pre-malignant B cell populations into immunodeficient mice.

2.2. CycD1//LC40 mice as potential model to study MCL development

One major obstacle to develop better medical therapies for MCL is the lack of satisfactory animal models for pre-clinical trials. The initial hallmark mutation of MCL is overexpression of CYCLIN D1 (CYCD1). At advanced stages, MCL transforms to more aggressive forms by acquisition of additional mutations and stimulation through the lymphoma microenvironment. One of these factors is provided by CD40 stimulation, which induces more aggressive and chemo resistant MCL (Rauert-Wunderlich *et al.*, 2018a). To mimic this MCL variant in mice, cycD1 mice were combined with LC40 mice (cycD1//LC40). It should be answered whether CYCD1 accelerates lymphoma development and whether it has an impact on the immunophenotype. In short, can cycD1//LC40 serve as a suitable mouse model for advanced MCL?

2.3. PiggyBac transposon screen to identify new drivers in B cell lymphoma

To identify new driver genes in the lymphoma development of cycD1 mice and LC40 mice, the two mouse strains should be crossed to PiggyBac transposon mice (PB). Tumors of both and control/PB cohorts should be collected and initial studies should be performed to determine which genes are involved in tumor evolution.

3. Results

3.1. Contribution of non-canonical NF- κ B signaling on CD40-induced B cell lymphoma development

Constitutive CD40 activation in B cells induced by the fusion protein LMP1/CD40 results in activation of the non-canonical NF- κ B pathway. LMP1/CD40//CD19-Cre (LC40) mice expressing LMP1/CD40 in B cells are characterized by an increased splenic weight induced by expanded B cells. Additionally, these B cells have an activated phenotype, preferentially reside in B cell follicles and are impaired in their germinal center reaction. To analyze the contribution of the non-canonical NF- κ B signaling to this phenotype RELB was inactivated in LMP1/CD40-expressing B cells. In RELB-deficient LC40 (RelBKO//LC40) mice, the splenic weight and B cells numbers remain elevated compared to controls but are slightly decreased compared to LC40 mice. B cells of RelBKO//LC40 mice were less activated and displayed an increased mobility compared to those of LC40 mice (Stojanovic, 2013; Zapf, 2017).

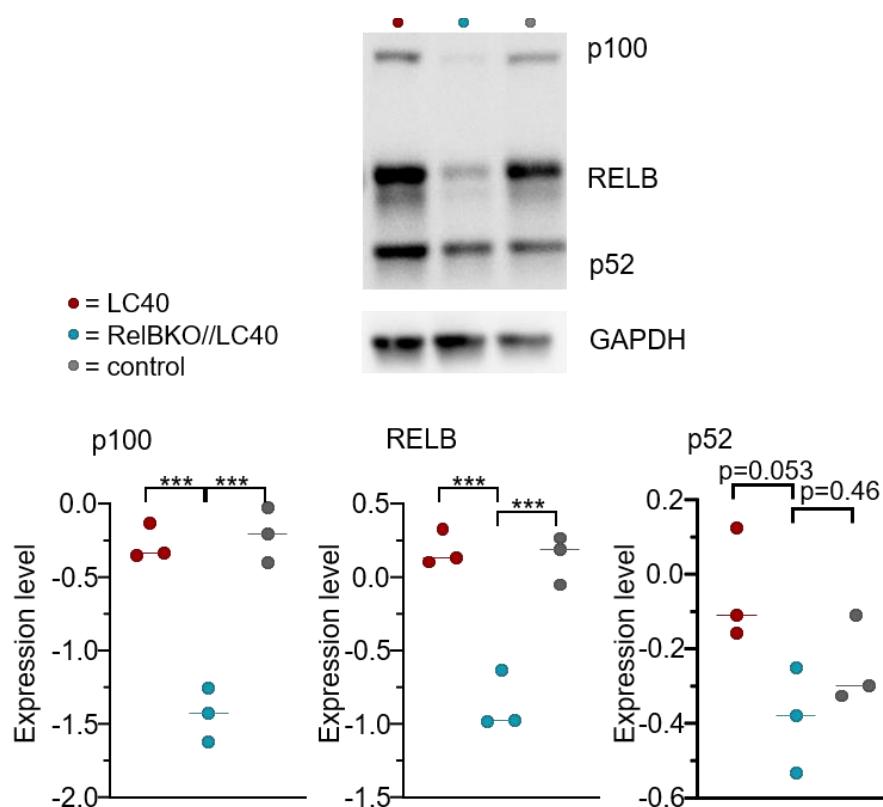


Figure 5 Determination of the expression of the non-canonical NF- κ B pathway components: A representative Western Blot with whole protein extracts from splenic B cells of LC40, RelBKO//LC40 and control mice after staining with an anti-RELB and anti-p100 antibody is shown. The graphs summarize the expression level of p52, RELB and p100 of three individuals per genotype. GAPDH was used as reference gene for normalization. Since values were lognormally distributed, they were transformed, and a one-way ANOVA with a Tukey's multiple comparison test was performed to test the statistical significance. The p values are indicated as *** ≤ 0.001 .

To ensure that *relB* was efficiently knocked out in the RelBKO//LC40 mice, the protein levels were measured by analyzing whole cell lysates of purified ex vivo B cells in Western Blot. It is shown that minor traces of RelB protein could be detected in the sample of RelBKO//LC40 mice but RELB levels were significantly decreased compared to B cells of LC40 and control mice (Figure 5). Since MACS-based B cell purification reached an average purification rate of ~95%, these traces of RELB protein were most likely due to some contamination of non-B cells. Moreover, the p100 protein levels were significantly decreased in B cells derived from RelBKO//LC40 mice compared to those from LC40 or control mice. This aligns with previous studies that functional RELB enhances the stability of p100 and absent or mutated RELB declines p100 protein levels (Maier *et al.*, 2003). Interestingly, the p52 protein levels of B cells from RelBKO//LC40 mice also tended to be diminished compared to the protein levels of B cells from LC40 mice. Thus, inactivation of RELB in LC40 mice efficiently decreases the activation of the non-canonical NF- κ B signaling pathway and is suitable to study which role this pathway plays in the development of B cell lymphoma caused by a chronic CD40-activation.

3.1.1. Impact of the non-canonical NF- κ B signaling on B cells of young LC40 mice

As previously shown by Kristina Stojanovic, RELB-deficient LC40 B cells are less activated than RELB-proficient LC40 B cells. She showed that, the surface proteins ICAM, ICOS-L and CD95 tend to be higher expressed on LC40 derived B cells than on RelBKO//LC40 derived ones. To further analyze the B cell activation in LC40 and RelBKO//LC40 mice, the surface expression of CD95, ICAM, ICOS-L and CD80, which are all known to be activated by NF- κ B signaling, were detected by FACS analysis of ex vivo B cells (Figure 6). CD95 signaling leads in combination with CD40 signaling to cell activation and proliferation (Benson, Hostager and Bishop, 2006). The RelBKO significantly diminishes the CD95 surface expression, but CD95 expression was still increased compared to control B cells. ICAM, an adhesion molecule involved in cell migration (Rothlein *et al.*, 1986) and supporting T/B cell interaction (Sanders and Vitetta, 1991), and CD80, a known T cell co-stimulator (Lanier *et al.*, 1995), were not significantly reduced after inactivation of RELB in LC40 B cells. Noteworthy, the surface expression of ICOS-L, a receptor ligand important for migration and survival of maturing germinal center B cells (Pratama *et al.*, 2015), was significantly lower expressed on B cells from RelBKO//LC40 mice compared to B cells from LC40 or control mice. This aligns with the strict dependency of an

ICOS-L upregulation on the non-canonical NF- κ B signaling pathway (Hu *et al.*, 2011). Therefore, the surface protein CD95 and ICOS-L are RELB-dependently upregulated in constitutively CD40-activated B cells, while the upregulation of ICAM and CD80 additionally relies on further signaling pathways such as canonical NF- κ B signaling.

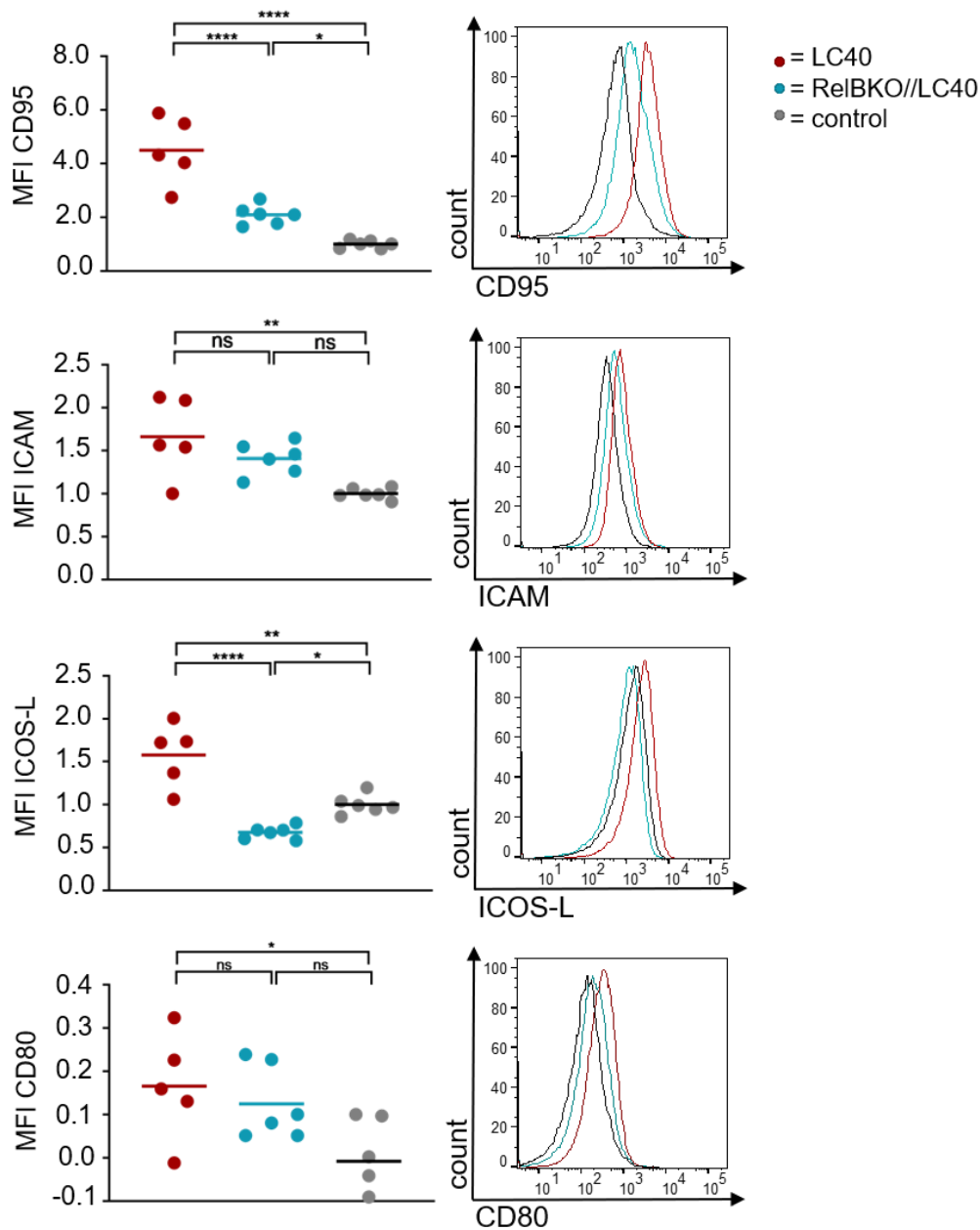


Figure 6 The RELB-dependent upregulation of activation markers on B cells was measured by FACS. Lymphocytes were pregated on CD19⁺ B cells and median fluorescence intensity (MFI) was determined of CD95, ICAM, ICOS-L and CD80. In each graph one dot represents the value of one individual mouse and for each activation marker one representative histogram overlay is shown next to the according graph. The average of all controls was used to normalize each sample. If all three genotypes had a log normal distribution instead of a linear distribution, values were transformed. This was only the case for CD80. Since all groups passed the Shapiro-Wilk test, a one-way ANOVA with a Tukey's multiple comparison test was performed to test the statistical significance. The p values are indicated as ns > 0.05, * ≤ 0.05, ** ≤ 0.01, **** ≤ 0.0001.

3.1.1.1. Identifying new RELB-dependent targets in constitutive CD40-activated B cells

Inactivation of the non-canonical NF- κ B pathway altered the phenotype of LC40 mice. To elucidate which genes are affected by the inactivation of RELB and therefore might cause the phenotypical changes, an RNA Seq experiment was performed before I started working on this project. Bioinformatical analysis revealed approx. 200 differentially expressed genes in B cells from LC40 mice compared to B cells from RelBKO//LC40 mice. In Figure 7, the top differentially genes are depicted in a heatmap. Generally, more genes were upregulated in B cells derived from LC40 mice compared to those from RelBKO//LC40 mice. This aligns with the generally lower activation status of B cells derived from RelBKO//LC40 mice in comparison to B cells obtained from LC40 mice.

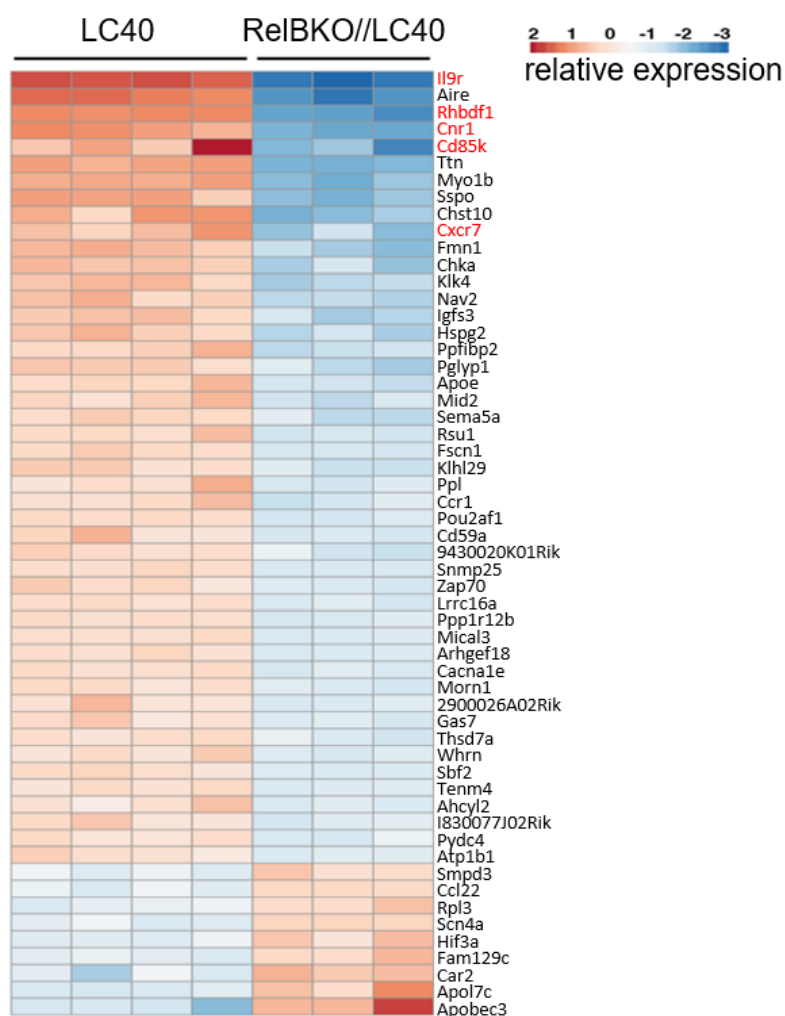


Figure 7 The top differentially expressed genes between LC40 (n=4) and RelBKO//LC40 (n=3) analyzed in splenic B cells. The RNA sequencing was performed at the Laboratory of Functional Genome Analysis (LAFUGA, Gene Center Munich) and bioinformatical analysis was performed by Daniel and Lothar Strobl. The genes indicated in red were further quantified.

Regarding the preliminary data that the RelBKO in LC40 mice facilitates B cell migration and reduces the age-related B cell expansion (Stojanovic, 2013; Zapf, 2017), the focus was set to genes involved in B cell migration, proliferation and lymphomagenesis. To validate five interesting candidates, qPCR experiments were executed (Figure 8).

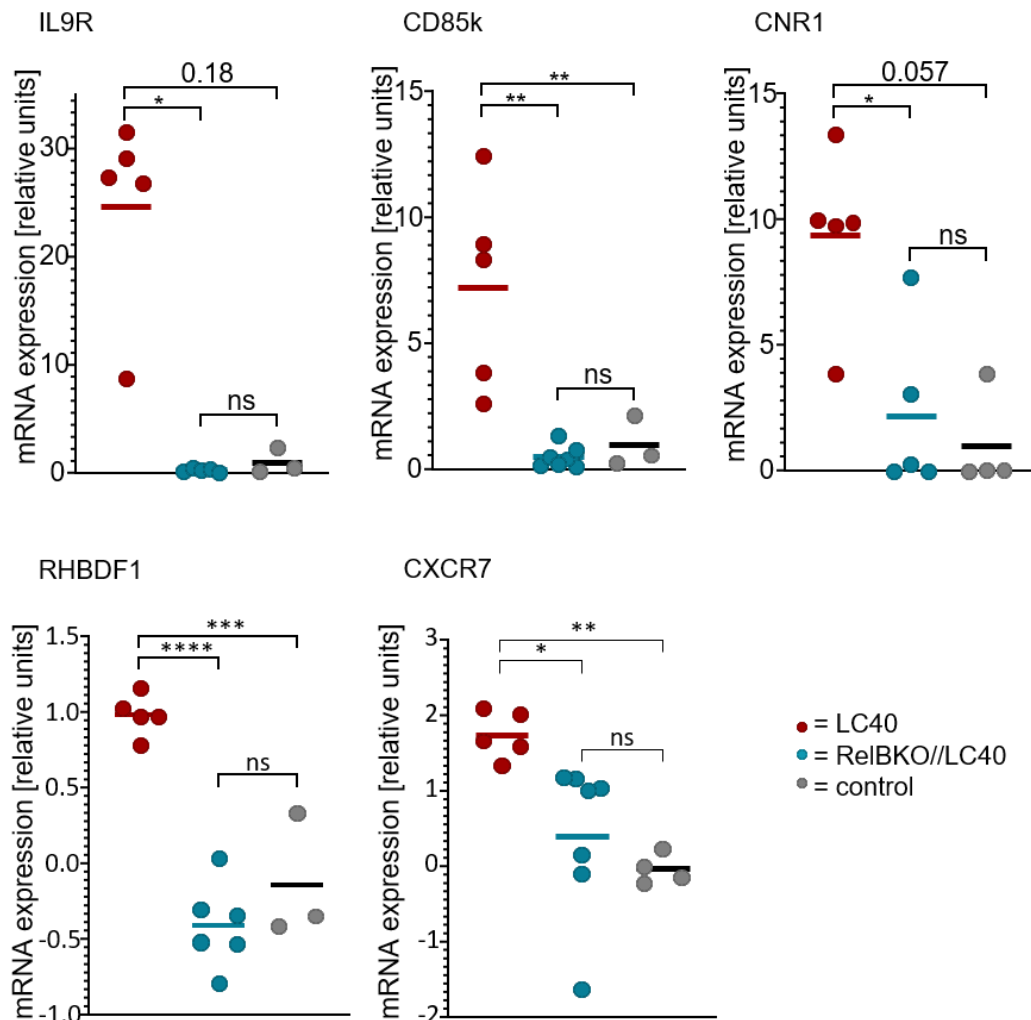


Figure 8 The validation of differentially expressed genes between the genotypes LC40 (red), RelBKO/LC40 (turquoise) and control (gray) was done by qPCR. RNA was extracted from CD43-depleted, MACS purified B cells. For statistical significance an ANOVA test was performed. If all three genotypes had a log normal distribution instead of a linear distribution, values were transformed. This was only the case for RHBDF1 and CXCR7. Since CD85k, RHBDF1 and CXCR7 passed the Shapiro-Wilk test, a one-way ANOVA with a Tukey's multiple comparison test was performed to test the statistical significance. For CNR1 and IL9R a non-parametric Kruskal-Wallis test was performed. In case the p value is not indicated as number, it is indicated as ns > 0.05, * ≤ 0.05, ** ≤ 0.01, *** ≤ 0.001, **** ≤ 0.0001.

Amongst these targets was CXCR7 which is a surface receptor involved in B cell migration (Humpert *et al.*, 2014). IL9 receptor (IL9R) is important in the recall response of memory B cell and induces proliferation (Takatsuka *et al.*, 2018). The leucocyte immunoglobulin-like receptor CD85k (or LiLRB4), an inhibitory receptor mostly expressed on dendritic cells,

monocytes and macrophages (Cella *et al.*, 1997). Additionally, it is ectopically expressed on neoplastic B cells (A. I. Colovai *et al.*, 2007). Further, the 7-transmembrane domain protein rhomboid 5 homolog 1 (RHBD1) activates the epidermal growth factor receptor and thereby induces proliferation and cell survival of cancer cells (Zou *et al.*, 2009). Moreover, the cannabinoid receptor 1 (CNR1) contributes to T cell dependent IgM production in B cells (Kaplan, 2013) and is upregulated in MCL (Gustafson, 2008). In general, the data of the qPCR and RNA Seq were congruent, and all analyzed targets had a higher mRNA expression in B cells of LC40 mice than in RelBKO//LC40 mice. Further, the qPCR revealed that the RelBKO reduced the mRNA expression back to control level, indicating that these genes are upregulated by chronic non-canonical NF- κ B signaling. Since the focus of this thesis was to determine the involvement of the non-canonical NF- κ B signaling on lymphomagenesis, the IL9R was selected for further investigations due to its proliferative capabilities. Additionally, CD85k was chosen because it is detectable on B cells derived from CLL patients but not on B cells of control groups (A. I. Colovai *et al.*, 2007).

3.1.1.2. CD40-induced upregulation of CD85k is dependent on RELB

To verify that the RELB-dependent upregulation of *CD85k* was not only at RNA level, but also at protein level, FACS analysis was performed to detect surface expression levels of this receptor. As expected, B cells of young LC40 mice had a significantly higher surface expression of CD85k than RelBKO//LC40 or control mice. The expression level of CD85k on B cells from RelBKO//LC40 mice was even back to control level (Figure 9A). In further *in vitro* experiments - using B cells of control and RelBKO mice - it was discovered that CD85k was not only upregulated by the LMP1/CD40 transgene but was even upregulated after *in vitro* anti-CD40 stimulation. In this experimental set up, the CD85k upregulation was significantly higher on control B cells than on RELB-deficient B cells, but CD85k was also slightly upregulated on CD40-stimulated RELB-deficient B cells (Figure 9B). Thus, this data demonstrates that CD85k is a suitable marker to detect activation of the non-canonical NF- κ B pathway, although a minor expression of CD85k might also be partially mediated by RELB-independent signaling pathways.

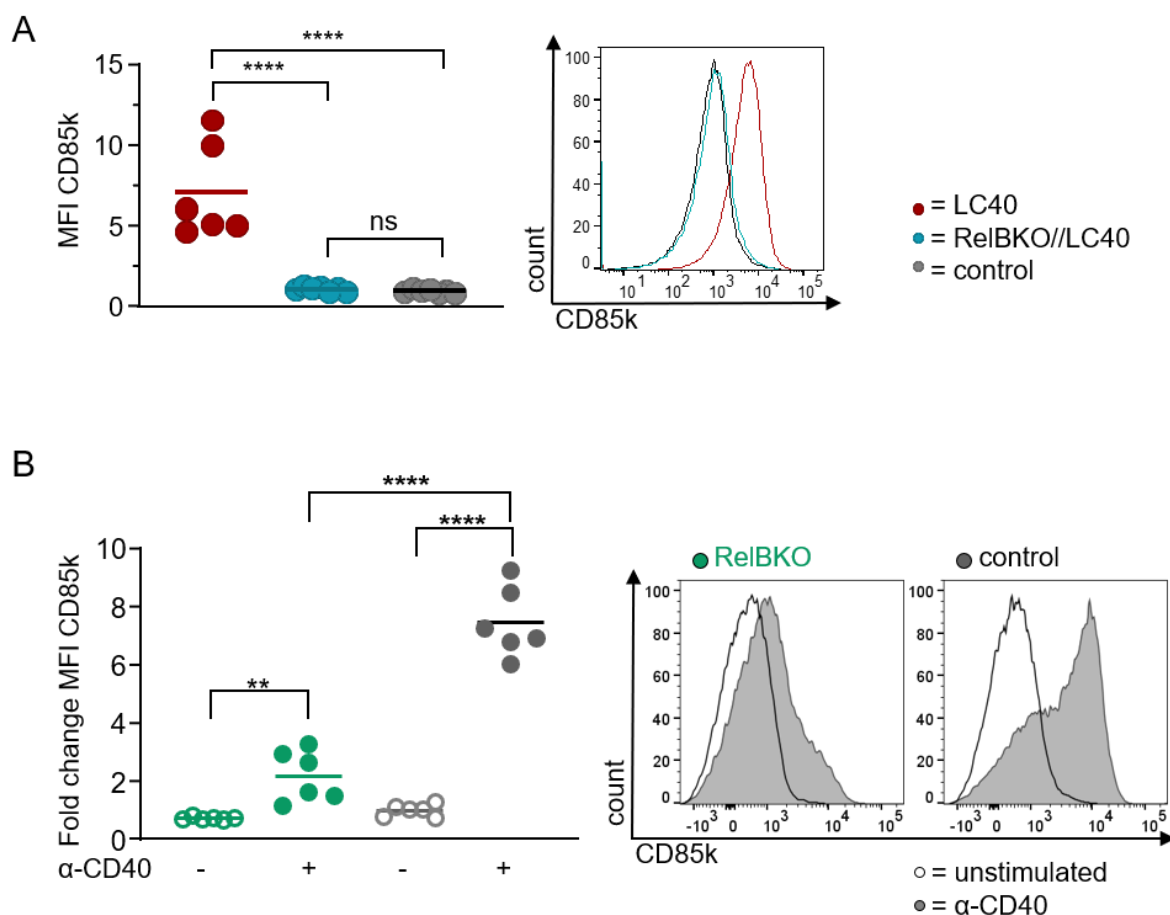


Figure 9 The CD85k expression level of B cells was determined by FACS. Lymphocytes were pregated on CD19⁺ B cells and to calculate the CD85k expression level the MFI was calculated. A prototypical histogram overlay of genotypes is shown on the right and the graph on the left side gives the summary of MFIs from all individuals. In panel A the genotypes LC40, RelBKO//LC40 and the control were tested. For normalization each value was divided by the control average. A one-way ANOVA with a Tukey's multiple comparison test was performed to test the statistical significance. In panel B MACS-isolated B cells from control and RelBKO mice were cultured with and without anti-CD40 stimulation for two days. For normalization the individual values were divided by the average the unstimulated control. A two-way ANOVA with a Tukey's multiple comparison test was chosen for statistical comparison. The *p* values are indicated as ns > 0.05, ** \leq 0.01, **** \leq 0.0001.

3.1.1.3. CD40-induced IL9R upregulation is dependent on RELB and induces *in vitro* cell proliferation upon IL-9 stimulation

IL9R was another target, which was upregulated on LC40 expressing B cells in a RELB-dependent manner. Our aim was to investigate, if the upregulation at mRNA level was also observable at protein level. In Figure 10 is shown that IL9R was higher expressed on the surface of B cells originating from LC40 mice compared to RelBKO//LC40 or control mice. Further experiments revealed that IL9R was also induced after CD40 stimulation of control B cells *in vitro*, but is strictly dependent on the presence of RELB, since IL9R surface expression could not be induced in B cells derived from RelBKO mice (Figure 10B).

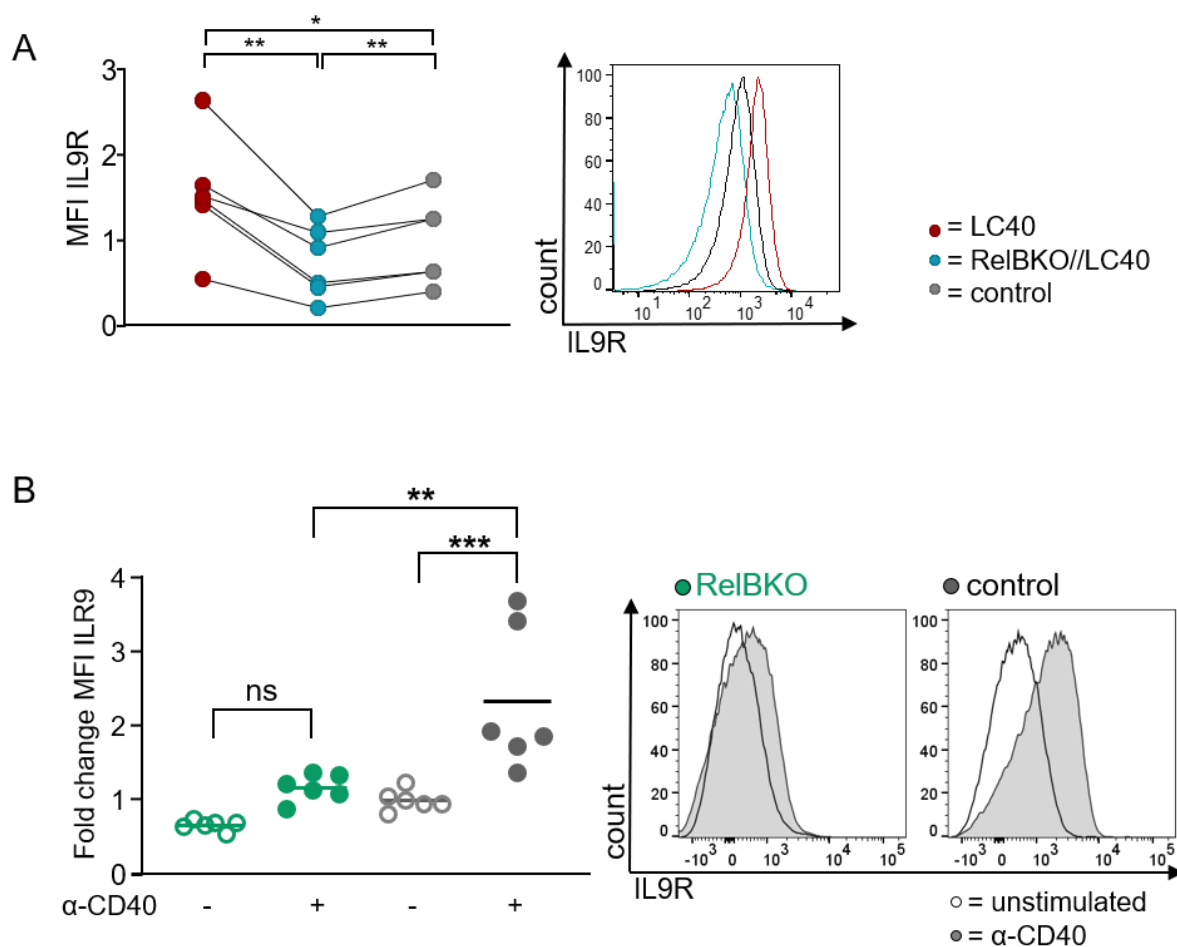


Figure 10 The IL9R expression level of B cells was determined by FACS. Lymphocytes were pregated on CD19⁺ B cells and the IL9R protein level was determined by calculating the MFI of each individual. A prototypical histogram overlay of the analysed genotype is shown on the right and the graph on the left side gives the summary of the individual MFIs. In panel A the genotypes LC40 (red), RelBKO//LC40 (turquoise) and the control (gray) was tested. In A four independent experiments were performed, though in two sets two LC40 and RelBKO//LC40 were analysed with one control. For normalization the individual values of each individual mouse were divided by the average the controls. Due to technical settings, each genotype has a high variance, but the genotypes always behave the same in correlation to each other. Values measured in the same experiment are connected with a line. For statistical comparison a repeated-measures one-way ANOVA (Tukey) was chosen. In panel B control (gray) and RelBKO (green) derived MACS-isolated B cells were cultured with and without anti-CD40 stimulation for two days. For normalization the individual values of each individual value were divided by the average the unstimulated controls. For statistical analysis a two-way ANOVA (Tuskey) was performed. The *p* values are indicated as ns > 0.05, * ≤ 0.05, ** ≤ 0.01, *** ≤ 0.001.

Previous studies already showed that IL9 stimulation enhances proliferation of lymphoma cell lines expressing IL9R (Lv *et al.*, 2016). Thus, considering the RELB-dependence of IL9R expression and the data provided by literature it is tempting to postulate that the difference in B cell expansion between RELB-proficient and -deficient LC40 mice (Stojanovic, 2013; Zapf, 2017) is partially due to their differential surface expression of IL9R. To provide further evidence of this theory, *in vitro* cell proliferation assays were performed by tracking the cell division rate with a CFSE assay after IL-9 and/or IL-4 stimulation. After each cell division, the

CFSE stain is equally divided between mother and daughter cells leading to a two-fold loss of brightness in both. Thus, the less intense the CFSE brightness is, the more cell divisions were done by the cells.

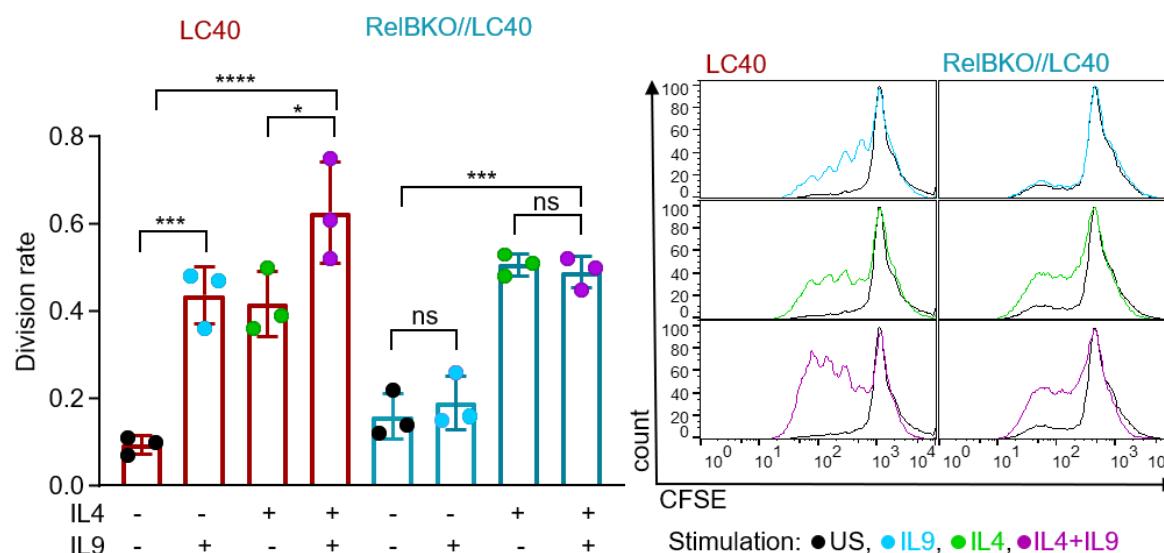


Figure 11 The proliferation of splenic B cells isolated from LC40 (red) and RelBKO/LC40 (turquoise) was measured with a CFSE assay after IL-9 and IL-4 stimulation. B cells were MACS-isolated and cultured with or without stimulation for three days. The FACS plots were pre-gated on living cells and the division rate was calculated with the proliferation assay of FlowJo. To visualize the CFSE dilution upon cell proliferation, a representative histogram of each condition is shown in an overlay with its according unstimulated control. The graphs summarize the experiments of three independent experiments. A two-way ANOVA with a Tukey's multiple comparison test was chosen for statistical comparison. The p values are indicated as ns > 0.05, * ≤ 0.05, *** ≤ 0.001, **** ≤ 0.0001.

In Figure 11 splenic B cells of LC40 and RelBKO//LC40 mice received an IL4, IL9, combined IL4/IL9 or no *in vitro* stimulation. The histograms on the right and the summarizing graph on the left show that only B cells with functional RELB underwent more divisions after IL9 stimulation. Since RELB-deficient B cells proliferated after IL4 stimulation, a general proliferation defect can be negated. Therefore, adding IL9 either on its own or in combination with IL4 enhanced only the division rate, if RELB was functional. Thus, it can be concluded, that only B cells of LC40 mice, but not B cells of RelBKO//LC40 mice are sensitive to an IL9 stimulation. Moreover, similar results were observed *in vitro* experiments using control or RelBKO B cells after providing a CD40 stimulation. Figure 12 depicts that only RELB-proficient cells increased their division rate after IL9 stimulation. A general division defect of RelBKO B cells is not possible since cells respond in proliferation after IL4 stimulation. The simultaneous *in vitro* stimulation of IL9 and IL4 stimulation barely enhances the proliferative response after IL4 stimulation. For the RelBKO genotype this was expected, since IL9 on its own could not

increase proliferation. This strengthens the hypothesis that B cells require functional RELB to induce an IL9 mediated proliferation.

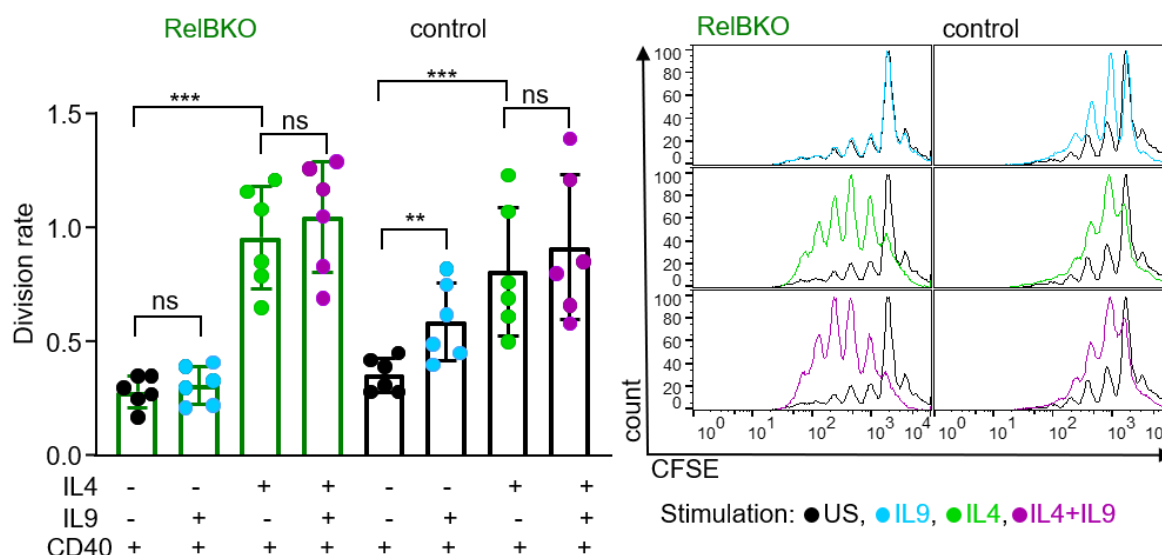


Figure 12 The division rate of control (gray) and RelBKO (green) derived B cells was measured after IL-9 and IL-4 stimulation with a CFSE assay. B cells were MACS-isolated and cultured with or without the indicated stimulations for three days. As basic stimulus all B cells were treated with an agonistic anti-CD40 antibody. The FACS plots were pre-gated on living cells and the division rate was calculated with the proliferation assay of FlowJo. To visualize the cell proliferation, a representative histogram of each condition is shown in an overlay with its according control. The graph summarizes the experiments and each dot represents values of one individual. A two-way ANOVA with a Tukey's multiple comparison test was chosen for statistical comparison. The *p* values are indicated as ns > 0.05, ** ≤ 0.01, *** ≤ 0.001.

3.1.1.4. T helper cells act as a potential IL9 source

In literature, one of the most discussed sources for IL9 are CD4⁺ Th cells (Goswami and Kaplan, 2011). To elucidate whether some Th cells were also producing IL9 in LC40 or RelBKO//LC40 mice, *ex vivo* isolated splenic CD4⁺ cells of LC40, RelBKO//LC40 and control mice were stimulated with PMA and ionomycin in combination with a protease inhibitor cocktail to block cytokine secretion. Intracellular (IC)-FACS analysis revealed, that the IL9 positive fraction of CD4⁺ cells in LC40 mice is significantly increased compared to those in RelBKO//LC40 and control mice (Figure 13). Considering the significant increase in LC40 mice, a positive feedback loop between IL9R positive B cells and CD4⁺ IL9-producing cells might be possible.

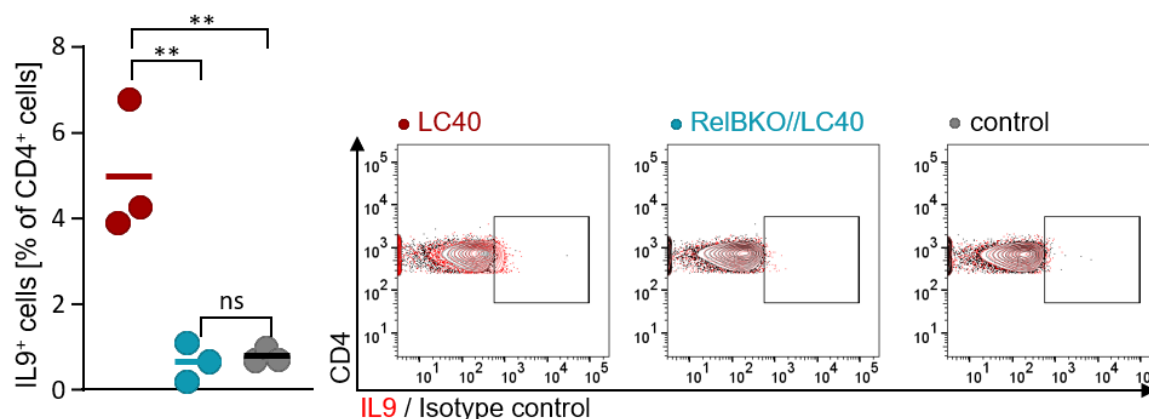


Figure 13 The IL9 expression of ex vivo short-term stimulated T-helper cells was detected by IC-FACS. For each genotype three mice were used to determine the percentage of IL9 expressing CD4+ cells. The panel on the right shows for each genotype one prototypical overlay of IL9 secreting CD4+ cells (red) and the isotype control (black). Since the Shapiro-Wilk test was passed positively, a one-way ANOVA with a Tukey's multiple comparison test was performed to test the statistical significance. The p values are indicated as $ns > 0.05$, $** \leq 0.01$.

3.1.2. IL9R and CD85k upregulation in human primary B cells after CD40 stimulation

Since the IL9R and CD85k upregulation after CD40 stimulation was observed in murine B cells, it was interesting to see whether CD40 stimulation also increases IL9R expression in human B cells. In this regard, human primary B cells were obtained from adenoids and co-cultured with CD40L or CD32 control feeder layer cells for two days. The feeder layer cells are a murine fibroblast cell line either expressing human CD40L or human CD32, which is a receptor for the Fc portion of immunoglobulins (De Andres *et al.*, 1999). The CD32 feeder layer cells only provide the basic stimulation induced by the feeder layer cells but no CD40 activation. Thus, these can be used to observe if the feeder layer induces unspecific activation which is not mediated by CD40 signaling. To analyze whether the CD40 stimulation induces activation of the non-canonical NF- κ B pathway in human B cells, I measured the amounts of nuclear p52 and RELB protein by WES simple protein analysis (Figure 14). As anticipated, both RELB and p52 were increased in the nuclear fraction of CD40-stimulated B cells in comparison to unstimulated ones. This indicates that the non-canonical NF- κ B signaling was induced by the CD40 stimulation. Additionally, primary human B cells receiving a CD40 signal upregulated both IL9R and CD85k on their cell surface (Figure 15).

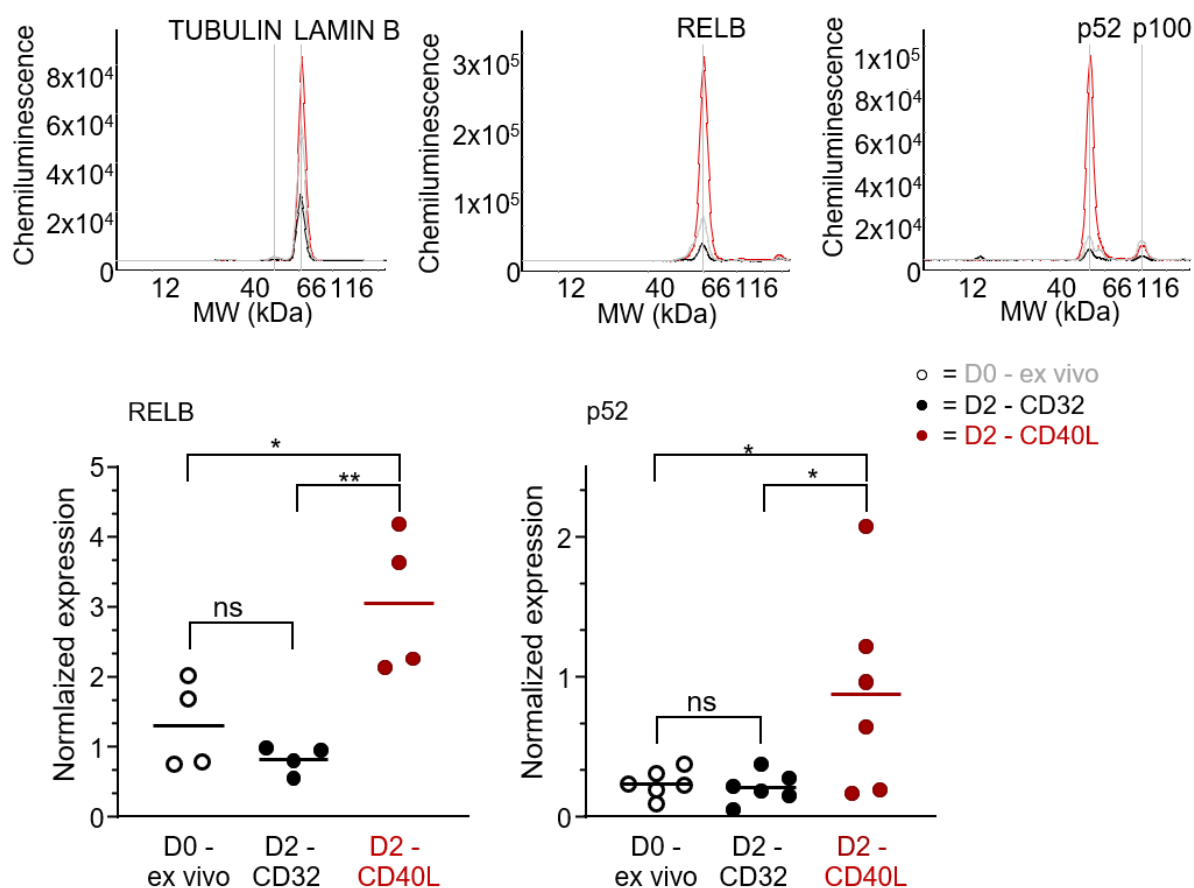


Figure 14 The protein levels of RELB and p52 in primary human B cells after CD40 stimulation were detected by WES simple protein. Human B cells were isolated from adenoids. To induce a CD40 stimulation B cells were cultured on CD40L feeder layer cells for two days. In parallel, B cells were cultivated on control CD32 feeder layer cells for two days (D2) and as a second control protein was also purified from ex vivo (D0) B cells. Only the nuclear fraction of the protein lysates was used. The detected chemiluminescence is shown for one representative set and in the graphs each dot represents one donor. Since the Shapiro-Wilk test was passed positively, a one-way ANOVA with a Tukey's multiple comparison test was performed to test the statistical significance. The *p* values are indicated as ns > 0.05, * ≤ 0.05, ** ≤ 0.01.

In general, this experiment demonstrated that human cells express IL9R and CD85k after CD40 stimulation as seen in murine B cells. Therefore, it seems likely that the observed RELB-dependency of IL9R and CD85k in mice is transferable to humans.

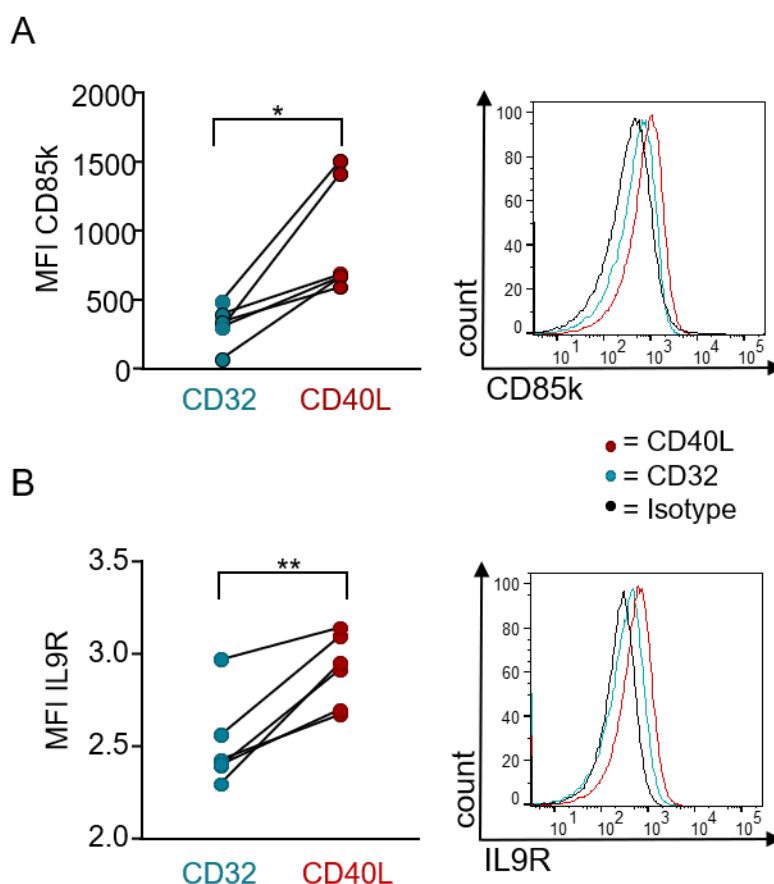


Figure 15 The surface expression of IL9R (A) and CD85k (B) on primary human B cell after CD40 stimulation was measured by FACS and the MFI was determined by FlowJo. CD40L feeder layer cells (red) were used for stimulation and CD32L feeder layer cells (turquoise) were used as control. In the graphs, the unstimulated and stimulated samples the same donor are connected by a line. For IL9R both conditions showed a lognormal distribution, thus values were transformed, and a paired *t* test was performed. For CD85k a Wilcoxon matched pairs signed rank test was performed, as not both conditions were normally distributed. The *p* values are indicated as * ≤ 0.05 and ** ≤ 0.01 .

In conclusion, this work identified genes, which are upregulated on B cells after CD40 stimulation in a RELB-dependent manner. Among these genes were CD85k and IL9R. The IL9R is of special interest, since it might be the reason why B cells derived from LC40 mice respond in proliferation after IL9 stimulation, while B cells of RelBKO//LC40 mice do not. This may give a possible explanation to why LC40 mice have an increased B cell expansion compared to RelBKO//LC40. Furthermore, the elevated B cell expansion of LC40 mice might already increase the risk to develop B cell lymphoma.

3.1.3. Lymphoma incidence is significantly reduced by RelBKO in LC40 mice

As previously described aging LC40 mice develop an aberrant B cell population, which is the potential pre-malignant population to grow into a tumor. The immunophenotype of this pre-

malignant population is CD23⁻, CD21⁻, B220^{low}, CD43⁺, very often IgM^{high} and sometimes CD5⁺ (Hömig-Hölzel et al., 2008). My colleague Stefanie Zapf showed that this aberrant population occurs with a more advanced age in RelBKO//LC40 mice and is less expanded. To show the outgrowth of the aberrant B cell population in old mice a representative example of each genotype is shown in Figure 16.

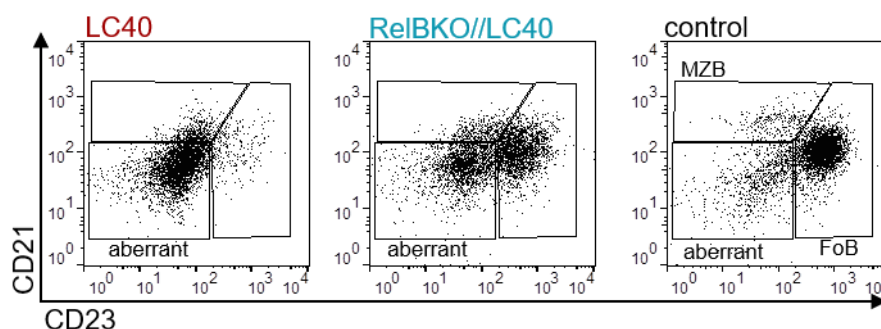


Figure 16 These FACS dot plots show a representative set of the CD21/CD23 immunophenotype of the old LC40 (red), RelBKO//LC40 (turquoise) and control (gray) mice. The mice had an approximate age of one year. Dot plots are pregated on lymphocytes and CD19⁺ B cells.

The dot plot of the control demonstrates that MZB (CD21⁺/CD23⁻) and FoB (CD21⁻/CD23⁺) cells can still be clearly separated in old control mice, while in LC40 mice this was not the case and only the aberrant B cell population remains. In RelBKO//LC40 mice, an aberrant and a healthy normal B cell population were detectable, though MZB cells already started to downregulate CD21. The delayed outgrowth of pre-malignant B cells already gives the first hint that the tumor burden of RelBKO//LC40 mice is diminished compared to LC40 mice. Indeed, Southern Blot analysis revealed that RelBKO//LC40 mice had less clonal B cell expansions. By combining Stefanie Zapf's and my data, we showed that LC40 mice with a BALB/c background reach a 100% lymphoma rate at the age of ~500 days (Figure 17).

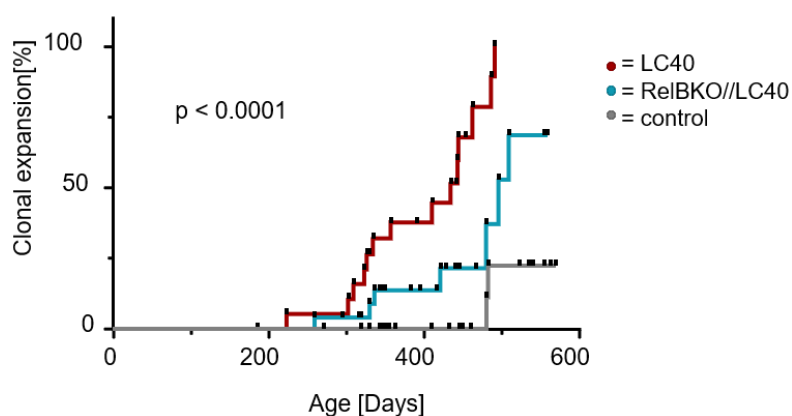


Figure 17 To determine the clonal B cell expansions in RelBKO//LC40 (turquoise) mice in comparison to control (gray) and LC40 (red) mice, the monoclonal and oligoclonal B cell expansions were detected by Southern Blot analysis. This Graph depicts the combined analysis performed by Stefanie Zapf and me. Black dots indicate the individual mice sacrificed at that specific time point. For statistical comparison a log-rank (Mantle Cox) test was performed. A table including all individuals is provided in the supplement.

At the same age and same background, RelBKO//LC40 mice had a tumor incidence rate of 75% and control mice 25%. Hence, the non-canonical NF- κ B pathway was accelerating the tumor development and risk about 25%.

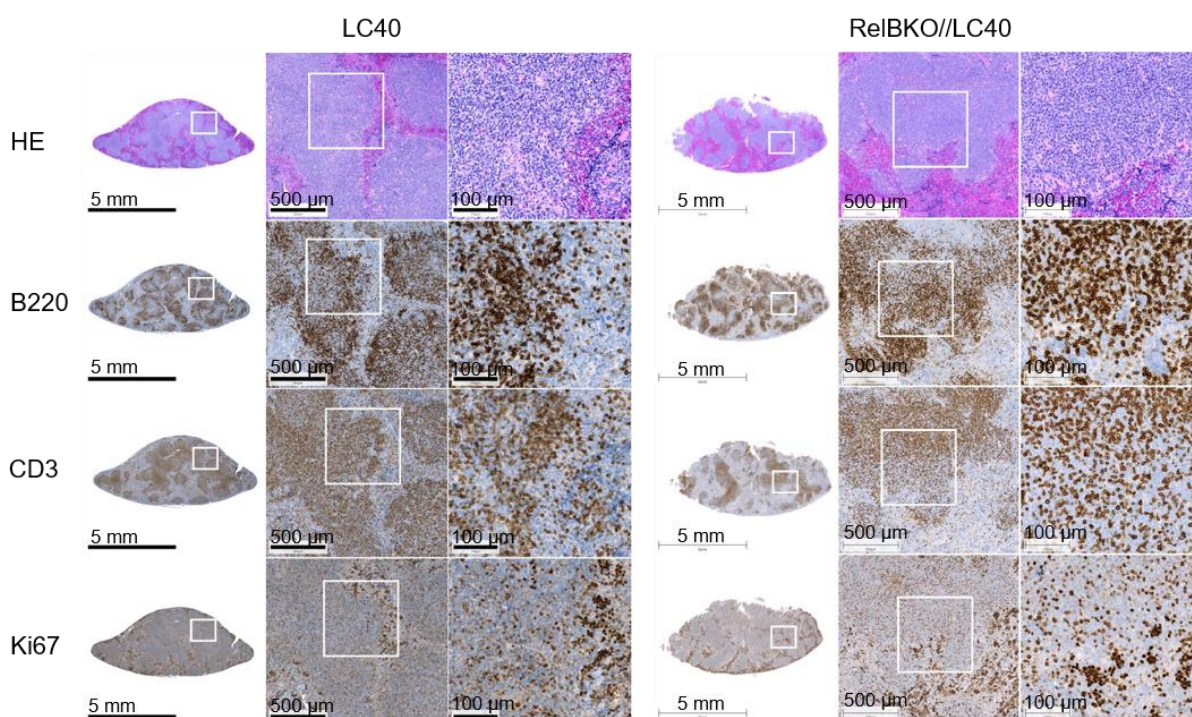


Figure 18 Immunohistochemistry was performed with tumorous spleen tissue of the LC40 and the RelBKO//LC40 genotypes. Histologies were performed by the Helmholtz core facility for analytical pathology (AAP). The HE staining gives an impression of the general follicle structure and further stainings show the amount of B220+ B cells, CD3+ T cells and the Ki67 proliferation activity.

In immunohistochemistry (Figure 18) it was shown that the spleen of LC40 and RelBKO//LC40 mice, which developed lymphomas, had a very similar morphology and barely can be distinguished. The spleen of both genotypes had an enlarged white pulp due to an increased B cell number. The follicles seemed to have lost their typical architecture due to small lymphocyte intermixes and B and T cells were not restricted to their usual areas. Furthermore, lymphomas of both genotypes were most likely indolent because Ki67, a marker for cell proliferation, gave only a weak signal within the follicles.

3.1.4. Identification of the B cell population inducing lymphoma in LMP1/CD40 mice

In 2008 Hömig-Hözl *et. al* described the immunophenotype of B cell lymphoma arising in LC40 mice with a mixed background as CD23⁻, CD21⁻, B220^{low}, CD43⁺ and defined this as the aberrant tumor population. This led to the hypothesis that the aberrant B cell population is the one causing the tumor.

3.1.4.1. Transplantation of LMP1/CD40-derived premalignant B cells into NSG mice

To prove this hypothesis, splenic B cells from two old, healthy LC40 mice with a C57BL/6 background were sorted into the aberrant and normal B cell population and transplanted into NOD scid gamma (NSG) mice. Since transitional B cells also have the CD23⁻/CD21⁻ phenotype, transitional B cells were excluded by gating on AA4.1⁻ B cells in the sorting strategy (Figure 19A). To ensure that each sorted B cell population has no contamination of the other population the purity of the two sorted populations was determined by FACS analysis (Figure 19B). Of each population, 3x10⁶ cells were injected into one NSG mouse. After six months the NSG mouse transplanted with the population AB14 started to show first signs of disease, thus all four NSG mice were sacrificed. FACS analysis of the blood revealed that B cells were circulating only in mice with a transplant of the aberrant population and the percentage of circulating B cells of the transplant AB14 was more than doubled compared to AB11 (Figure 20).

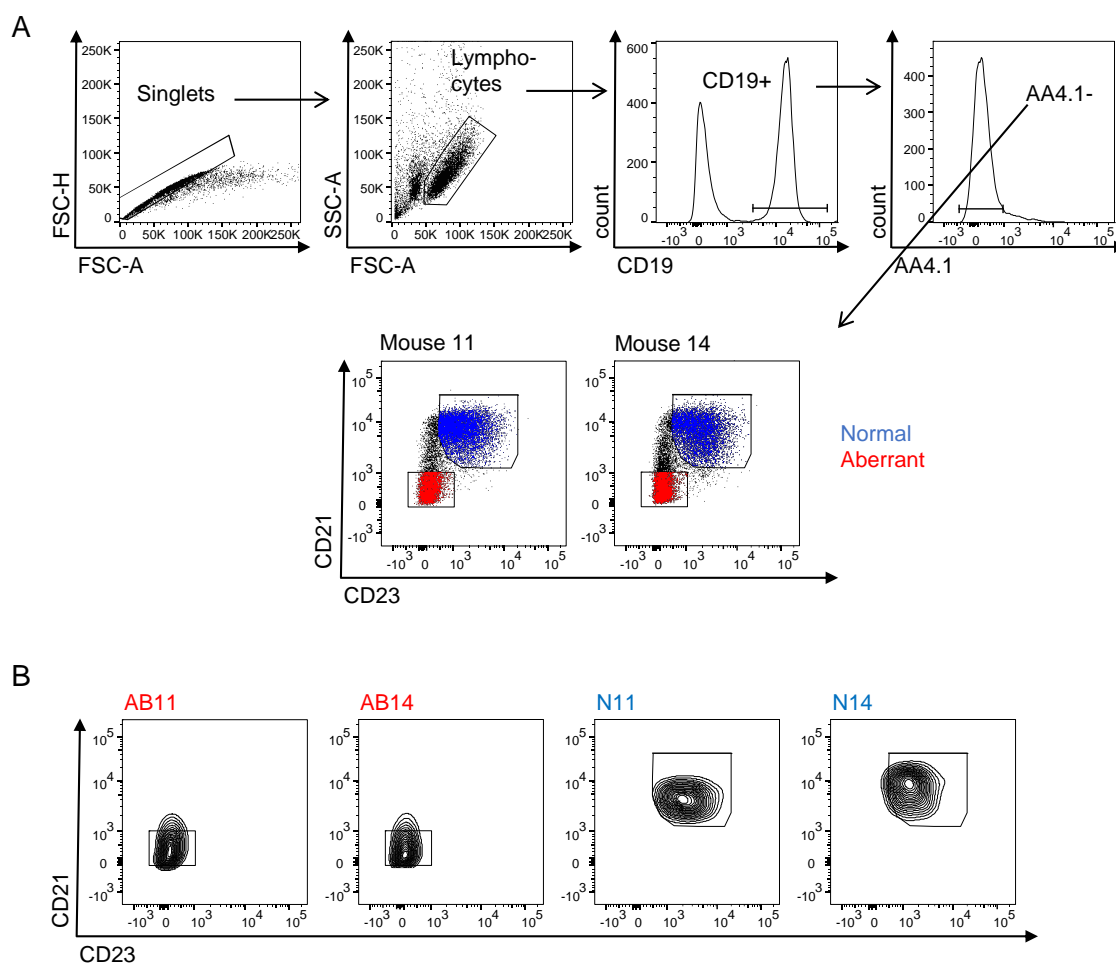


Figure 19 A shows the detailed FACS gating strategy of the cell sort of LC40 donor mice #11 and #14. B cells were sorted into normal (N) CD21⁺/CD23⁺ B cells (blue) and aberrant (AB) CD21⁻/CD23⁻ B cells (red). In B the purity check of both sorted populations from both mice can be seen.

In the spleen, it gets even clearer, that only B cells of the aberrant population were able to engraft and proliferate successfully in NSG mice. Further the percentage of B cells located in the spleen is higher in transplant AB14 than AB11 (Figure 21A), though both populations kept their aberrant CD23⁻/CD21⁻ phenotype (Figure 21B). Of special note was the appearance of spleen AB14, the engrafted B cells form tumorous follicles and the spleen was enlarged compared to a wildtype control and the spleen of the NSG mouse transplanted with the N14 population (Figure 21C). The engraftment and proliferation of the aberrant CD23⁻/CD21⁻ population, but not the normal CD23⁺/CD21⁺ B cell population, provides evidence, that the aberrant population was the premalignant B cell population that caused lymphoma in LC40 mice.

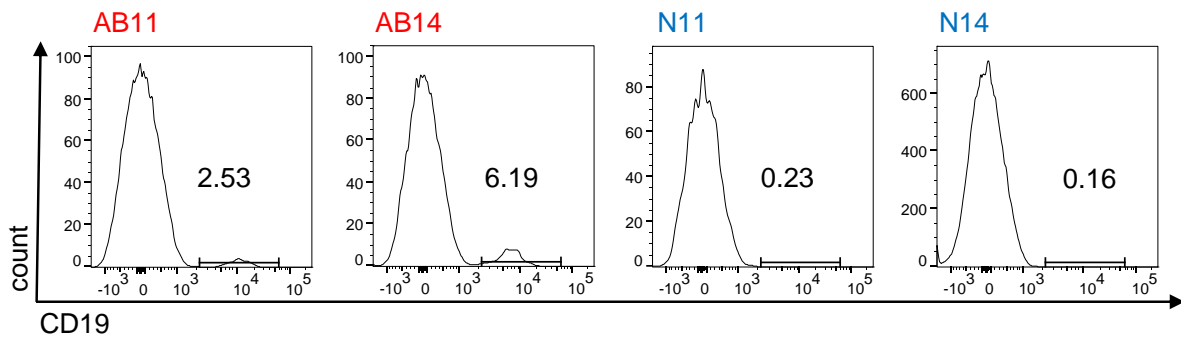


Figure 20 B cells were only detected in the blood of NSG mice receiving an aberrant B cells population transplant. The histograms indicate the percentage of B cells (CD19+) in the blood of each recipient NSG mouse on the day of scarification. B cells are pregated on singlets and lymphocytes. Recipients of the aberrant population were named AB and those of the normal population N.

To prove that the AB14 population is a real, transplantable tumor population, it was MACS-purified and 4.5×10^6 cells were re-injected into another NSG mouse. This time, engraftment and proliferation were accelerated, and the enlarged spleen of the recipient mouse was harvested after six weeks (Figure 22A). FACS analysis showed that the enlarged spleen was due to an expanded B cells population of the CD23⁻/CD21⁻ immunophenotype.

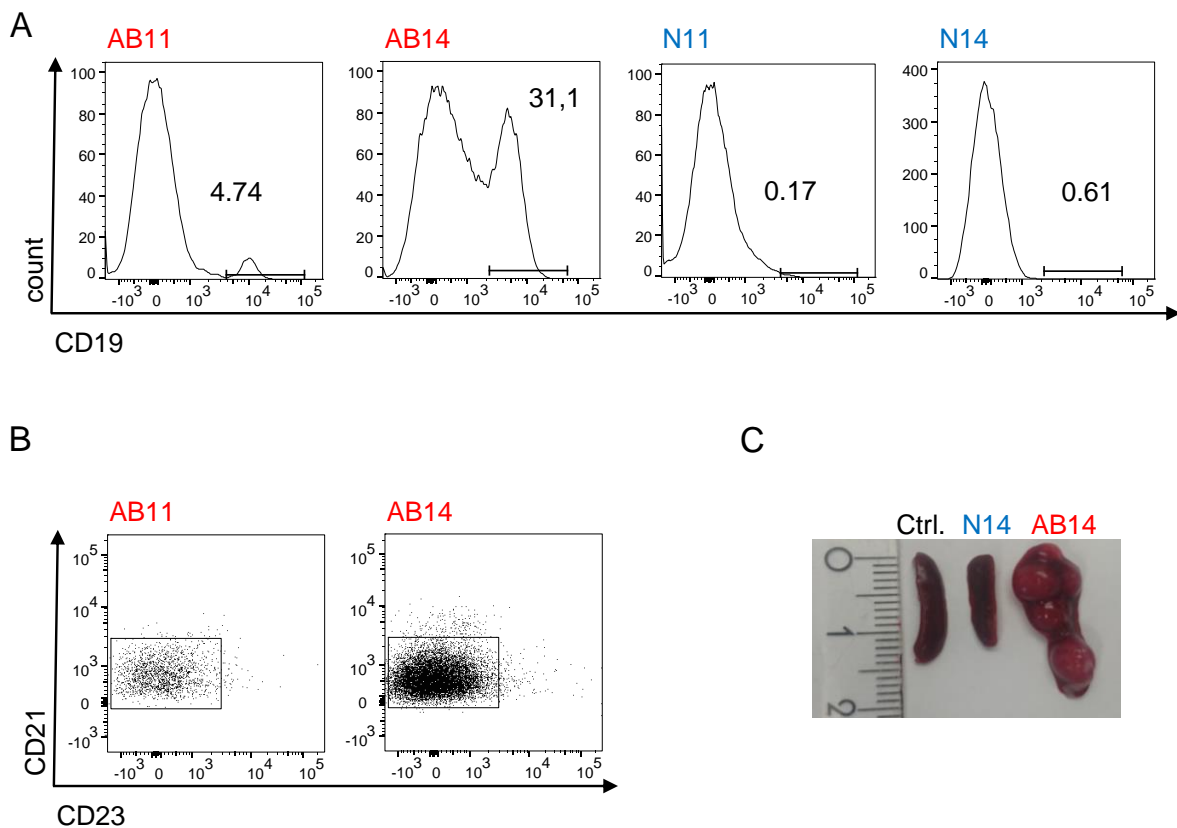


Figure 21 B cells expand only in the spleen of NSG mice receiving an aberrant B cells population. In panel A cells were pregated on singlets and lymphocytes. The numbers indicate the percentages of B cells. In panel B it is shown that the CD19⁺ splenic cells of the aberrant donor transplants keep their CD23⁻/CD21⁻ phenotype. The picture in

C shows a control spleen and the spleens of the NSG mice receiving the transplant of the normal population of donor #14 (N14) and the aberrant population of donor #14 (AB14).

To further enrich these lymphoma cells, 3×10^6 cells of the N₂ frozen re-transplanted AB14 B cell population were re-transplanted again into one NSG mouse. After six weeks the recipient mouse was sacrificed. A clear B cell enrichment was detectable by FACS. Further BCR sequencing revealed a monoclonal B cell expansion in both re-transplantations (Figure 22B). Since the mouse did not show any signs of sickness before these six weeks, I conclude that the aggressive B cell tumor was rather stable and did not gain further aggressiveness.

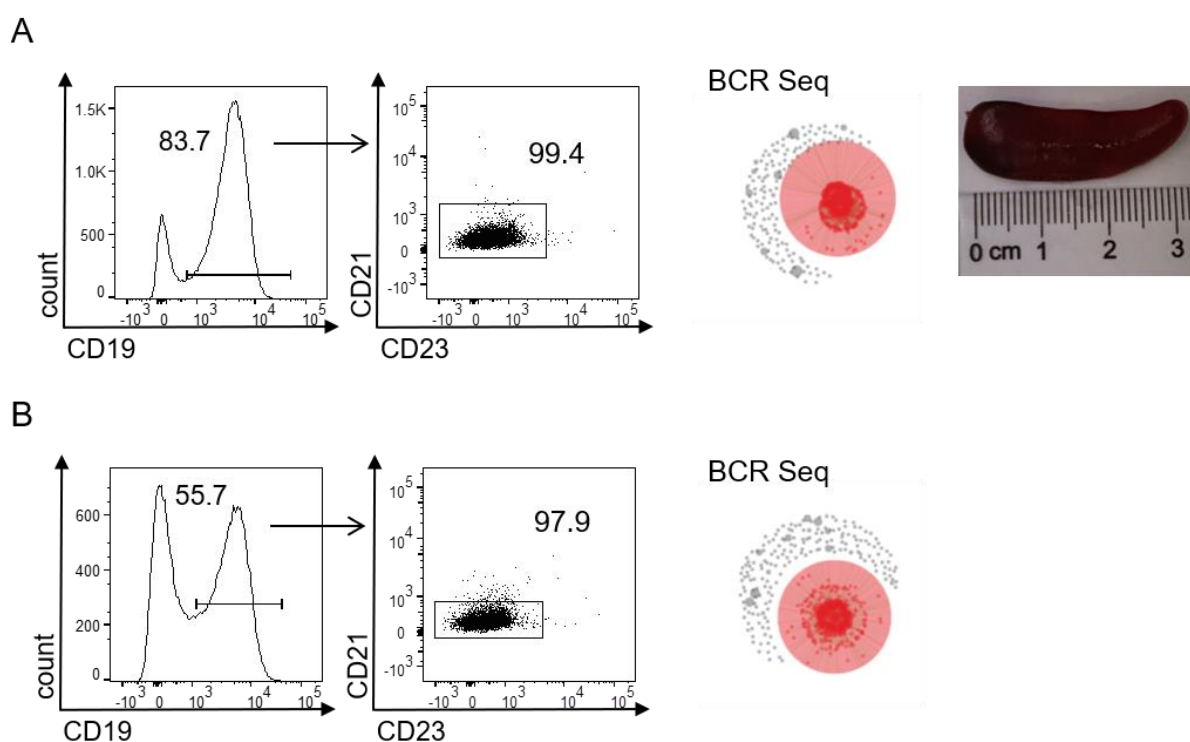


Figure 22 The re-transplanted B cells of the AB14 population engraft and expand repeatedly. In panel A the direct re-transplanted B cells of recipient mouse AB14 is shown. In panel B the second re-transplanted is shown. In both panels CD19+ cells were pregated on singlets and lymphocytes and for B cells an additional dot plots shows the CD23-/CD21- phenotype. For both transplantations BCR sequencing of the Ig heavy chain revealed a monoclonal expansion. One clone is defined by its CDR3 sequence and constitutes a node of the clonality network. The size of the node scales with the third root of the read counts assigned to it. In panel A an additional picture of the spleen of the recipient mouse illustrates the B cell expansion.

3.1.4.2. Generation of a murine LC40 lymphoma cell line

Since it is always an interest to reduce animal experiments and to facilitate an experimental set-up, purified B cells of the first re-transplant were also cultured *in vitro* to see whether these lymphoma cells can be enriched without the need of NSG mice. After several weeks of adapting to the *in vitro* culture conditions, B cells started to expand and behaved like a

lymphoma cells line. This means that cells did not compromise in proliferation after freezing and thawing and they had an approximate doubling rate of 48 hours. The immunophenotype was still like a full grown LC40 tumor, since the cells were CD23⁻/CD21⁻, CD43⁺ and IgM^{high} and CD5⁺ (Figure 23). This cell line will be a good tool to further investigate why chronic CD40 signaling leads to B cell lymphoma.

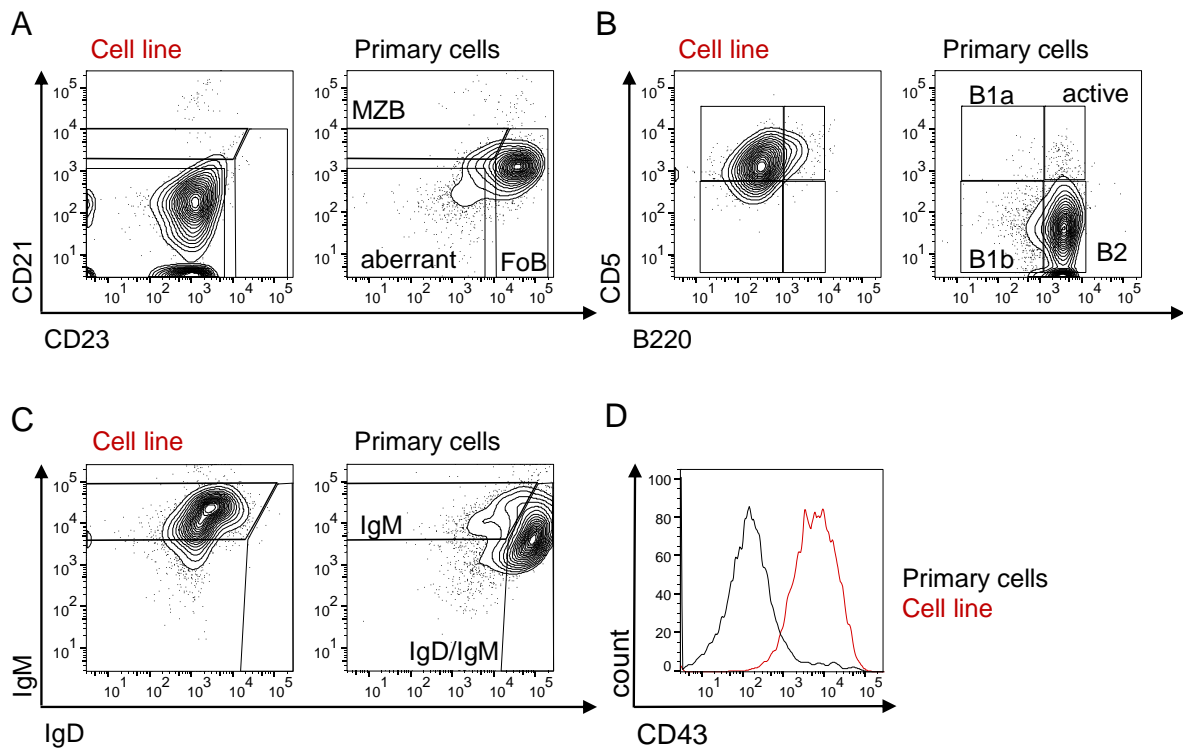


Figure 23 The immunophenotype of the murine LC40 cell line compared to primary murine B cells. In all panels, cells were pregated on living cells and primary cells were additionally pregated on CD19. In panel A the CD21/CD23 phenotype is shown, in panel B the B1 cell phenotype, in panel C the IgM/IgD phenotype and in panel D is a histogram indicating that the cells of the LC40 cell line express CD43.

3.2. CycD1//LC40 mice as MCL model

As described before (1.4), the hallmark mutation of MCL is a *CYC1* overexpression due to the translocation of *cycD1* to the *igh* locus. Furthermore, infiltrating T cells result in CD40 stimulation of MCL cells increasing their proliferation (Anderson, 2000) and inducing chemoresistance to BTK-inhibitors, which makes this disease difficult to cure (Rauert-Wunderlich *et al.*, 2018a). Currently, no sufficient mouse model is available to study the transformation of this disease. Thus, E μ CycD1 (*cycD1*) mice were crossed with LMP1/CD40 mice (*cycD1*//LC40) to investigate if the double transgenic mouse is a suitable model for pre-clinical studies for these more aggressive MCL cases.

3.2.1. CYCD1 overexpression does not affect the phenotype of young LC40 mice

Firstly, the *cycD1* expression was analyzed in splenic B cells derived from 3-4 months old *cycD1*//LMP1/CD40 (*cycD1*/LC40), *cycD1*, LC40 and control mice by qPCR.

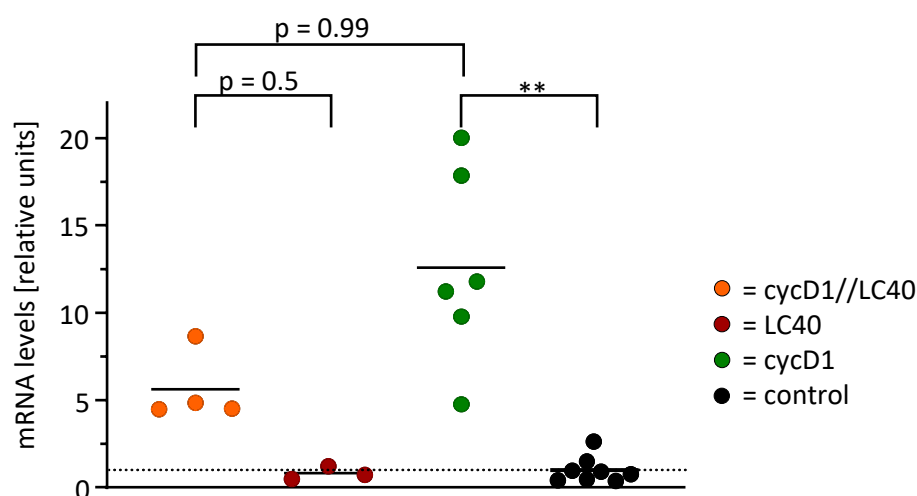


Figure 24 *CycD1* mRNA levels were detected by qPCR. As reference genes *RNAPo2* and *YWHAZ* were used. For normalization each value is divided by the average of all controls. Each dot represents a sample derived from one individual mouse of the respective genotype *cycD1*//LC40 (orange), LC40 (red), *cycD1* (green) and control (black). The non-parametric Kruskal-Wallis test was performed for statistical comparison. The p values are indicated as ** ≤ 0.01 . The dotted line indicates the value of 1 relative unit.

As Figure 24 shows, *cyD1* single transgenic (*cycD1*) mice have significantly elevated *cycD1* mRNA levels compared to control mice. LC40 and control mice have a similar *cycD1* expression level, while for *cycD1*//LC40 mice *cycD1* mRNA levels were increased by trend in comparison to LMP1/CD40 and control mice. The high variance of the *cycD1* mRNA levels in *cycD1* and

cycD1//LC40 mice could be an effect of the random insertions of the *cycD1* transgene, therefore not every individual might have the same number of the inserted *cycD1* transgene. Nevertheless, every single individual containing the *cycD1* transgenic insertions had higher mRNA level than control or single transgenic LC40 mice. Secondly, a cohort of young cycD1//LC40 mice was analyzed with their age-matched single transgenic LC40 and cycD1 and control littermates. The splenic weight of cycD1//LC40 mice was comparable to that of young LC40 mice, though no further increase in splenic weight was visible (Figure 25). CycD1 mice had a splenic weight comparable to control mice. The same applied to the total count of splenic B cell numbers, as cycD1//LC40 mice had elevated numbers compared to control mice and cycD1 mice but similar B cell numbers compared to LC40 mice (Figure 25).

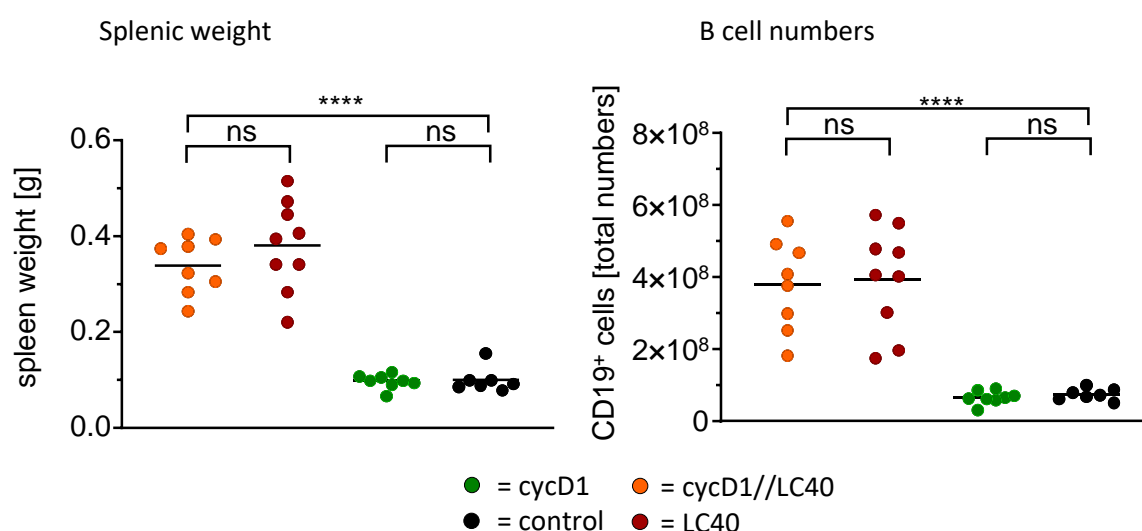


Figure 25 The splenic weight of young cycD1//LC40 (orange), LC40 (red), μ CycD1 (green) and control (black) mice is depicted in the left graph. Mice were between three and six months old and one dot represents the value of an individual mouse. In the right graph the total splenic B cell numbers of the same mice are shown. To receive the total B cell number, the percentage of CD19+ cells – pregated on living cells - was determined by FACS and was multiplied by the counted number of living splenocytes. For statistical analysis a one-way ANOVA with a Tukey's multiple comparison test was performed. The p values are indicated as ns > 0.05, **** \leq 0.001.

Generally, the immunophenotype of young cycD1//LC40 was the same as the immunophenotype of LC40 mice. FACS analysis could not reveal any differences provoked by adding the CYCD1 overexpression to LC40 mice. Compared to cycD1 and control mice, LC40 and cycD1//LC40, had an increased number of MZBs (CD21⁺/CD23⁻) and FoBs (CD21⁻/CD23⁺) (Figure 26). Expectably, cycD1 mice show no difference to control mice.

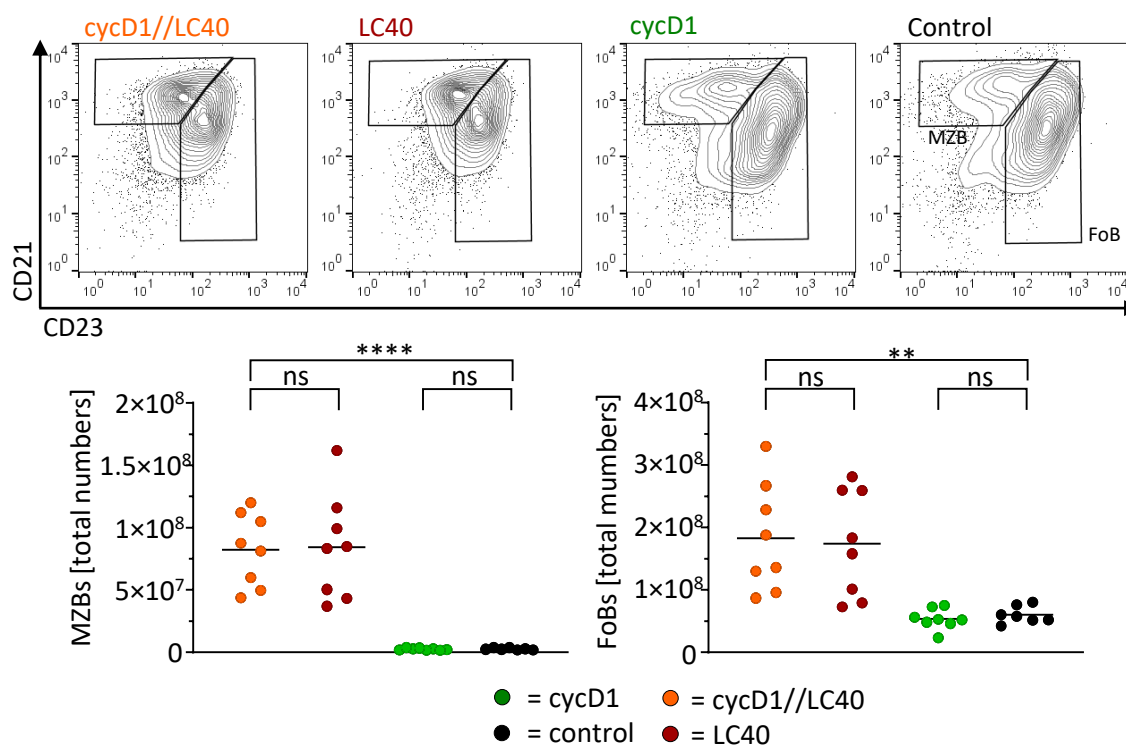


Figure 26 The immunophenotype of three to six months old *cycD1//LC40* (orange), *LC40* (red), *E μ CycD1* (green) and control (black) mice was determined by FACS analysis. As an example, the MZB (CD21⁺/CD23⁻) and FoB (CD21⁻/CD23⁺) staining of splenic B cells is shown. In the upper panel FACS plots of one representative experiment including each genotype is depicted. Pregating was done on lymphocytes and CD19⁺ B cells. In the graphs below the total number of MZBs and FoBs is summarized. The value of one individual is represented in one dot. For statistical analysis a one-way ANOVA with a Tukey's multiple comparison test was performed. The *p* values are indicated as *ns* > 0.05, ** ≤ 0.01, **** ≤ 0.001.

3.2.2. Lymphoma development in *cycD1//LC40* mice

Of special interest is the effect of the CYCD1 overexpression on aged *LC40* mice. For this purpose, a cohort of *cycD1//LC40*, *LC40* and control mice in the C57BL/6 background were aged and analyzed when first signs of disease appeared. The splenic weight and the B cell numbers were comparable in aged *LC40* and *cycD1//LC40* mice and significantly increased compared to control mice (Figure 27A). To determine the B cell lymphoma incidence the splenic weight and B cell expansion have to be considered. The clonal B cell expansion was detected by BCR sequencing of the complementarity-determining region 3 (CDR3) of the IgH. Depending on the mutated CDR3 region, clones were identified and clustered into clonal networks. If one clone reached at least 10% of all read counts, it is considered as an expanded clone and indicated in color (Figure 27C).

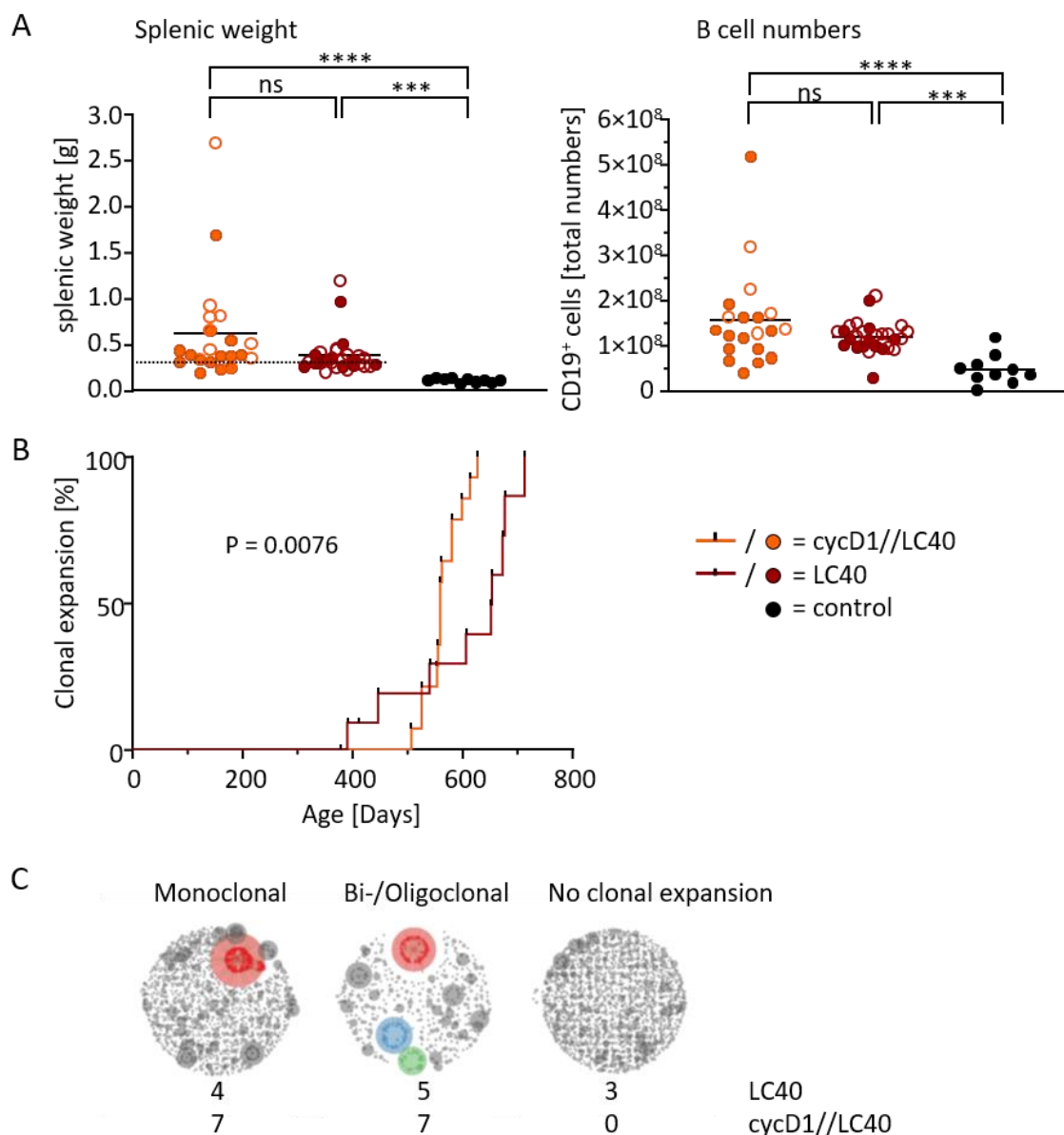


Figure 27 The monoclonal B cell expansion, splenic weight, and B cell numbers of aged cycD1//LC40 and LC40 mice. Mice were sacrificed as soon as first signs of disease were encountered. In A the splenic weight of aged cycD1//LC40 (orange), LC40 (red) and control (black) mice as well as the total number of B cells is shown. To receive the total B cell number, the percentage of CD19⁺ cells – pregated on living cells - is determined by FACS and was multiplied by the counted number of living splenocytes. One dot represents the value from one individual. Filled dots represent individuals which were randomly chosen to be analyzed in BCR sequencing. The dotted line indicates the average splenic weight observed in young mice. For statistical analysis a Kruskal-Wallis test was performed. The p values are indicated as ns > 0.05, *** ≤ 0.001, **** ≤ 0.0001. In B and C, the clonal B cell expansion was detected by BCR sequencing of the IgH. In C a representative c-net plot is shown for a monoclonal expansion, bi-/oligoclonal expansion and no clonal expansion. Clones are defined by a unique V(D)J rearrangement that contained more than 10% of the total reads. The expanded clones are colored and if several clones were expanded in one sample, each clone received a different color. Each clone constitutes a node of the clonality network, which size scales with half of the third root of the read counts assigned to it. How often each case appears in each genotype is indicated by the number below the c-net plot. BCR sequencing and the bioinformatical analysis was performed at Roland Rads lab. In B the Kaplan-Meier graph shows with which likelihood cycD1//LC40 and LC40 mice develop a clonal B cell expansion within the time course of ~ 2 years. A black dot represents the time point when one individual was analyzed.

The three LC40 individuals with no clonal expansion of their IgH had an age of 1-1.5 years. In all remaining LC40 mice a clonal expansion was detectable. The median survival of LC40 mice was 654 days (~21.8 months) and the oldest mouse with a clonal B cell expansion reached an age of 713 days (~23.7 months). A clonal B cell expansion could be detected in all analyzed *cycD1*//LC40 mice, which had a median survival of 559 days (~18.6 months) and the oldest mouse reached an age of 627 days (~20.9 months) (Figure 27B). Thus, both mutants developed clonal B cell expansions during aging and have a splenomegaly compared to control mice. Further, both mutants achieve an advanced age before getting sick, therefore the lymphoma development is rather indolent for both. Since *cycD1*//LC40 showed a significantly faster development of the disease than LC40 mice, it seems that the overexpression of *CYCD1* accelerates the lymphoma development.

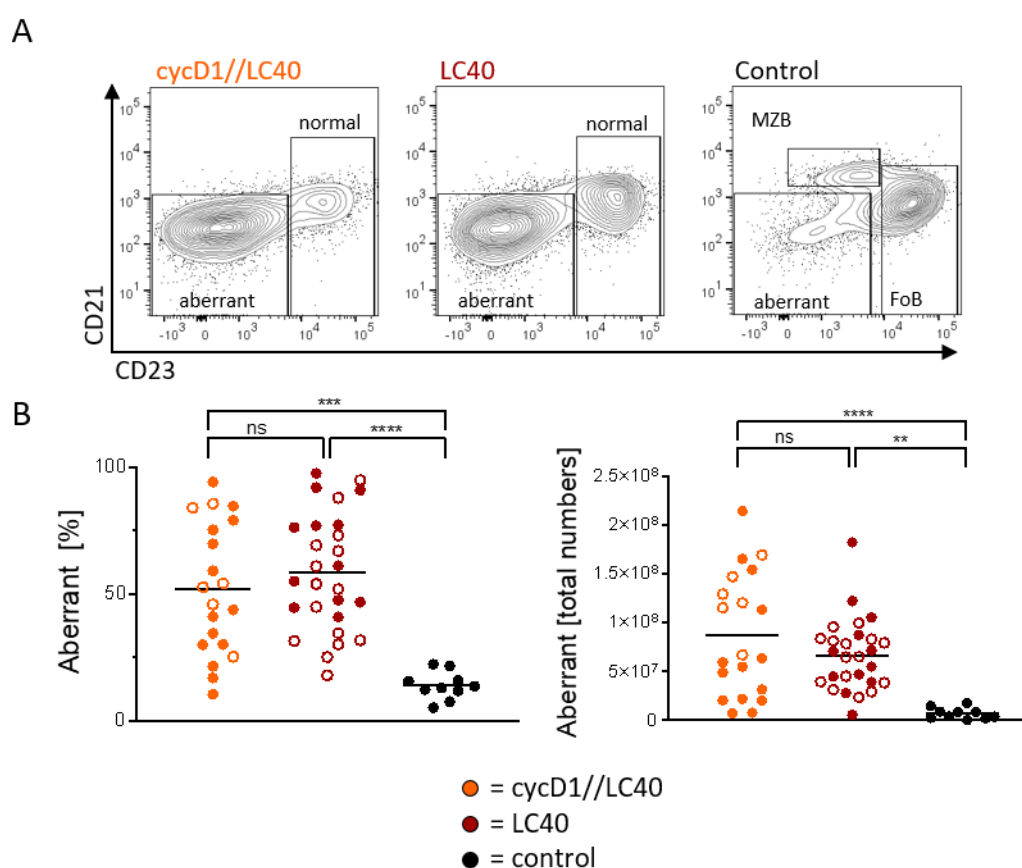


Figure 28 The immunophenotype of aged *cycD1*//LC40 (orange), LC40 (red) and control (black) mice was detected by FACS analysis. Cells were pre-gated on lymphocytes and CD19⁺. In the upper panel a representative of each genotype of the CD21/CD23 staining of splenic B cells is shown. The graph below gives the summary, while each dot represents one sample. A one-way ANOVA with a Tukey's multiple comparison test was performed to test the statistical significance. The *p* values are indicated as ns > 0.05, *** ≤ 0.001, **** ≤ 0.0001.

A characteristic feature of the lymphoma development of LC40 mice is the outgrowth of an aberrant CD23⁻/CD21⁻ population. Hence, FACS analysis was performed and revealed, that

the aberrant population occurred to the same extent in both mutant mice (Figure 28). Further, both mutants had a significant increase of this population compared to aged control mice. Generally, the immunophenotype of B cells derived from *cycD1*//LC40 lymphoma mice was the same as the immunophenotype of those derived from single mutant LC40 mice. Apart from the similar CD23⁻/CD21⁻ phenotype, both mutant mice showed an increase in the percentage of B220^{low} B cells in their spleen and a tendency to have an increase of CD5⁺ aberrant B cells (Figure 29B). Additionally, all mutant B cells expressed the BCR. Most B cells expressed high levels of IgM and showed a downregulation of IgD (Figure 29A).

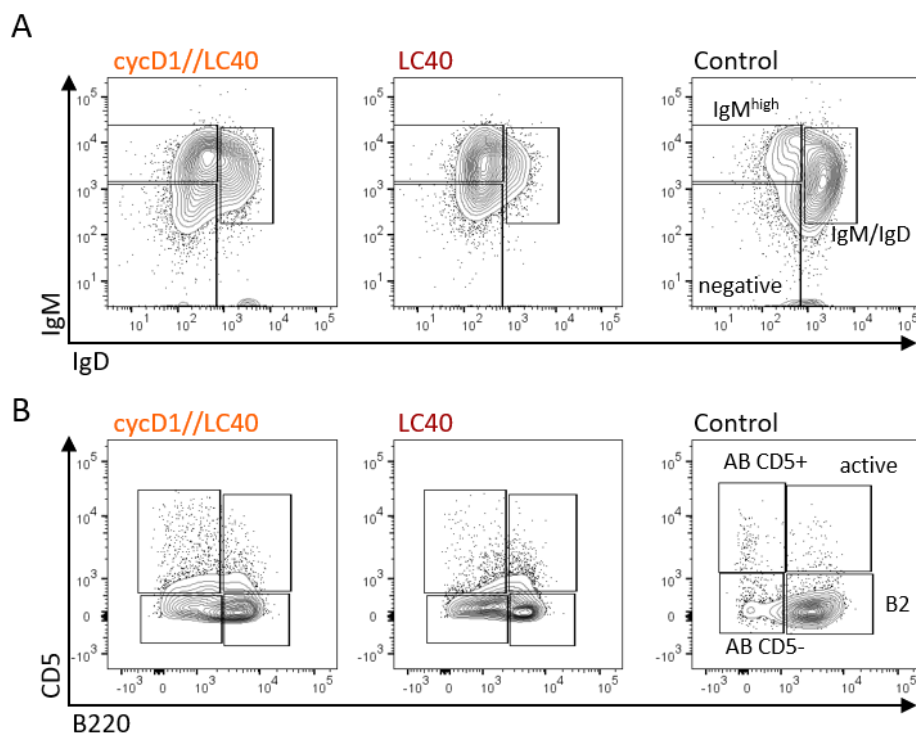


Figure 29 The immunophenotype of aged *cycD1*//LC40 (orange), LC40 (red) and control (black) mice was detected by FACS analysis. The upper panel shows a representative set of an IgM/IgD staining, while the lower panel depicts one example of each genotype of the B220/CD5 staining. In both cases cells are pregated on lymphocytes and CD19⁺.

Although the immunophenotype of tumors derived from *cycD1*//LC40 and LC40 was the same, *cycD1*//LC40 mice had an accelerated tumor development, as they showed first signs of disease at an earlier time point.

3.2.3. The impact of C57BL/6 and BALB/c background on lymphoma development in LC40 mice

Surprisingly, the background of LC40 mice had a tremendous impact on the tumor development of these mice. This matter came to attention as the LC40 mice studying the non-canonical NF- κ B pathway were on a BALB/c background and the littermates of the *cycD1*/LC40 mice were on a C57BL/6 background.

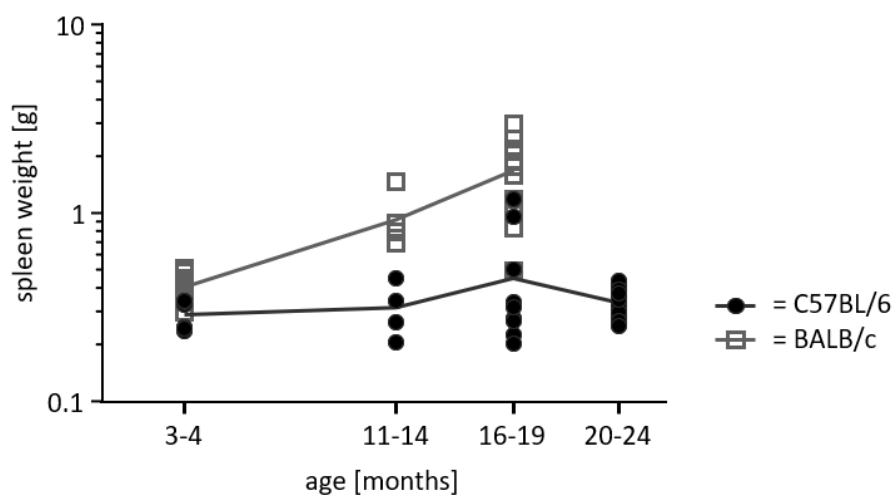


Figure 30 The age-related splenomegaly of LC40 mice depends on their genetic background. Each data point represents the value of one individual belonging to the indicated age group. BALB/c mice are shown in gray/rectangle and C57BL/6 mice in black/circle.

The immunophenotype of the lymphoma was the same regardless of the background, however the tumor expansion is accelerated in BALB/c mice. Firstly, the age-related splenomegaly is increased in BALB/c mice compared to C57BL/6 mice (Figure 30). Secondly, all LC40 BALB/c mice showed first signs of disease before reaching 20 months and had to be sacrificed, while some LC40 mice on the C57BL/6 background survived up to 24 months without any signs of lymphoma. Thus, to accelerate future lymphoma studies it might be recommended to use the BALB/c background.

3.3. PiggyBac transposon screen for identification of new cancer genes

As described before (3.2.2), LC40 mice with a C57BL/6 background need more than one year to develop indolent mono- and oligoclonal B cell lymphoma and *cycD1* mice do not develop any spontaneous lymphoma. Therefore, secondary mutations need to be acquired for lymphomagenesis. A transposon-induced mutagenesis screen provides the opportunity to induce and detect such mutations and to pinpoint new driver genes involved in the evolution of B cell lymphoma. Hence, the LC40 or the *cycD1* mice were crossed with the PiggyBac (PB) mouse model to receive LMP1/CD40//PB//ATP2//CD19-Cre (LC40//PB) and $E\mu$ CycD1//PB//ATP2//CD19-Cre (*cycD1*//PB) mice. Due to CD19-Cre, the PB transposase is exclusively expressed in B cells and enables transposon mobility only in B cells. To induce gain of function mutations, it is essential for the transposon to insert in sense orientation upstream of the expressed gene, so the internal promoter activates gene transcription. For loss of function mutations, the orientation and position of the insertion are less relevant. Due to a bi-directional polyA site, the transposon disrupts transcription in both orientations. Thus, the insertion pattern is often more randomly distributed throughout the gene (for a more detailed description see 1.5.2).

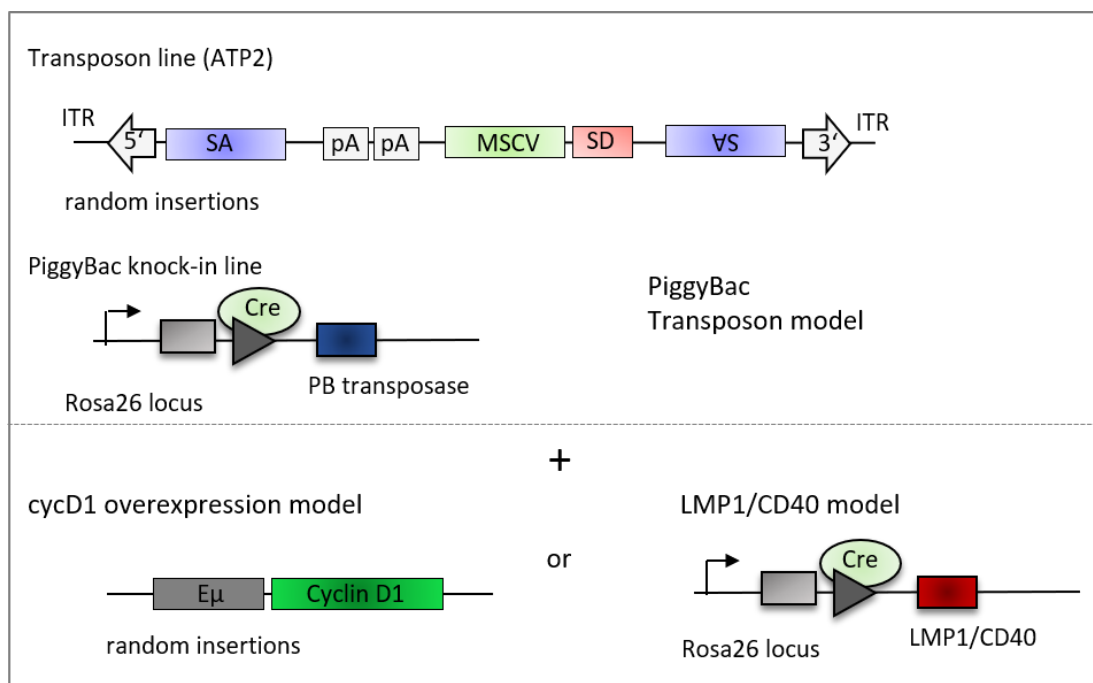


Figure 31 Schematic mouse model of PiggyBac system including the PiggyBac (PB) transposase inserted into the *rosa26* locus together with a loxP flanked stop-cassette and ATP2 transposon with two splice acceptors (SA), one splice donor (SD), bidirectional polyA site (pA) and the MSCV promoter. Mice bearing the PB system in combination with CD19-Cre were crossed with either $E\mu$ CycD1 or LC40 mice. CD19-Cre results in excision of the stop cassette in B cells resulting in the B-cell specific expression of the transposase and LC40.

The *cycD1*//PB was expected to unravel secondary driver genes involved in MCL, due to its initial *cycD1* hallmark mutation, while the LC40//PB model was used to reveal further mutations of tumors depending on a constitutively active CD40 signaling. Potentially, this could also include MCL, since late stages of MCL are triggered by a CD40 stimulation but any other B cell lymphoma type is just as likely to be generated by the random mutagenesis induced by the transposons in combination with LC40. A third cohort of control//PB mice, which did not bear any further transgene apart from the PiggyBac system, was utilized to determine which driver genes appear without preliminary transgenic mutations and which mutations are exclusive for the *cycD1*//PB, respectively the LC40//PB model.

3.3.1. Lymphoma development of PB mice

Transgenic mice of all three cohorts – LC40//PB, *cycD1*//PB and control//PB – were aged and sacrificed when first signs of disease were visible.

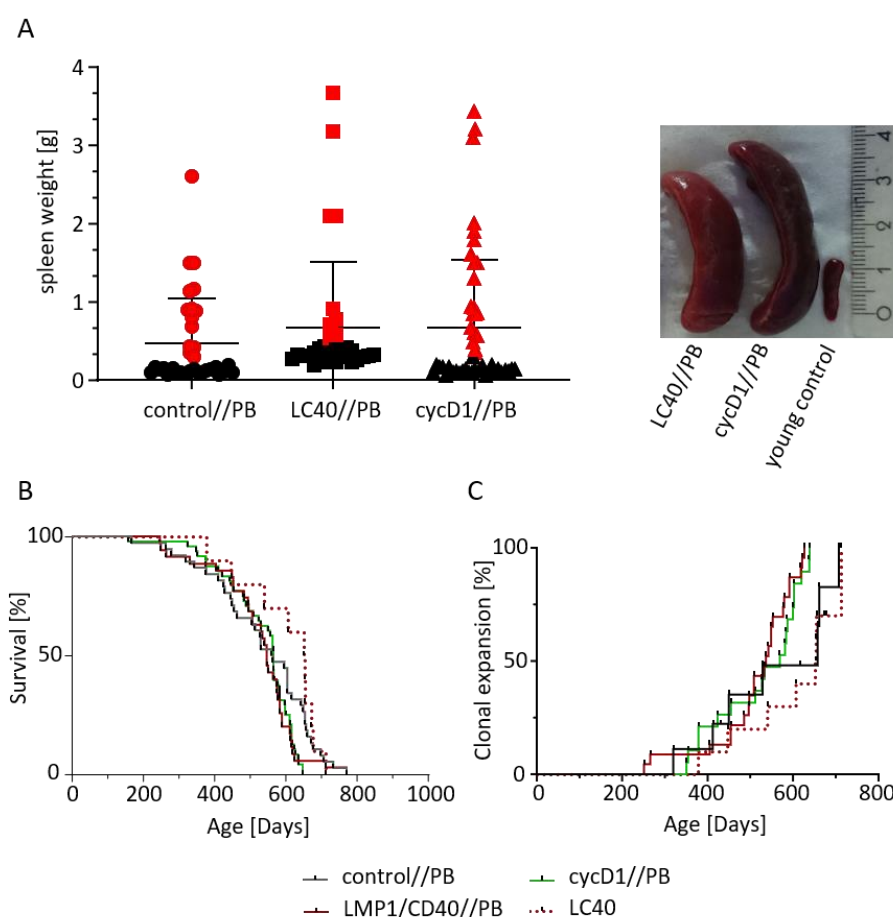


Figure 32 Splenic weight, survival, and development of a clonal B cell expansion of aged control//PB, LC40//PB and *cycD1*//PB mice. In A the splenic weight is summarized in the graph on the left. If the splenic weight of an individual is above the regarding genotypes' splenic weight of young mice without PB, the data point is red. The picture on the right gives an example of an enlarged spleen of an LC40//PB, *cycD1*//PB mice in comparison to a spleen of a young control mouse. Panel B and C depict the survival curve respectable the clonal B cell expansion

of control//PB (black), LC40//PB (red), *cycD1*//PB (green) mice and LC40 mice without PB (red-dotted) mice. Mice were sacrificed when first signs of disease were observed. Individual mice are indicated by a black dot. For the survival curve all sacrificed mice are indicated. The clonal B cell expansion was determined by BCR sequencing and since not all sacrificed mice were sequenced yet, the Kaplan Meier curve of the clonal expansion contains less individuals than the survival curve. The decision which samples should be used for BCR sequencing was based on the splenic weight and individuals with a splenomegaly were selected. BCR sequencing was performed at Roland Rads Lab.

The cohort of the LC40//PB included 34 mice with a median age of 525 days, the *cycD1*//PB cohort had 48 individuals with a median age of 532 days and the number of control//PB mice was 37 with a median age of 537 days. Due to the random mutagenesis induced by the ATP2 transposons, some mice had to be sacrificed before they reached an age of one year, and some even reached the age of ~2 years. The oncogenic potential was proven, because LC40 mice without the PB system had a longer disease-free life than LC40//PB mice. As the median survival and the age variation of mice bearing the PB system was independent of the transgenic background, the survival curves do not show any significant difference between these genotypes (Figure 32B).

Table 1 Listed summary of LC40//PB, *cycD1*//PB and control//PB mice used to identify driver genes in B cell lymphoma. The sample ID, age, SP weight and results from the BCR sequencing are given. If BCR sequencing was not performed for a sample yet, it is indicated as NA.

control//PB				LC40//PB				<i>cycD1</i> //PB			
sample ID	Age (Days)	BCR Seq	SP weight	sample ID	Age (Days)	BCR Seq	SP weight	sample ID	Age (Days)	BCR Seq	SP weight
35433	708	biclonal	0.347	31025	496	biclonal	0.315	33068	423	monoclonal	1.5
35805	662	monoclonal	1.5	31027	508	monoclonal	0.233	34684	526	monoclonal	0.84
38861	529	monoclonal	0.877	31028	508	oligoclonal	0.293	35774	599	biclonal	0.919
41608	280	monoclonal	2.6	31031	536	oligoclonal	2.1	38269	378	monoclonal	3.2
32005	618	oligoclonal	0.142	32006	618	oligoclonal	0.309	39627	583	monoclonal	0.354
36783	658	monoclonal	0.689	32897	532	monoclonal	0.187	40056	454	oligoclonal	0.67
44823	412	monoclonal	0.89	32898	454	monoclonal	0.233	40062	568	biclonal	0.287
45806	450	monoclonal	1.13	32899	579	biclonal	3.67	40066	511	monoclonal	0.86
38825	531	NA	1.5	35430	497	oligoclonal	0.32	40373	650	NA	0.94
42906	655	NA	0.157	39425	251	monoclonal	0.398	40375	580	oligoclonal	0.39
42908	655	NA	0.292	40321	405	monoclonal	0.532	40376	637	NA	3.1
49415	518	NA	0.64	42505	266	monoclonal	0.425	41391	619	biclonal	0.56
42904	597	NA	0.8	40318	485	oligoclonal	3.17	41395	350	monoclonal	1.9
				44914	454	monoclonal	2.1	42030	378	monoclonal	1.6
				41018	621	oligoclonal	0.71	43130	586	biclonal	1.29
				43894	585	NA	0.25	43136	445	biclonal	1.78
				41269	576	biclonal	0.58				
				44915	626	monoclonal	0.37				

Considering the splenic weight, many mice had developed an age-related splenomegaly, since their splenic weight is increased compared to the splenic weight of young mice in their respective genotype without the PB system (Figure 32A). The threshold of an age-related splenomegaly was higher for the LC40//PB genotype, since young LC40 mice already had an increased splenic weight. The age-related splenomegaly indicated that the PB system induced lymphomagenesis in all transgenic backgrounds and potentially favored a more aggressive lymphoma development. Further, the range of splenic weight showed a high variation in all

three genotypes, which could be due to the differently hit genes by the transposons. The clonal B cell expansion was measured by BCR sequencing of splenic tissue and results were summed up in a Kaplan Meier curve, which indicates the probability of developing a clonal B cell expansion in the given time period (Figure 32C). Since the sequenced samples had been preselected for an increased splenic weight, the clonal B cell expansion should align with the lymphoma development. Since the splenic weight, age and BCR sequencing result of mice, which were used to identify the genes hit by the transposon-based mutagenesis, are of special interest, this data is given in Table 1.

To reveal whether the PB induced mutagenesis changed the immunophenotype of the B cells, FACS analysis was performed. It appeared that mice, which most likely beared lymphoma, developed the aberrant $CD23^-/CD21^-$ population in their spleen, which is not present in young control mice. The size of this aberrant population varied amongst individuals and was independent of the genetic cohort they belong to (Figure 33). Since the numbers of the aberrant population aligned with the expansion of the total $CD19^+$ B cell numbers, it can be concluded, that the B cell expansion is mainly due to the aberrant population.

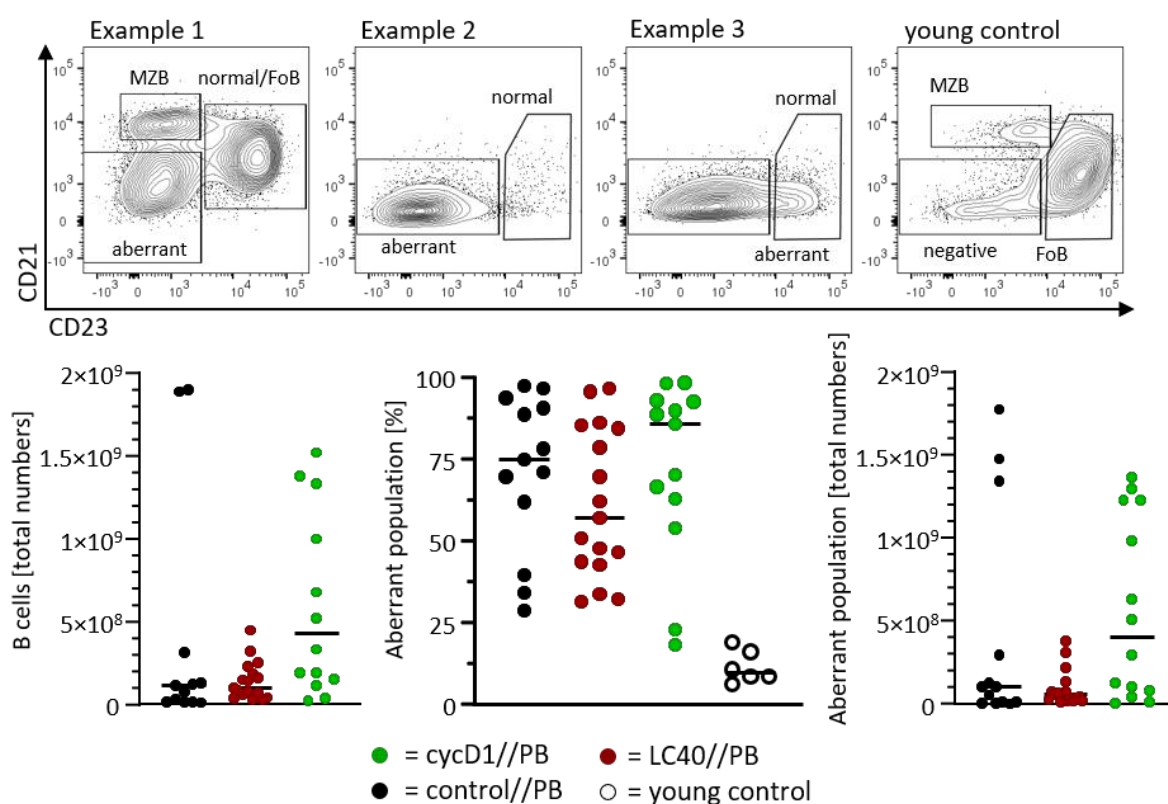


Figure 33 Example FACS blots of PB mice for the stainings CD23/CD21. Pregating was performed on singlets, lymphocytes and $CD19^+$ B cells. The example 1 and 2, and young control (white) are derived from the same experiment and the example 3 was analyzed in a different experiment. The depicted dot plots are examples of

different lymphomas, which occurred in all three genotypes. The graphs below the dot plots summarize the results for the aberrant CD23-/CD21- population. Total B cell numbers were determined by the percentage of CD19+ cell in FACS and used to calculate the total cell number of the aberrant population. The values of mice which were sequenced for common insertion site (CIS) analysis are depicted in the graph. Each dot represents one individual.

Moreover, the aberrant population tended to be B220^{low} (Figure 34). In some cases, these cells also tended to be CD5⁺, however this is also independent of the genetic background and varied among individuals (Figure 34). Since the CD5⁺ phenotype appeared in a range, it is difficult to cluster these mice.

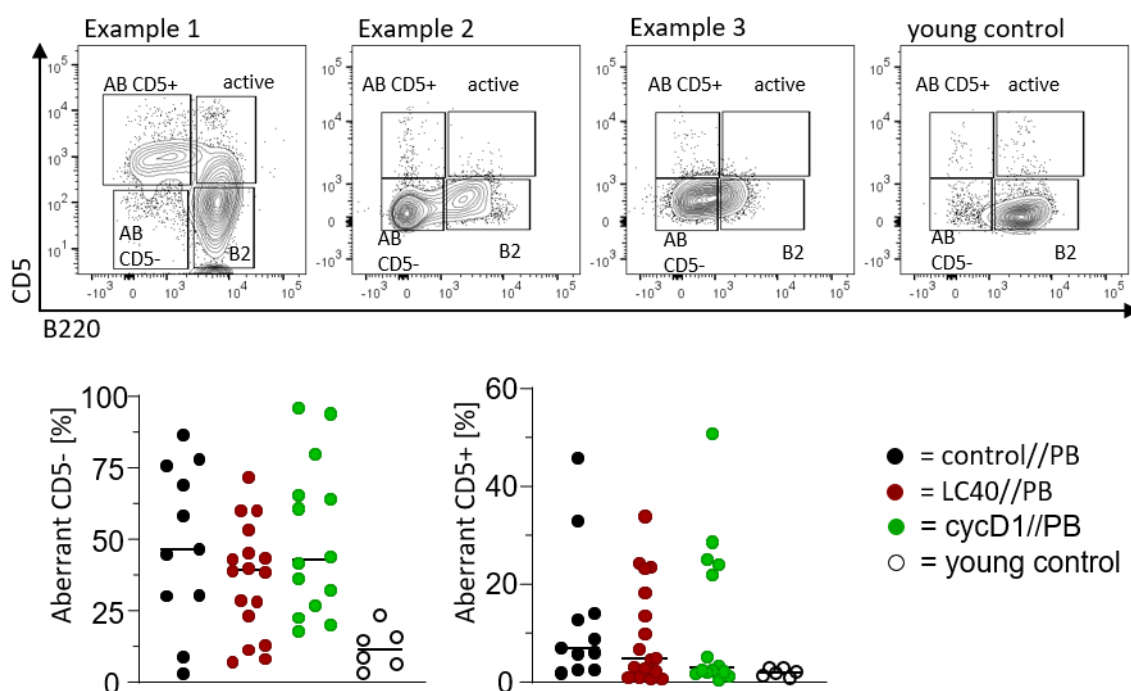


Figure 34 Example FACS blots of PB mice for the stainings B220/CD5. Pregating was performed on singlets, lymphocytes and CD19+ B cells. The examples 1 and 2, and young control (white) are derived from the same experiment and the example 3 was analyzed in a different experiment. The depicted dot plots are examples of different lymphomas, which occurred in all three genotypes. The values of mice which were sequenced for common insertion site (CIS) analysis are depicted in the graph. Each dot represents the value of one individual.

In the exemplary FACS plots one mouse with a clear CD5⁺ population is shown (Figure 34, Example 1) and two with none (Example 2, 3). In addition, many mice had a B cell population which upregulated IgM and downregulated IgD compared to young controls. Similar to the development of the aberrant population, the population size of B cells with an IgM upregulation differed a lot between the single mice and was not necessarily genotype specific (Figure 35).

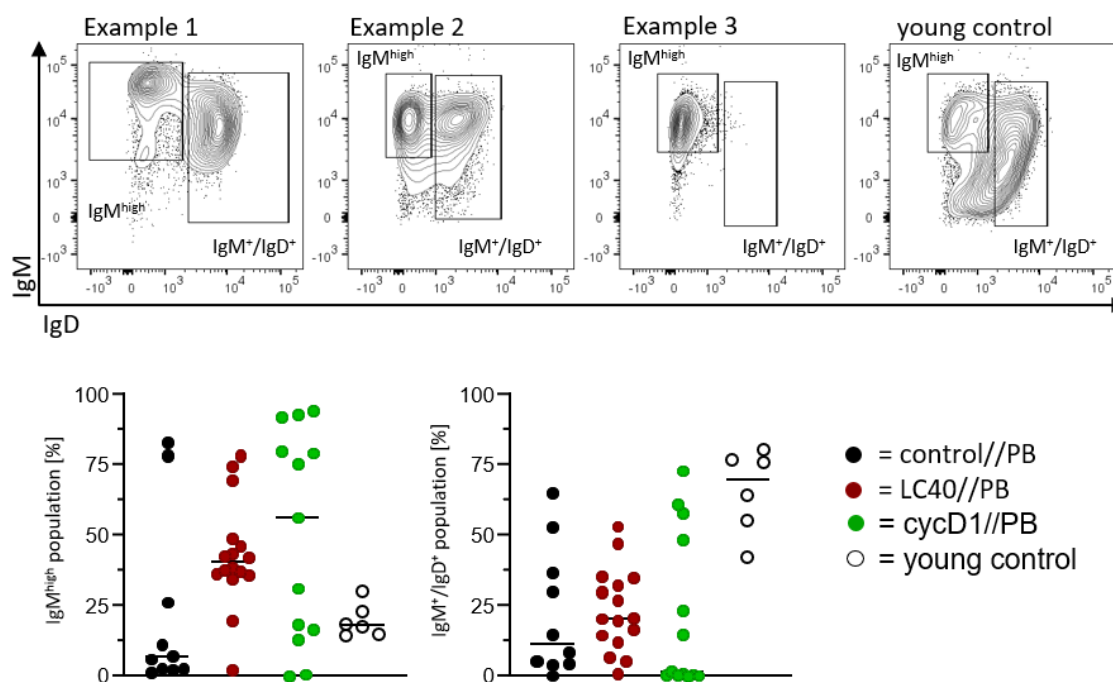


Figure 35 Example FACS plots of PB mice for the stainings IgM/IgD. Pregating was performed on singlets, lymphocytes and CD19+ B cells. The cycD1//PB (green), LC40//PB (red) and young control (white) are derived from the same experiment and the control//PB (black) was analyzed in a different experiment. The depicted phenotypes are not genotype specific. The graphs below the dot plots summarize the results. Each dot represents the value of one individual, which was also used for CIS analysis.

3.3.2. Identification of new driver genes

To elucidate new driver genes quantitative transposon insertion site sequencing (QiSeq) was performed to elucidate the position and insertion orientation of the ATP2 transposons in the genome. For further analysis, only samples of lymphoma mice were considered, and only insertions with a read coverage ≥ 4 were included into the analysis. The karyoplot gives an overview of the insertion sites across the entire genome (Figure 36). Generally, the insertions were spread out across all chromosomes, although two exceptions occurred. Firstly, more transposons seemed to have jumped into chromosome two. Since this chromosome served as initial donor locus, this could be a possible explanation for this observation. Secondly, less insertions were detected in chromosome Y, since approximately half of the analyzed cohorts were female mice.

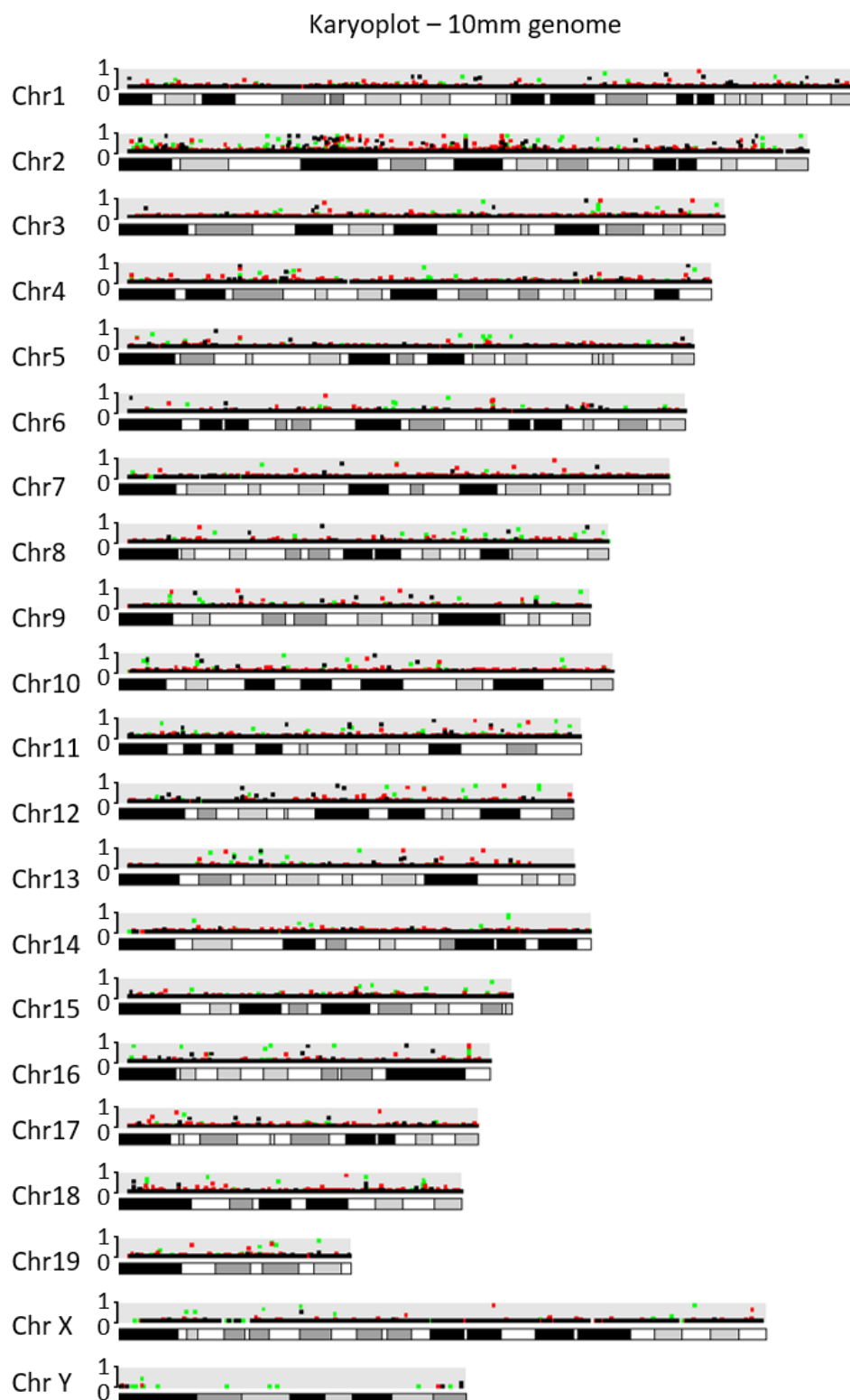


Figure 36 Overview of the ATP2 insertions is shown in a karyoplot. The basic scaffold shows all murine chromosomes and builds the x-axis of the graph to indicate at which position a transposon inserted. The y-axis of the graphs indicates the relative read coverage, therefore the higher a dot is positioned, the more relevant and dominant is this specific insertion. One dot represents one insertion, overlap between the genotypes is possible due to graphical limitations. *CycD1//PB* is represented in green, *LC40//PB* in red and control//PB in black. Only insertions with a read coverage higher than three were considered for these calculations.

To determine which insertion sites occurred more frequently within the genome, TAPDANCE (Transposon Annotation Poisson Distribution Association Network Connectivity Environment) analysis was performed. This algorithm identifies common insertion sites (CIS), which are genomic regions that bear transposon insertions in at least two individuals of the screen. The CIS are of special interest, since these indicate which mutations are potentially tumorigenic. For the following analysis, the size of a CIS covered 30k bp. The region chr2: 100630604-103694219 was excluded from the analysis since it is the transposon donor locus. Additionally, the CIS locus of the *sfi1* gene on chromosome 11 was excluded since it is a known artificial site (Rad *et al.*, 2010). The number of CIS had a high variance between the individual samples (Figure 37). Surprisingly, the entire cohort of LC40//PB mice had a rather low number of CIS per sample in comparison to *cycD1*//PB and control//PB mice. For the LC40//PB cohort, the individual with the highest number of CIS counted 21 CIS, while the individual with the highest CIS number of the *cycD1*//PB group had more than 250 CIS and the control//PB a bit more than 100 CIS. Generally, the individuals of LC40//PB cohort contain more than 21 insertions, but these did not appear in other mice, thus these were not shared and no CIS. Furthermore, the LC40 genotype is able to develop lymphoma in the absence of transposon-induced mutations, therefore less insertions might be necessary for the lymphoma development in this genotype compared to the other two. Few samples of the *cycD1*//PB and control//PB samples also had a small number of CIS. Reason for this might be that aggressive tumor drivers were initially hit e.g. *ikzf3* was hit in sample 40376 of the *cycD1*//PB group. One sample (41269) had only transposon insertions, that were not shared with other splenic samples, thus zero CIS are indicated in this case.

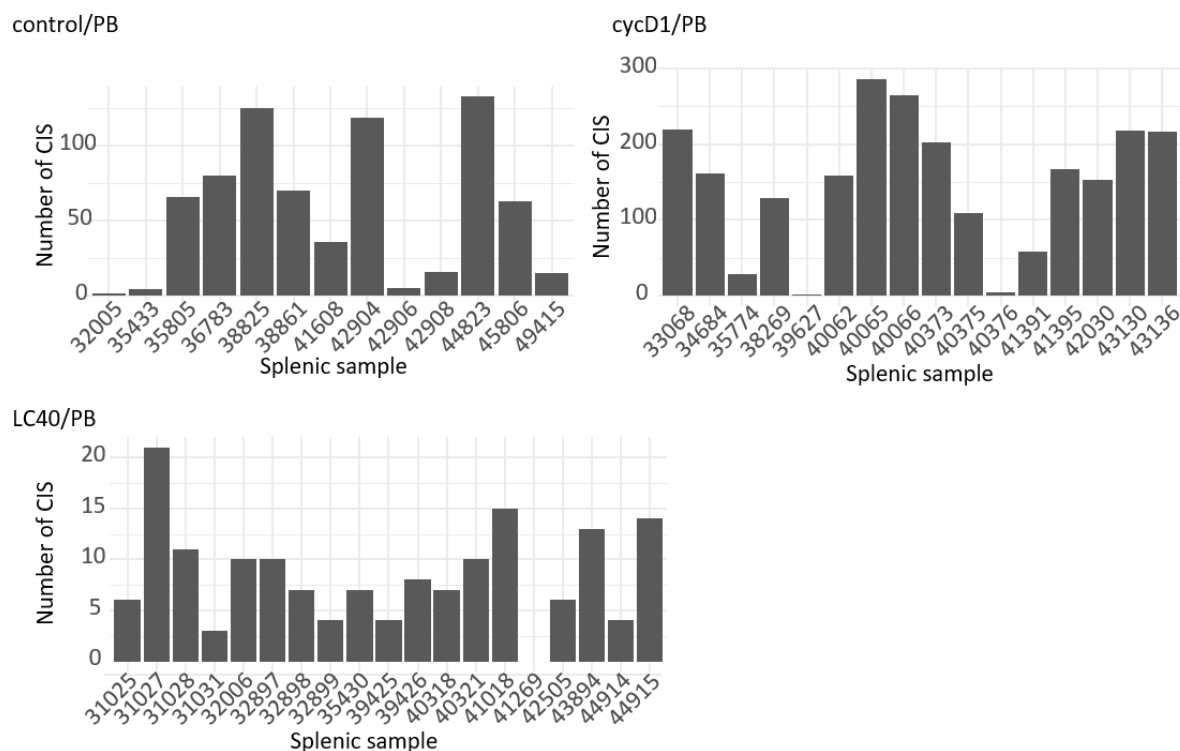


Figure 37 Numbers of common insertion site (CIS) for each splenic sample is given. The different samples are indicated with their identifier number. According to the genotype samples are grouped into three respective graphs. The indicated number serves as identifier for each individual. Only insertions with a read coverage ≥ 4 were accounted.

To select which gene was hit within a CIS region, the UCSC Genome Browser is a helpful tool, since it indicates the insertion position, orientation, and number within a genomic region. In case the UCSC Genome Browser did not clearly pinpoint to one gene, the normalized read coverage of genes within the respectable CIS region was analyzed. The normalized read coverage suggests which insertion is the most dominant in each sample, thus helps to select the most relevant hit gene within one gene region. Based on these analyses, the most relevant genes were selected for each CIS and heatmaps indicate the top frequently hit genes within each genotype (Figure 38). CIS which could not be allocated to a specific gene, because the transposons clustered at an intergenic region, are indicated as “intergenic”. The LC40//PB cohort had a limited number of CIS. Thus, each single CIS was analyzed for this genotype. Since the top CIS of the genotypes cycD1//PB and the control//PB were chosen based on how frequently they appeared in different samples, the hit genes had a huge overlap between samples. No specific pattern, which might indicate that certain genes excluded each other, could be observed in these two genotypes.

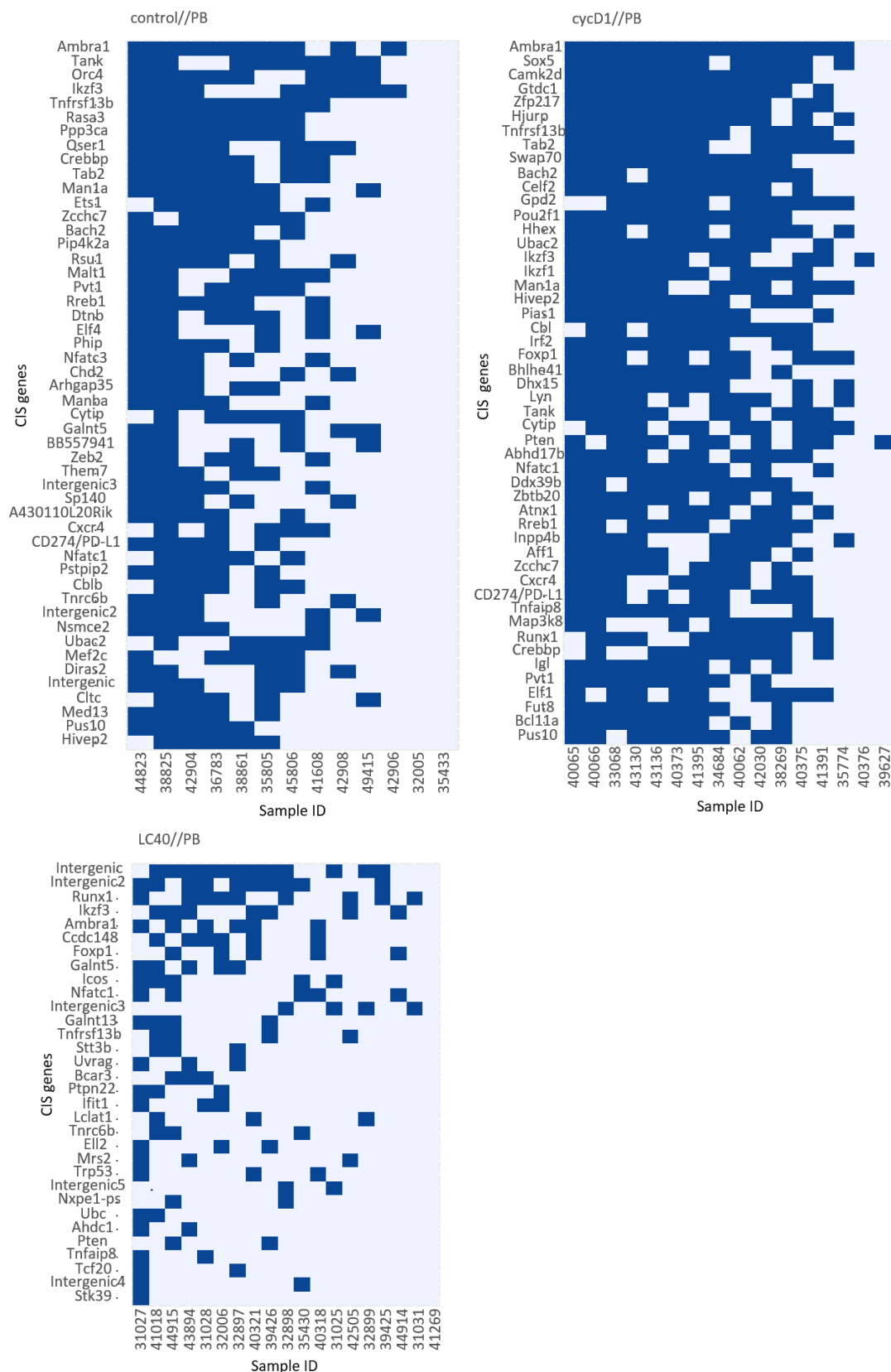


Figure 38 Heatmaps of top hits are represented in separate tables for control//PB, cycD1//PB and LC40//PB. If the gene is hit in a specific sample the parcel is colored in dark blue. As the LC40 genotype has a limited number of CIS, all CIS are shown. For control and cycD1//PB mice only the top 50 hits are shown. The hits are sorted by the number of samples where they occurred, while the most frequently hit gene is on top of the heatmap.

For the LC40//PB cohort, *runx1* and *ikzf3* were the most frequently hit genes and it seems that these excluded each other. While *runx1* appeared in nine samples and *ikzf3* in seven samples, they only overlapped in two samples. Genes, which were top frequently hit genes in all three genotypes were *ambra1* and *tnfrsf13b* (or TACI). A gene which seemed to be more exclusively important for lymphomagenesis in LC40//PB mice was *ccdc148*. For *cycD1*//PB, *sox5* and *hhex* were genes, which only appeared in the top hit genes of this group. *Phip*, which interestingly regulates *cycD1* transcription (De Semir *et al.*, 2018), was a top hit gene amongst the control//PB cohort.

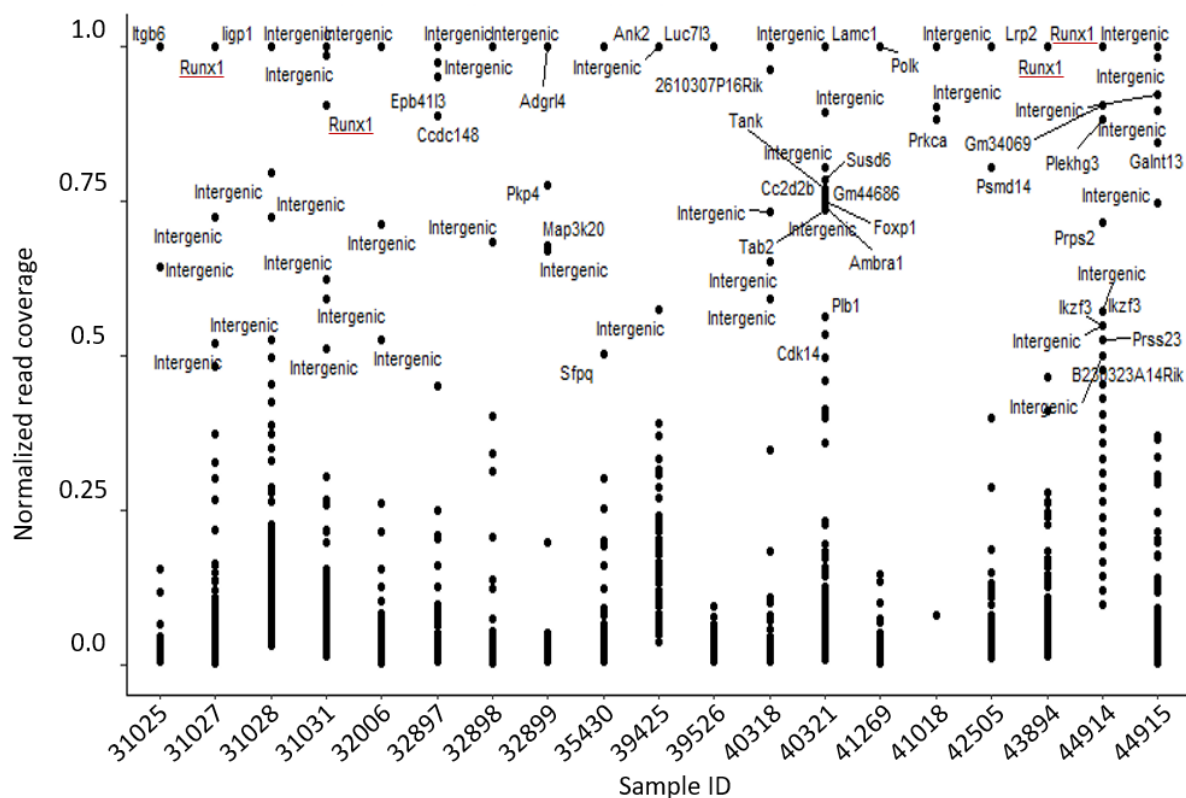


Figure 39 Normalized read coverage of all LC40//PB sample. All insertions with a read coverage higher than 3 were accounted. The normalized read coverage is determined by normalizing the read coverage against the highest read coverage of the respective sample. Each sample is represented with its unique identifier number. For insertions with a read coverage > 0.5 the gene names are indicated, if no gene is directly hit, it is indicated as intergenic. *Runx1* is underlined in red to facilitate reading.

The read coverage of an insertion gives further information, whether a gene might be an early initial tumor driver or rather plays a more important role in tumor progression. A high read coverage directly aligns with a higher cell number bearing this insertion, thus is more likely to be a dominant event appearing early. To be able to compare the read coverage between different samples, it is essential to make sure each read coverage is weighted equally and does not differ due to technical differences or the potentially different clone sizes between

samples. To achieve this, the normalized read coverages were calculated by dividing a single read coverage by the highest read coverage appearing in the according sample. Thus, the normalized read coverage serves as tool to draw a conclusion about the chronological appearance of hit genes and the tumor evolution. In Figure 39-41, the normalized read coverage of all directly hit genes are indicated for each sample. Genes with a normalized read coverage above 0.5 were defined as genes with a high normalized read coverage and their names are given in the graphs. For the LC40 cohort *runx1* had a high normalized read coverage in four out of 19 samples (Figure 39). Hence, *runx1* was a very dominant hit gene and was potentially an initiator of the disease. Considering that *runx1* did not occur as a gene with a high normalized read coverage in the control//PB cohort and only in one sample of the cycD1//PB group, it seemed that *runx1* was of special importance for lymphomagenesis in the LC40 background.

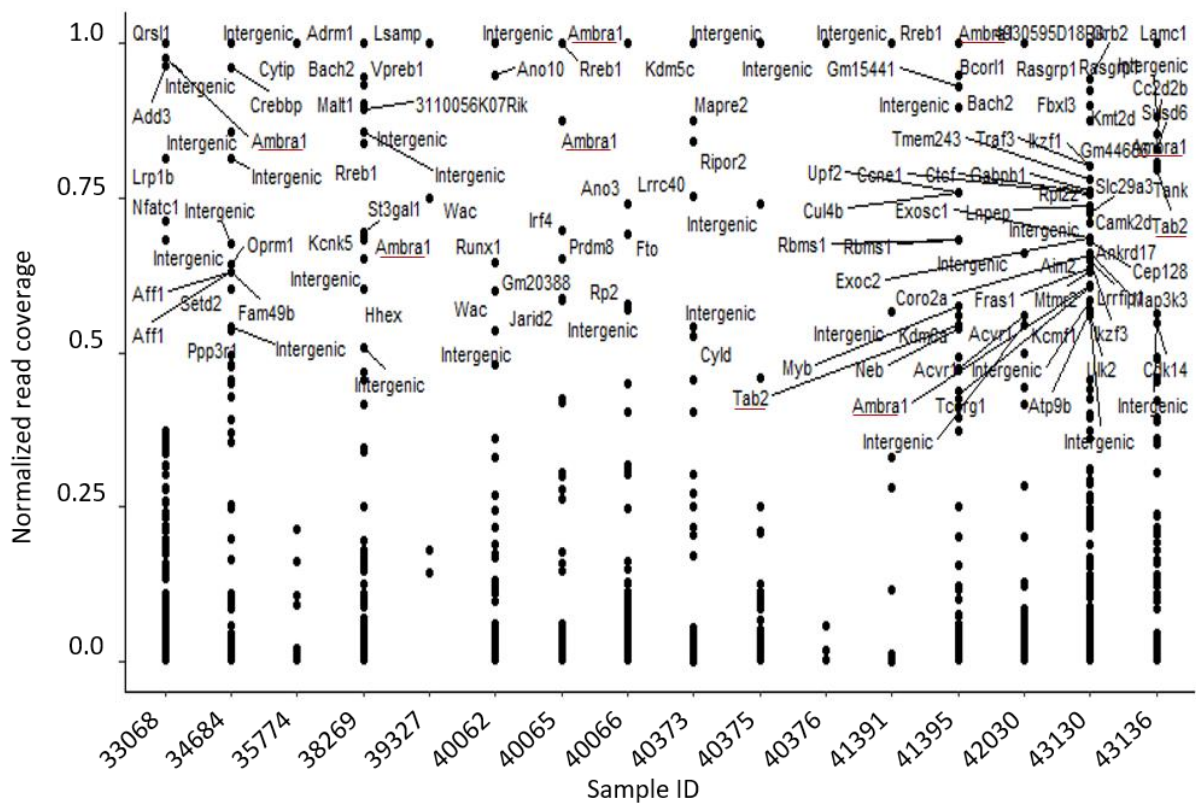


Figure 40 Normalized read coverage of all *cycD1*//PB samples. All insertions with a read coverage higher than 3 were accounted. The normalized read coverage is determined by normalizing the read coverage against the highest read coverage of the respective sample. Each sample is represented with its unique identifier number. For insertions with a read coverage > 0.5 the gene names are indicated, if no gene is directly hit, it is indicated as intergenic.

For the *cycD1*//PB group, the frequently hit genes *ambra1* and *tab2* appeared with a high normalized read coverage in several samples, which leads to the conclusion that those two could potentially be early mutations in lymphomagenesis. Genes, which are frequently hit

genes, but do not have a high normalized read coverage, are usually mutations promoting the late stages of lymphoma. Interestingly, *tnfrsf13b* (or TAC1) is frequently hit, but not amongst the genes with a high normalized read coverage (Figure 40). Hence, it is more likely that this TNFR is a gene that was hit at a later stage of tumor development and favored further tumor expansion.

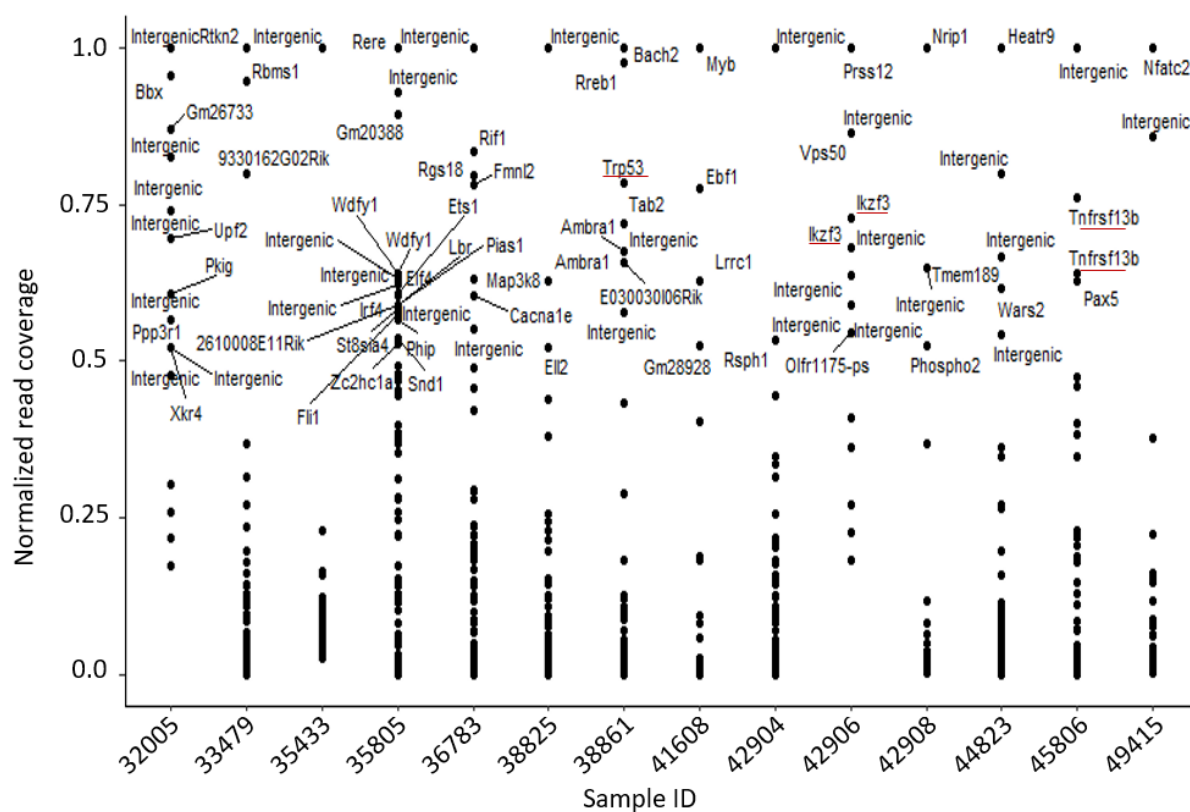


Figure 41 Normalized read coverage of all control//PB samples. All insertions with a read coverage higher than 3 were accounted. The normalized read coverage is determined by normalizing the read coverage against the highest read coverage of the respective sample. Each sample is represented with its unique identifier number. For insertions with a read coverage > 0.5 the gene names are indicated, if no gene is directly hit, it is indicated as intergenic.

For the control//PB cohort barely any targets appeared as common initial driver genes, as the genes with a high read coverage were mostly unique in the different samples (Figure 41). Amongst the genes with a high normalized read coverage were e.g. genes as *trp53*, *ikzf3* and *tnfrsf13b*, though all only exist as high read coverage genes in one single sample.

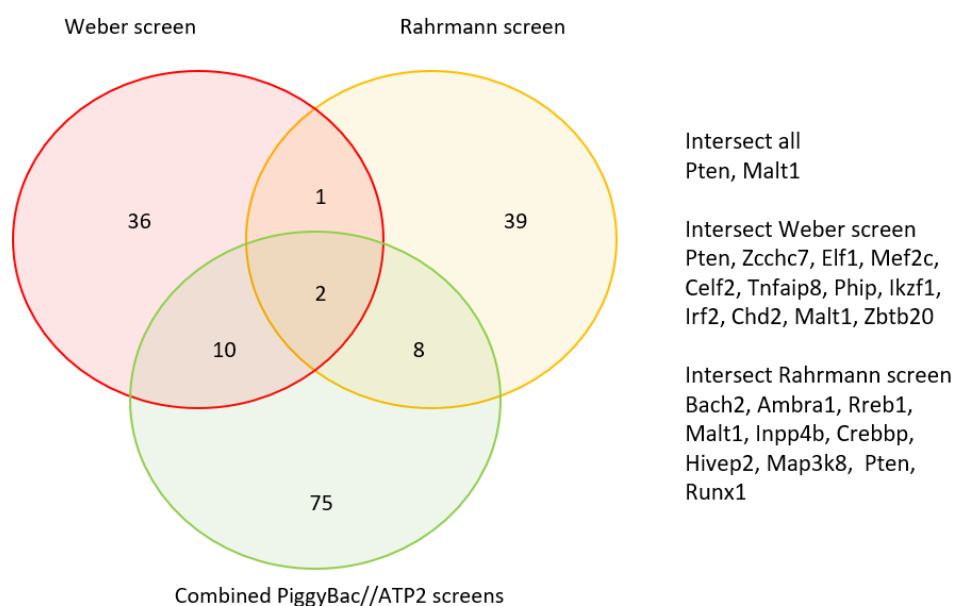


Figure 42 The Venn diagram displays the intersection between the PB screen of this thesis and two screens performed by Weber *et al.* and Rahrman *et al.* 2 top hit genes appear in all three screens. The intersecting genes between our PB//screen and the Weber *et al.* screen, as well as our screen and the Rahrman *et al.* screen are indicated on the right. The 75 top targets not intersecting with another screen are indicated in red in Fig 41.

Naturally, it is of interest which new driver genes could be discovered by our transposon screen and were not unraveled by former studies yet. Therefore, the frequently hit genes of all three genotypes were combined and compared to the top 50 hits of published screens (Rahrman *et al.*, 2019; Weber *et al.*, 2019). In the Weber screen, Blm^{m3} mice, which have an increased rate of loss of heterozygosity, were combined with the PB transposase. Due to the transposon design, only tumor suppressors were detected in this screen. Therefore, the intersecting genes of our PB//ATP2 screen and the Weber screen are mainly of an inactivating nature and more likely to be tumor suppressors. In the Rahrman screen, the transposon had a gene activating and inactivating capacity, thus both tumor suppressors and oncogenes were discovered. This study differs from ours, as they used Sleeping Beauty (SB) as transposase. Furthermore, their screen analyzed 7 mice, which had a trans-genetically inhibited *trp53* mutation and 23 mice, which had no further transgenic modification apart from the SB system. Therefore, the Rahrman screen differs from ours concerning the used transposase and partially also in the additional transgene, which was combined with the transposon system. The overview of the comparison of the three screens is given in a Venn diagram (Figure 42). It is shown that some genes were hit in all three screens, therefore these genes induced lymphoma regardless of the genetic background. Additionally, many frequently hit genes only appeared in one screen. This is most likely due to the different experimental set-up and proves

that transposon-based mutagenesis revealed cancer drivers which are specifically important in a certain genetic background. Additionally, this comparison indicates that 75 genes of your transposon screen were no top hit genes in the other studies, and we could identify new cancer drivers. These 75 genes are marked in red in the overview of the molecular function of the top hit genes in our study (Figure 43).

Gene	Present in genotype	CR	Sig	TR	RM	Oth	Gene	Present in genotype	CR	Sig	TR	RM	Oth
A430110L2							Lyn	Cy					
20Rik	Ctrl						Malt1	(Cy,) Ctrl					
Abhd17b	Cy						Man1a	Cy, Ctrl					
Aff1	Cy						Manba	Ctrl					
Ahdc1	L						Map3k8	Cy, (Ctrl)					
Ambra1	L, Cy, Ctrl						Med13	Ctrl					
Arhgap35	Ctrl						Mef2c	Ctrl					
Atnx1	Cy						Mrs2	L					
Bach2	Cy, Ctrl						Nfatc1	L, Cy					
BB557941	Ctrl						Nfatc3	Ctrl					
Bcar3	L						Nsmce2	Ctrl					
Bcl11a	Cy						Nxpe1-ps	L					
Bhlhe41	Cy						Orc4	Ctrl					
Camk2d	Cy						Phip	Ctrl					
Cbl	Cy						Pias1	Cy, (Ctrl)					
Ccdc148	L						Pip4k2a	Ctrl					
CD274	Cy, Ctrl						Pou2f1	Cy					
Celf2	Cy						Pstip2	Ctrl					
Chd2	Ctrl						Ppp3ca	Ctrl					
Cltc	Ctrl						Pten	L, Cy					
Crebbp	Cy						Ptpn22	L					
Cxcr4	Cy, Ctrl						Pus10	Cy, Ctrl					
Cytip	Cy, Ctrl						Pvt1	Cy, Ctrl					
Ddx39b	Cy						Qser1	Ctrl					
Dhx15	Cy						Rasa3	Ctrl					
Diras2	Ctrl						Rreb1	Cy, Ctrl					
Dtnb	Ctrl						Rsu1	Ctrl					
Elf1	Cy						Runx1	L, Cy					
Elf4	Ctrl						Sox5	Cy					
Ell2	L, (Ctrl)						Sp140	Ctrl					
Ets1	Ctrl						Stk39	L					
Foxp1	L,Cy, (LC40)						Stt3b	L					
Fut8	Cy						Swap70	Cy					
Galnt13	L						Tab2	Cy, Ctrl					
Galnt5	L, Ctrl						Tank	Cy, Ctrl, (LC40)					
Gpd2	Cy						Tcf20	L					
Gtdc1	Cy						Them7	Ctrl					
Hhex	Cy						Tnfaip8	L, Cy					
Hivep2	Cy, Ctrl						Tnfrsf13b*	L, Cy, LC40					
Hjurp	Cy						Tnrc6b	L, Ctrl					
Icos	L						Trp53	LC40					
Ifit1	L						Ubac2	Cy, Ctrl					
Igl	Cy						Ubc	L					
Ikzf1	Cy						Uvrag	L					
Ikzf3	L, Cy						Zbtb20	Cy					
Inpp4b	Cy						Zcchc7	Cy, Ctrl					
Irf2	Cy						Zeb2	Ctrl					
Lclat1	L						Zfp217	Cy					

CR = chromatin regulation
 Sig = signaling
 TR = transcriptional regulation
 RM = RNA metabolism
 Oth = other/unkown

Figure 43 This table indicates the general molecular function of all top hit depicted in the heatmaps of Fig32. Genes were written in red when they did not intersect with the top hits of the Rahrman et al. and Weber et al. screen. Additionally, it is indicated in which genotypes the CIS appear. Genotypes noted in brackets hits which have a normalized read coverage of >0.5 in a least one sample of the respective genotype and therefore might be as well important for lymphomagenesis although these were not amongst the top hit genes. The human gene database and DAVID Bioinformatics Resources 6.8 (Huang DW) were mainly used for primary literature research about the single hits. Tnfrsf13b is an exception as it does not appear in the 50 hits of the Rahrman or Weber

screen, but the Rahrman screen as a less frequent hit gene, but codependent on the Trp53 inhibition. Thus, Tnfrsf13b is marked with a star.

To give an impression what basic molecular function the top hit genes have, literature research was performed. The overview is provided in a table and most genes play a role in signal transduction or transcriptional regulation (Figure 43). To draw a conclusion whether a gene is a tumor suppressor or an oncogene, the insertion pattern must be analyzed. For the genes *pten*, *ambra1*, *tab2*, *tnfrsf13b*, *runx1*, *ccdc148* and *sox5*, the insertion pattern is schematically depicted in Figure 44. *Pten* and *ambra1* are already known tumor suppressors, thus these were chosen to serve as a proof of principle that we can discover relevant driver genes in the performed PB transposon screen. For both genes, the transposon insertions were distributed randomly in the entire gene locus and were in sense as well as anti-sense direction. Thus, the transposon insertion pattern suggests that both genes were inactivated by the transposons. *Tab2*, *ccdc148* and *sox5* were selected, because these genes were not described in one of the other transposon screens and unique frequently hit genes of our screen. For *tnfrsf13b* it has to be noted that it did not appear in the most frequently hit genes of the other transposon screen but appeared in the Rahrman screen as a less frequently hit gene with a dependency on the *tpr53* inhibition. Nevertheless, *tnfrsf13b* was not exclusive to our screen, it is of special interest, as it is a TNFR which activates similar pathways as CD40. Both, *tab2* and *tnfrsf13b* showed a rather activating insertion pattern, because insertions happened to be in the first intron upstream of a second transcription start site. Most insertions were in sense orientation. Insertions, which were in anti-sense could be rather irrelevant because these were upstream of the transcription start site, thus did not inactivate gene transcription, or only had a very low read coverage and could be a random bystander insertion of little importance. *Tab2* was a relevant hit gene for the control//PB and the *cycD1*//PB cohort, while *tnfrsf13b* was a target in all three, although it occurred more often in control//PB and *cycD1*//PB mice. *Ccdc148* was a frequently hit gene exclusive for the LC40//PB group. The insertion pattern indicates that this gene got inactivated and therefore was most likely a tumor suppressor. For the *cycD1*//PB cohort, *sox5* is an exclusive top hit gene, which got inactivated, thus most likely also had a tumor suppressor function. *Runx1* was already discovered in the Rahrman screen, but was also chosen for further description, since it is the top frequently hit gene for the LC40//PB and *cycD1*//PB cohort and also one of the most dominant tumor drivers for LC40//PB mice. Accordingly, *runx1* seems to be of special interest in the context of B cell lymphoma receiving a constitutive CD40 activation. *Runx1* had a more

complex pattern, but since the insertions were more randomly distributed and appeared in both directions it was most likely an inactivating mutation (Figure 44). In conclusion the transposon-based mutagenesis screen identified new lymphoma drivers.

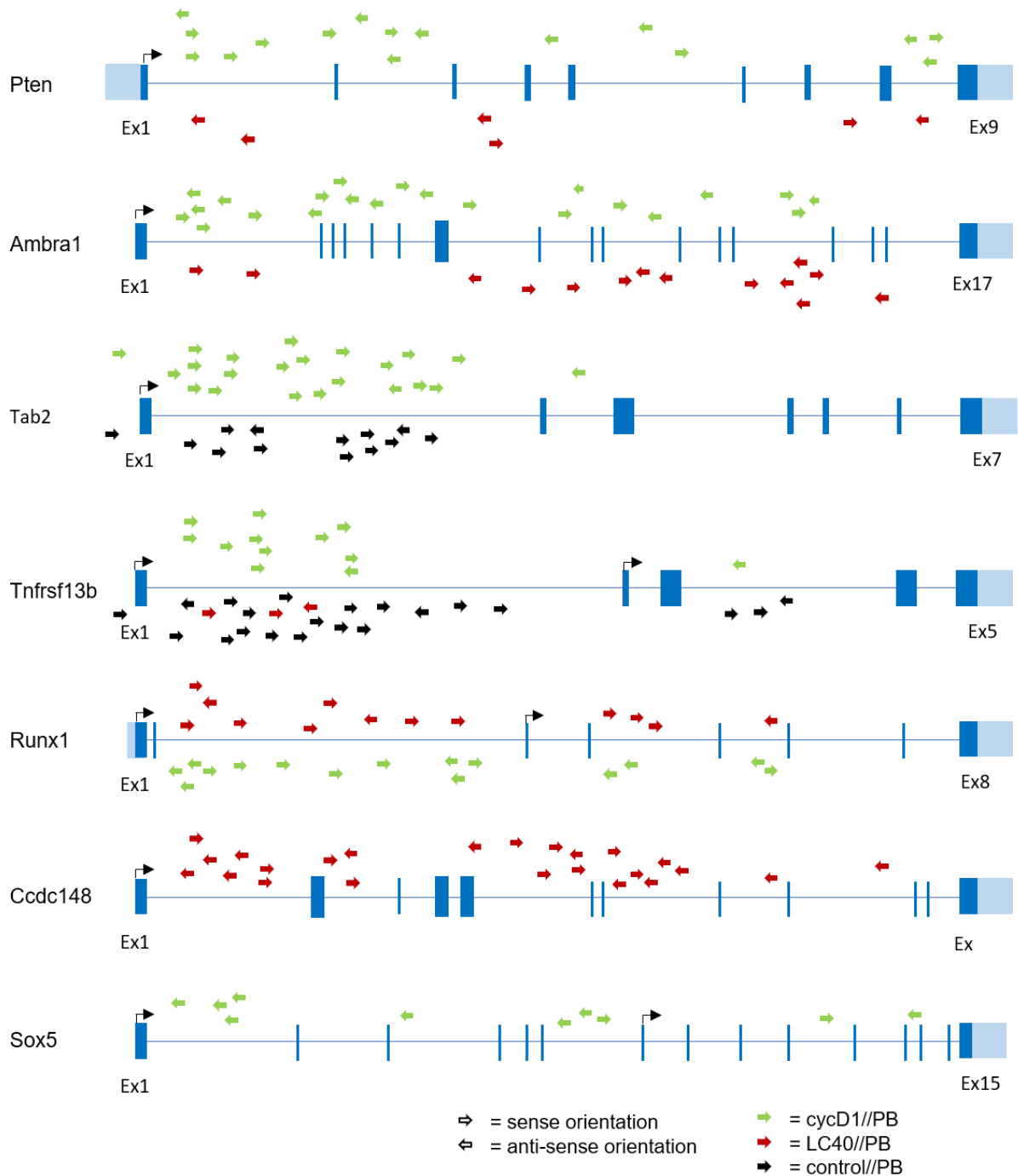


Figure 44 Transposon insertion pattern for selected genes derived from the USCS Genome Browser. *Pten* and *Ambra1* are shown as known tumor suppressors in B cells. *Tab2* and *tnfrsf13b* (or *taci*) depict the transposon insertion pattern of an activated gene. The transposon insertion pattern for *Runx1*, *ccdc148* and *sox5* pictures an inactivating pattern. Each arrow represents one insertion with a read coverage higher than 3. The insertions of the control//PB cohort (black) are not indicated for *Ambra1*, since it is similar to *cycD1*//PB (green) and *LC40*//PB (red).

4. Discussion

To date, there are first line therapeutic options for most B cell lymphoma entities however, treatments for patients with refractory lymphomas remains elusive. Therefore, further research is required to better understand this disease and to be able to provide a satisfactory treatment for all future patients.

The objective of this thesis was to investigate the evolution of pre germinal center B cell lymphoma. As a central mouse model, LC40 mice were used, since these mice lack germinal centers in their spleen, show a B cell expansion and an indolent B cell lymphoma development. To unravel the influence of the non-canonical NF- κ B signaling on the B cell lymphoma development in LC40 mice, the lymphoma incidence was compared between RELB-deficient and RELB-proficient LC40 mice. Further, the transcriptional profile of B cells derived from LC40 and RelBKO//LC40 mice were compared to elucidate NF- κ B regulated genes which contributed to lymphoma development.

Moreover, CD40 signaling accelerates the tumor progression of MCL. Therefore, it was investigated whether the combination of a CYCD1 overexpression, the hallmark of MCL, and the constitutive CD40 signaling (*cycD1*//LC40 mice) is a suitable model to study MCL development in mice.

Finally, it was of high interest to discover secondary mutations, which are involved in the lymphomagenesis of a chronic CD40 activation. Since, the combined effect of a chronic CD40 signaling and CYCD1 overexpression on lymphomagenesis was investigated, it was of an additional interest to understand which mutations apart from CD40 advance the lymphoma development of MCL with a *cycD1* hallmark mutation. For this objective a close to random mutagenesis was induced by the PiggyBac system and combined with either LC40 mice or *cycD1* mice.

4.1. Role of non-canonical NF- κ B signaling to B cell lymphoma

LC40 mice are a well-established model to study the influence of chronic CD40 activation on lymphoma development. B cell lymphoma developed by these mice manifest a CD23⁻, CD21⁻, CD43⁺, B220^{low}, partially CD5⁺ and IgM⁺ immune phenotype. An aberrant B cell population of the same immune phenotype starts to grow out at the age of six month (Zapf, 2017). This led to the hypothesis that this aberrant B cell population is the premalignant B cell population

mediating lymphoma development. In this work, transplantation of the sorted premalignant B cell population, but not of the remaining normal B cells into NSG mice gave rise to tumors. Thus, further evidence is provided that the development of B cell lymphoma in LC40 mice originate from a slowly growing premalignant, aberrant B cell population. Further B cells of LC40 mice receive a chronic activation of the non-canonical NF- κ B pathway prompting in splenic weight increase, a B cell expansion and upregulation of CD95, ICAM and CD80 in young mice (Hömig-Hölzl, 2008). Thus, the non-canonical NF- κ B pathway was prognosed to have a high contribution to lymphomagenesis induced by chronic CD40 signaling. Therefore, my previous colleagues Kristina Stojanovic and Stefanie Zapf crossed RelBKO mice with LC40 mice to establish mice bearing constitutive CD40 activated B cells with a disruption of the non-canonical NF- κ B signaling pathway. They could show that the inhibition of the non-canonical NF- κ B pathway diminished the elevated B cell expansion and splenic weight of young LC40 mice, although it was still increased compared to controls. Moreover, the premalignant, aberrant B cell population was also detected in young RelBKO//LC40, but grows out slower than in LC40 mice, leading to a decreased age-related splenomegaly in RelBKO//LC40 mice compared to LC40 mice. The combined data of Stefanie Zapf and I revealed that aged RelBKO//LC40 mice had 25% fewer clonal B cell expansion than LC40 mice an observed time course of ~1.5 years. Therefore, we conclude that the inactivation of RelB resulted in 25% reduced tumor risk. Our observation that the activation of the NF- κ B signaling pathway promotes B cell expansion and lymphoma aligns with other studies. Transgenic mice overexpressing NIK or a non-degradable mutant of NIK display B cell hyperplasia due to an activation of the non-canonical NF- κ B pathway (Sasaki *et al.*, 2008). Additionally, the B cell specific deficiency of TRAF3 – a negative regulator of the non-canonical NF- κ B pathway – results in B cell lymphoma development in mice (Moore *et al.*, 2012). Moreover, the constitutive activation of the non-canonical NF- κ B signaling also favors the development of canine ABC-DLBCL, since the activity of non-canonical NF- κ B signaling is upregulated in primary canine DLBCL samples and siRNAs directed against *relB* induced apoptosis in a canine DLBCL cell line (Seelig *et al.*, 2017). In addition, the non-canonical NF- κ B pathway also has an oncogenic capacity in humans, since a TRAF3 deletion frequently coexists with a BCL6 dysregulation in about 15% of all DLBCL patients (Zhang *et al.*, 2015). Moreover, *relB* was detected as an oncogenic driver in human primary mediastinal large B-cell lymphoma by whole exome sequencing (Mottok *et al.*, 2019). Thus, hyperactivation of the non-canonical

NF- κ B pathway appears to be an oncogenic driver in several species pointing to its central role in tumor development. Therefore, it seems highly likely that an inactivation of the non-canonical NF- κ B pathway via inactivation of RELB might result in a similar reduction of lymphoma development as shown for RelBKO//LC40 mice compared to LC40 mice.

Although the tumor risk is reduced and the lymphoma development is delayed, RelBKO//LC40 mice still do develop lymphoma. In these cases, the immunophenotype and the immunohistopathologic characteristics look similar to tumors of LC40 mice. Thus, other pathways must also contribute to the lymphoma development of these mice. Recently, a study showed that the deletion of *nfkbie* – an inhibitor of the NF- κ B p50-p65 and p50-c-REL complexes –also induces indolent B cell lymphoma with an immunophenotype of CD21⁻, CD23⁻, CD43⁺, B220^{low} and occasionally CD5⁺ (Della-Valle *et al.*, 2020). This immunophenotype also resembles the immunophenotype of lymphomas arising in LC40 mice and RelBKO//LC40 mice, therefore it may be possible that the canonical NF- κ B signaling pathway may be the driving force of the remaining tumor risk of RelBKO//LC40 mice.

Since the premalignant, aberrant B cell population already appears at an age of six months, it might be possible that young LC40 mice have a predisposition to develop lymphoma probably caused by the hyperactivation of the non-canonical NF- κ B pathway. This aligns with decreased splenic weight and B cell numbers in young RelBKO//LC40 compared to LC40 mice. Several RELB-regulated genes may contribute to the development of lymphoma in LC40 mice. One example is CD95, which is lower expressed on B cells of RelBKO//LC40 mice compared to B cells from LC40 B cells, but still higher compared to control B cells. CD95 (or Fas), is classically known to induce apoptosis in cancer cells (Trauth *et al.*, 1989) and was even declared to have a tumor suppressor function (Peng *et al.*, 1996). In contrast to this, recent studies indicate that CD95 is also able to mediate pro-survival signals (Guégan and Legembre, 2018) and if B cells receive an antigen specific survival signal via the BCR or an antigen-independent signal via CD40 they are rescued from CD95 induced apoptosis (Koncz and Hueber, 2012). Furthermore, CD95 promotes growth of chemo-resistant tumor cells (Ametller *et al.*, 2010) and induces cancer stemness via STAT1-dependent type one interferon signaling in human breast cancer or squamous carcinoma (Qadir, 2017). Additionally, it was not possible to trigger apoptosis via CD95 in 90% of B cell acute lymphoblastic leukemia (Karawajew, 1997). Hence, the role of CD95 in cancer development is highly complex and considering that its upregulation in LC40

RelB-proficient B cells aligns with the higher lymphoma incidence of these mice, it could be possible that CD95 escapes the CD95 mediated apoptosis and even supports tumor outgrowth in this genetic background. Moreover, the RELB-dependent upregulation of ICOS-L surface expression could be confirmed in LC40-expressing B cells. Additionally, it was discovered that the inactivation of RELB in LC40-derived B cells even leads to a significant reduction compared to control B cells. Regarding that ICOS-L is essential for B cells to interact with follicular T helper cells (Weinstein *et al.*, 2014), the RELB-dependent upregulation on LC40 derived B cells aligns with the preferred location of LC40 relB-proficient B cells in B cell follicles. Thus, the RELB-dependent upregulation of the activation marker CD95 and ICOS-L on B cells derived from LC40 mice might contribute to their increased B cell expansion and location site.

While B cells of LC40 mice are trapped in their B cell follicles in the spleen and lymph nodes and have reduced B cell numbers in blood, bone marrow and peritoneal cavity, knocking out relB in LC40 mice replenishes the B cell numbers in blood, bone marrow and the peritoneal cavity back to control levels. In the spleen and the lymph nodes the inactivation of RelB reduces the B cells numbers compared to the numbers in LC40 mice (Stojanovic, 2013; Zapf, 2017). Thus, the non-canonical pathway might also contribute directly or indirectly to B cell migration. Therefore, the RNASeq comparing the gene expression between B cells of young RelBKO//LC40 and LC40 mice was screened for genes involved in B cell migration and especially for genes that might promote lymphomagenesis. Generally, more genes were upregulated in LC40 derived B cells than in RelBKO//LC40 derived B cells, which might be due to the diminished activation B cells of RelBKO//LC40 mice receive compared to B cells of LC40 mice. For the selected targets CD85k (or LiLRB4), IL9R, CNR1, RHBDF1 and CXCR7 (or ACKR3) qPCR could validate their higher expression in B cells of LC40 mice than in B cells of RelBKO//LC40 mice. Additionally, qPCR revealed that the inactivation of RELB in LC40 derived B cells brings the expression level back to the level of control B cells. In the following the potential involvement of the selected top *relB*-dependently upregulated genes is further discussed.

CXCR7 - a protein involved in lymphocyte migration - is attracted by CXCL12 and thereby omits the migratory capacity of CXCR4 (Humpert *et al.*, 2014). B cells in CXCR4-deficient mice migrate better into splenic follicles, hence the upregulated CXCR7 may indirectly explain why B cells of LC40 mice are trapped inside B cell follicles by a decreased sensitivity to CXCR4.

Moreover, the CXCR7 upregulation and loss of CXCR4 is detectable on MALT lymphoma patient sample and correlates with the disease progression (Deutsch *et al.*, 2013). This provides evidence that CXCR7 upregulation is not only important for B cell migration but also involved in lymphoma development. In conclusion, CXCR7 might be a reason why B cells in LC40 mice are trapped in the B cell areas of the white pulp, which is an environment where they receive constant stimulation and eventually mutate to malignant cells.

Earlier data revealed, that in vitro anti-CD40 stimulation of murine B cells leads to an upregulation of CNR1 (Noe *et al.*, 2000). In this work it is shown, that CNR1 is upregulated via the non-canonical NF- κ B signaling pathway. Potentially, CNR1 may play a role in B cell migration, as CNR1 facilitates the adhesion of murine, encephalitogenic T cell in inflamed brain vessels in vivo (B. Rossi *et al.*, 2011). Since CNR1 is upregulated on B cells of LC40 mice and these B cells are trapped in their B cell follicles, it could be hypothesized that CNR1 might have a similar effect on B cell adhesion in B cell follicles as for encephalitogenic T cell in inflamed brain vessels. Further CNR1 is also upregulated in MCL (Islam *et al.*, 2003). Interestingly, the CNR1 upregulation in MCL patients can be correlated to SOX11 expression. In SOX11⁺ MCL cases, CNR1 is upregulated, while CNR1 is barely upregulated in SOX11⁻ MCL patients (Wasik *et al.*, 2014). The small fraction of patients being SOX11⁻ and having a hypermutated Ig are classified as leukemic non-nodal MCL, while the SOX11⁺ MCL cases belong to the classic MCL entities and reside within lymph nodes (Swerdlow *et al.*, 2016). In conclusion, the upregulation of CNR1 in the SOX11⁺ classic entities of MCL might also be a reason why these cells stay within the lymph nodes and do not migrate into other lymphoid organs as the leukemic non-nodal MCL subtype, which has no upregulation of CNR1. Therefore, it is likely that the RELB-dependent upregulation of CNR1 in B cells of LC40 mice, is partially responsible for their preferred location within B cell follicles of the spleen and lymph nodes.

One of the newly discovered *reB*-dependent upregulated genes is CD85k (or LILRB4, ILT3). Apart from the mRNA expression, its *reB*-dependent upregulation induced by CD40 stimulation could also be shown on protein level. In general, CD85k belongs to an inhibitory receptor family (LILRs) bearing a long cytoplasmic tail consisting of variable sets of immunoreceptor tyrosine-based inhibitory motifs (Cheng *et al.*, 2011). It is expressed on dendritic cells (DC), monocytes, and macrophages. While CD85k expression could not be detected on healthy human B cells, it was observed on CD5⁺ neoplastic B cells of CLL patients

(A. Colovai *et al.*, 2007). Besides, stimulation of CD85k in patient derived CLL cells inhibits the activation of the Akt pathway and CD85k was already detectable on CLL progenitors (Zurli *et al.*, 2017). Thus, the expression of CD85k on LC40 derived B cells but not on B cells from RelBKO//LC40 mice could potentially serve as an early indicator for the higher lymphoma risk of LC40 mice compared to RelBKO//LC40 mice. In tumor cells, it is generally discussed that LILRs prevent T cell priming to help cancer cells evading anti-tumor immune responses (Anderson and Allen, 2009). Moreover, soluble CD85k induces the in vitro differentiation of human CD8⁺ T suppressor cells which inhibit T cell activity against allographic tumor transplants (Suciu-Foca *et al.*, 2007). Therefore, it may be possible that lymphoma cells or their progenitors benefit from expressing CD85k by inducing the differentiation of CD8⁺ T suppressors cells which helps them to escape immune surveillance. Since the CD85k expression is dependent on RelB, this may explain why RelBKO//LC40 mice have a decreased lymphoma burden.

The IL9R is composed of the IL9R α -chain and the common γ -chain, which exists also in other interleukin receptors. Its signal transduction involves JAK1 and JAK3 activating the signal transducer and activation transcription factors STAT-1, STAT-3 and STAT-5 (Bauert *et al.*, 1998; Hornakova *et al.*, 2009). Further, this receptor is able to activate ERK MAP kinase signaling (Demoulin *et al.*, 2003) and has the potential to regulate NF- κ B signaling (Richard *et al.*, 1999). Several studies discovered an overexpression of IL9 or IL9R in T cell lymphoma, and B cell diseases as CLL and DLBCL (Lv *et al.*, 2013; Chen *et al.*, 2014; Vieyra-Garcia *et al.*, 2016). In all three lymphoma types, IL9R signaling promotes tumor growth and in DLBCL it is even involved in supporting drug resistance (Lv *et al.*, 2016). Further, IL9 provokes the in vivo expansion of CD5⁺ and preferentially CD5⁻ B1 cell populations (Vink *et al.*, 1999). As the outgrowth of the aberrant population in the LC40 and RelBKO//LC40 mice resembles a B1 cell like phenotype, it might be possible that IL9R directly supports the outgrowth of this premalignant tumor population. Since B cells of RelBKO//LC40 mice do not express the IL9R and therefore did not show a proliferative response after IL9 stimulation, this might be a reason for the delayed and reduced tumor development in RelBKO//LC40 mice compared to LC40 mice. Additionally, a higher percentage of IL9 expressing Th cells was detected in LC40 mice compared to control or RelBKO//LC40 mice. This aligns with the discovery that patients suffering from B cell Non-Hodgkin lymphoma have higher IL9 levels in their sera than healthy controls. Further the same study revealed that neutralizing IL9 inhibits tumor growth of A20 murine lymphoma

transplants in mice (Feng *et al.*, 2011). This study explained that IL9 does not only trigger the tumor growth, but also declines the numbers of regulatory T cells, which might mediate anti-tumor immunosuppression. In our experimental set up the premalignant B cells from LC40 have an upregulation of IL9R and more IL9 expressing Th cells, thus this may promote the tumor development in both ways. Firstly, the direct growth advantage of the increased IL9R levels and secondly, the potential decrease of an anti-tumor immune reaction. In addition, this hints to a positive feedback loop between B and T cells, leading to an increased B cells expansion due to an increased availability of the stimulation reagent and a higher receptor density on the responding cell. Furthermore, IL9 - provided by T follicular helper cells - drives germinal center (GC) development (Wang *et al.*, 2017) and its receptor signaling participates in the regulation of the humoral recall response of memory B cells (Takatsuka *et al.*, 2018). Interestingly, LC40 and RelBKO//LC40 mice are unable to form GCs (Stojanovic, 2013). In literature it is described, that CD40 stimulation is required to initiate the GC formation, but also must cease to successfully form GCs. Thus, B cells of LC40 and RelBKO//LC40 mice might be blocked in forming GCs because the CD40 signal cannot be switched off. Additionally, LC40 derived B cells had IL9R upregulated in a relB-dependent manner but are unable to proceed their natural development. Thus, these trapped pre-germinal center stage cells receive IL9R-induced proliferation and eventually manifest mutations leading to lymphoma.

In conclusion, the B cell lymphoma development of LC40 is dependent on the non-canonical NF- κ B signaling pathway. Thereby, the RELB regulated genes such as IL9R, CD85k may contribute to lymphoma development.

4.2. CycD1//LC40mice as a Mantle Cell Lymphoma (MCL) model

The characteristic hallmark mutation of MCL is a *CYCD1* overexpression due to a translocation of the *cycD1* gene to the IgH locus, occurring during early B cell development. Another common feature of conventional MCL is its low number of IGHV mutations, because it is bypassing the germinal center and barely undergoes somatic hypermutation. This indicates its pre-germinal center origin. The *CYCD1* overexpression on its own is not sufficient to induce lymphoma development but further secondary mutations must be acquired at later B cell stages. Functionally, these secondary mutations can be involved in DNA repair, cell cycle progression or cell apoptosis, thus the disease is highly diverse in its genetic profile (Jares, Colomer and Campo, 2007; Puente, Jares and Campo, 2018). One of the many secondary

factors advancing MCL progression is CD40 activation. In vitro CD40 stimulation of MCL cell lines and MCL cells directly derived from patients promotes cell cycle progression and proliferation (Andersen *et al.*, 2000; Castillo *et al.*, 2000). Additionally, further in vitro studies, indicate that CD40 stimulated MCL cell lines develop chemoresistance to the BTK-inhibitor ibrutinib by activating NF- κ B signaling (Rauert-Wunderlich *et al.*, 2018b). Since patients who develop ibrutinib resistance have a poor overall survival, and the induction of its resistance is linked to CD40 stimulation, it is of high interest to further investigate the function of CD40 in MCL. Up to date no suitable mouse model was available to study the influence of CD40 signaling on MCL. Single mutant LC40 mice already share several features of MCL as they do not form germinal centers and develop indolent lymphoma. Tumor cells derived from LC40 mice have a similar immunophenotype as MCL, since these are CD23⁻, often IgM⁺, and partially CD5⁺ (Hömig-Hölzel *et al.*, 2008; Aqil *et al.*, 2018). Therefore, *cycD1* mice were crossed to LC40 mice to receive mice bearing the initial MCL hallmark *CYCD1* overexpression and a B cell specific constitutive CD40 activation. B cells of double mutants did not show any immune phenotypical differences to single mutant LC40 neither at a young age nor at an aged stage. Both transgenic mice evolved the CD21⁻, CD23⁻, B220^{low}, often IgM⁺ and occasionally CD5⁺ aberrant lymphoma population. Another study revealed, that transgenic mice which harbor a *CYCD1* overexpression and produce an autoreactive BCR give rise to MCL like neoplasms with the same immunophenotype (Hayakawa *et al.*, 2018). This provides further evidence that LC40 and *cycD1*//LC40 derived lymphomas can be classified as MCL-like according to their immune phenotype. Since LC40 mice already had the immune phenotype of MCL, the *CYCD1* overexpression probably could not further push the immune phenotype towards MCL. BCR sequencing could reveal, that *cycD1*//LC40 mice developed clonal expansions at a slightly younger age than LC40 mice, and the splenic weight as well as the B cell expansion was more pronounced than in single LC40 mice. *CYCD1* might accelerate lymphomagenesis by promoting cell cycle progression (Du, Tong and Ye, 2013). Further, constitutively nucleic *CYCD1* decreases genome stability and contributes to tumor induction (Aggarwal *et al.*, 2009). Therefore, it

seems that CYCD1 overexpression accelerated the tumor development of LC40 mice leading to the conclusion that cycD1//LC40 mice could serve as a potential mouse model for MCL.

4.3. Influence of the strain background on lymphoma development in LC40 mice

The prior investigations comparing RelBKO//LC40 and LC40 mice were performed in a BALB/c background and therefore were continued in this background. The EμCycD1 as well as the PiggyBac transposase and ATP2 transposon mice were obtained in a C57BL/6 background. Additionally, the C57BL/6 background is used more often in genetic screens than the BALB/c background, therefore the PB transposon screen and investigations about the combined effect of an CYCD1 overexpression in LC40 mice were both carried out in a C57BL/6 background. Since single transgenic LC40 mice with a C57BL/6 background served as a control group in both studies, LC40 with both backgrounds were analyzed. Interestingly, it appeared that LC40 with a C57BL/6 background did not show the same age-related splenomegaly and lymphoma development as it was detected in LC40 with a BALB/c background. As the monoclonal expansion in the C57BL/6 cohort was determined by BCR sequencing and in the BALB/c cohort by Southern Blot, it was not possible to directly compare the lymphoma incidence. Strikingly, the LC40 mice with a mixed C57BL/6 and BALB/c background and reach a lymphoma incidence of 60% (Hömig-Hölzel *et al.*, 2008), instead of 100% in the pure BALB/c background. Thus, it is likely that the tumor expansion must be dependent on the genetic background. Generally, it is known, that classic laboratory inbred strains contain various single nucleotide polymorphisms (SNPs) and sequencing revealed that BALB/c mice differ in about 3.9×10^6 SNPs from C57BL/6 mice (Keane *et al.*, 2011). These genetic differences can lead to a variation in their phenotypes, though as the number of SNPs is very high it is difficult to pinpoint which SNPs are relevant. BALB/c mice have a defect in DNA double strand break repair mechanism, particularly in non-homologous end joining compared to C57BL/6 mice (Okayasu *et al.*, 2000). Therefore, it is likely that secondary mutations manifest faster in a BALB/c background than a C57BL/6 background. Moreover, ATM-deficient mice with a BALB/c background develop T cell lymphoma faster than ATM-deficient mice with a C57BL/6 background (Genik *et al.*, 2014). As ATM is a serin kinase involved in the initiation of DNA-repair, this gives another example of BALB/c mice having a higher likelihood to establish mutations and therefore might be more prone to develop lymphoma. In the regard on MCL, the BALB/c background might be even more favorable, as ATM-deficiency occurs in combination with CYCD1 overexpression in ~50%

of MCL cases and contributes to pre-germinal center lymphoma in mice (Yamamoto *et al.*, 2015).

4.4. New drivers of B cell lymphoma development

A major task of this thesis was to investigate new oncogenic drivers in initiation and progression of B cell lymphoma. To reach this goal, the PiggyBac (PB) transposon system was used to randomly induce mutations, that aggravate B cell expansion and therefore cancer. The transgenic mice containing the conditionally activated PB transposase activated by CD19-Cre and the ATP2 transposons were crossed with *cycD1*, LC40 or wildtype mice. While the screening of *cycD1*//PB mice should identify secondary mutations involved in MCL, the screening of LC40//PB mice should discover genes supporting the lymphomagenesis of LC40 mice and control//PB mice served as a control to decide whether a gene generally induces lymphoma or is specific for LC40 or *cycD1* dependent B cell lymphoma development. Generally, the transposon-based mutagenesis induced lymphoma in control and *cycD1*//PB mice and could accelerate the tumor development in LC40//PB mice compared to single mutant LC40 mice. Interestingly, the LC40//PB cohort had a limited number of common insertion sites (CIS), compared to *cycD1*//PB and control//PB mice. This might be due to the oncogenic potential that chronic CD40 signaling has on its own, thereby requiring fewer secondary mutations for lymphoma development. In the performed PB transposon screen most genes are involved in signal transduction or gene regulation e.g. transcription factors. This was also observed in other transposon screens in example in the studies published by Weber *et al.*, and Rahrman *et al.* Nevertheless, our screen could unravel 75 genes not ranking in the most frequently hit genes of these two screens. This demonstrates the power of transposon screens for the identification of new oncogenic drivers. The unique newly identified target genes potentially might be due to a different experimental set-up and also due the additional transgenes the *cycD1*//PB and LC40//PB mice had in our screen. Moreover, by comparing which genes intersect in these screens, targets which have a more generic oncogenic power and are less dependent on the different genetic background can be identified. Among those intersecting genes are e.g. *pten*, *malt1*, *runx1* and *ambra1*, which also appeared in all three genotypes of our screen. The targets *tab2*, *ccdc148*, *tnfrsf13b* and *sox5* were new frequently hit genes in our screen. Therefore, their potential contribution to lymphomagenesis is described in more detail below. *Runx1* is not a newly identified gene, but it is the most frequently hit gene and a rather early appearing gene in the LC40//PB group.

Since this group had generally fewer CIS, *runx1* must be of special importance for CD40-induced lymphomagenesis and was selected for further description in the next paragraph.

The runt-related transcription factor 1 (RUNX1) was hit by transposons in an inactivating pattern in *cycD1//PB* and *LC40//PB* mice. Therefore, RUNX1 is more likely to have a tumor suppressor function in MCL and CD40 induced B cell lymphoma. Of special note is the high normalized read coverage *runx1* yielded in several LC40 samples. Thus, *runx1* is not only a top CIS in this genotype, but also has the potential to be one of the initial drivers of CD40-induced lymphoma. Generally, RUNX1 is a master transcription factor and coordinates DNA demethylation by recruiting the DNA demethylation machinery in hematopoietic cells (Suzuki *et al.*, 2017). Moreover, it contributes to the survival and development of early B cell progenitors and the transition to the late pre-B cell stage of B cell development (Niebuhr *et al.*, 2013). The hematopoietic-specific double knock-out of RUNX1 and RUNX3, induced by poly-inosinic-polycytidylic acid, results in a disrupted hematopoiesis and bone marrow failure in 82% of all mice. Within the remaining 12% this double knock-out mediated leukocytosis due to a defective DNA repair which facilitates leukemia development (Wang *et al.*, 2014). Further, RUNX3 represses the expression of RUNX1 in human B cells and this RUNX1 downregulation mediates proliferation of EBV-transformed B cells (Spender *et al.*, 2005; Brady *et al.*, 2009). The EBV latent membrane protein 1 (LMP1) signaling is functionally like a constitutively activated CD40 signaling and both induce proliferation (Kilger *et al.*, 1998). Thus, it could be speculated that RUNX1 might mediate proliferation in constitutively activated B cells – like LC40 derived B cells - in the same manner. In conclusion, RUNX1 might contribute to the lymphomagenesis in LC40 derived B cells by promoting proliferation.

A unique top CIS for the *LC40//PB* cohort was the coiled-coil domain containing protein 148 (CCDC148). Currently, its function is unclear. It is hypomethylated in T helper cells of patients suffering from Chronic Fatigue Syndrome (Ekua W Brenu, 2014) and it is potentially involved in the restless leg syndrome (Akçimen *et al.*, 2020). Currently, CCDC148 has not been described in the context of B cell lymphoma context, thus it is a perfect example of the power of transposon-based cancer screens, as new unknown targets arise attention, which might help to further understand lymphoma development in future. As the insertion pattern is in an inactivating manner, *ccdc48* is more likely to be a tumor suppressor.

TAK1-Binding Protein 2 (TAB2) is a regulatory subunit of the TAK1 kinase complex and facilitates the TAK1 signal transduction by binding to the K63 ubiquitin chain of TRAF6 (Kanayama *et al.*, 2004). Thus, TAB2 activates MAP kinase signaling and NF- κ B signaling (Shi and Sun, 2018). Furthermore, SUMOylation of TAB2 leads to an impaired formation of the TAK1 kinase complex and downregulates MAP kinase and NF- κ B signaling activity (Gu *et al.*, 2020). Since TAB2 has a close relationship with TAK1, it is interesting to see, that inhibition of TAK1 results in increased death of ABC-DLBCL and is even able to vanquish ibrutinib resistance (Wu *et al.*, 2019). As the potential of TAK1 inhibition is achieved by inhibiting the chronic NF- κ B activation, TAB2 might be another target to receive similar result. In the PB transposon screen *tab2* was hit in an activating pattern in the *cycD1*//PB and control//PB groups. Thus, TAB2 seems to have an oncogenic function, which aligns with the general oncogenic potential of increased NF- κ B signaling.

Another interesting target activating NF- κ B signaling is TNFRSF13B (or TACI), which induces isotype switching in B cells and is expressed by plasma cells (Castigli *et al.*, 2005; Tellier and Nutt, 2017). Additionally, TNFRSF13B is involved in the regulation of BAFF mediated B cell survival (Smulski *et al.*, 2017). In multiple myeloma, TNFRSF13B is upregulated and already discussed as a potential target for novel anti-tumor therapies (Novak *et al.*, 2004; Xu and Lam, 2020). The TNFRSF13B receptor has two isoforms and in the performed transposon-screen the shorter isoform of the gene was activated in all three genotypes, but particularly in *cycD1*//PB and control//PB mice. Both isoforms of TNFRSF13B are able to induce NF- κ B signaling by co-localizing with TRAF-6 and MyD88, but the shorter gene version has an increased capacity to bind BAFF and APRIL ligands (Garcia-Carmona *et al.*, 2018). Therefore, the shorter isoform promotes a stronger NF- κ B signaling activation than the longer isoform and has a stronger oncogenic potential. This increased oncogenic potential might be the reason why in particular the shorter isoform is activated by the transposons. Since B cells derived from LC40//PB B cells already receive a constitutive NF- κ B pathway activation via CD40 signaling, the benefit of additional stimulation via the TNFRSF13B might not be as pronounced as for B cell derived from *cycD1*//PB and control//PB mice. Thus, *cycD1*//PB and control//PB derived B cells show more activating transposon insertion for *tnfrsf13b* than LC40//PB derived B cells. Further similarities of CD40 and TNFRSF13B in lymphoma development might be their relevance in lymphoma progression. In MCL, TNFR CD40 signaling promotes drug-resistance to the Bruton's tyrosine kinase inhibitor ibrutinib and facilitates the disease progression (Rauert-

Wunderlich *et al.*, 2018a). Considering that the *tnfrsf13b* is frequently hit in many *cycD1//PB* derived samples but did not appear as a dominant insertion with a high normalized read coverage, this suggests its importance for lymphoma development at a later stage in lymphoma with a *cycD1* hallmark mutation like MCL. Therefore, the transposon-induced activation of *tnfrsf13b* provides further evidence, that TNFR mediated NF- κ B activation plays an essential role in tumor progression of lymphomas like MCL.

Generally, SRY (Sex Determining Region Y)-Box 5 (SOX5) is essential in chondrogenesis. In the performed transposon-screen *sox5* is amongst the *cycD1//PB* top CIS hits and the insertion pattern revealed an inactivating, therefore rather a tumor suppressor function. In regard of *CYCD1*, it is interesting to know that SOX5 expression regulates the exit time at the G1-S transition in neural progenitors by controlling the feedback repressor pathway via WNT signaling (Martinez-Morales *et al.*, 2010). Moreover, SOX5 serves in combination with SOX6 and SOX21 as a tumor suppressor in glioblastoma by supporting the expression of CDK inhibitors and decreased p53 protein turnover (Kurtsdotter *et al.*, 2017). In human B cells, SOX5 is highly expressed at late stages of B cell differentiation, including activated CD21^{low} B cells and atypical memory B cells. Its overexpression results in reduced proliferation and had barely any effect on plasma blast differentiation (Rakhmanov *et al.*, 2014). Furthermore, SOX5 overexpression in human multiple myeloma leads to decreased cell proliferation and an increase in apoptosis, by upregulating the protein levels of p27 and β -catenin (Edwards *et al.*, 2014). Therefore, it might be possible that *cycD1//PB* mice disrupt *sox5* to increase their proliferative potential and enhance lymphomagenesis.

In conclusion the PB transposon screen identified known oncogenic drivers and new candidates involved in lymphoma development and with a further detailed analysis of this data it will be possible to detect more new regulatory elements affecting lymphoma development. For the target validation identified in LC40//PB, the LC40 lymphoma cell, which was generated after transplantation experiments of LC40 derived B cells in NSG mice could be a helpful tool.

5. Material and Methods

5.1. Mouse strains

CD19-Cre

The Cre-recombinase was inserted into the B cell specific CD19 locus (Rickert, Roes and Rajewsky, 1997). If combined with transgenic systems bearing a lox-P region, the deletion efficiency in periphery B cells reaches about 95%. In this thesis the CD19-Cre line was crossed with LSL-PB mice, LMP1/CD40^{fl/fl} mice and RelB^{fl/fl} mice to create B cell specific knock-ins and knock-outs. Further CD19-Cre^{+/-} or CD19-Cre^{-/-} mice were also used as controls.

LMP1/CD40^{fl/stop}

LMP1/CD40^{fl/stop} mice were generated in the Zimmer-Strobl laboratory. The fusion protein consisting of the transmembrane part of the viral LMP1 and the intracellular part of CD40 leads to a chronic CD40 activation. This transgene was inserted into the rosa26 locus. A loxP-flanked stop-cassette was inserted before the transgene, thus expression of the transgene was induced by crossing these mice to CD19-Cre mice leading to a ligand-independent activation of CD40 signaling in B cells (Hömig-Hölzel *et al.*, 2008).

RelB^{fl/fl}

These mice were donated by Falk Weih (Fritz-Lippmann Institute, Jena). The 4th exon of the relB gene was loxP-flanked. Since the 4th exon contains the start of the homologous Rel domain, a cut out of this region induced by the Cre-recombinase leads to a dysfunctional RelB protein and a RelB knock-out (Weih *et al.*, 1995). These mice were combined with CD19 to obtain a B cell specific RelBKO. Further, these mice were crossed to LMP1/CD40//CD19-Cre mice to create the RelBKO//LMP1/CD40//CD19-Cre line, which has a B cell specific constitutive CD40 activation combined with a disruption of the non-canonical NF-κB signaling.

EμCycD1 (cycD1)

These mice were a kind gift of the Yale University (USA) and first described by Katz *et al.*, 2014. Random transgenic insertions of *cyclinD1* controlled by the Eμ promoter were inserted into the genome to induce a B cell specific overexpression of *cycD1*. These mice were crossed to LMP1/CD40//CD19-Cre mice to receive EμCycD1//LMP1/CD40//CD19-Cre (cycD1//LC40) mice or combined with the PiggyBac system for the transposon screen. Single transgenic EμCycD1 (cycD1) mice were used to one control group to study the combined effect of LMP1/CD40 and the cyclinD1 overexpression in young mice.

ATP2

ATP2 mice contain the transposons required for a transposon-based screen. Initially about 25 copies of the transposon were inserted into chr2: 100630604-103694219, which marks the donor locus. A scheme of the construct is depicted in Figure 4. Without the transposase the transposons are immobilized. Thus, these mice were crossed with LSL-PB//CD19-Cre mice to allow mobilization of the transposon induced by the PiggyBac transposase. When both components of the PiggyBac system are combined, mutagenesis and cancer is induced (Rad *et al.*, 2010). ATP2 and LSL-PB mice were kindly provided by Roland Rad (TranslaTUM, Munich).

LSL-PB

LSL-PB mice have the *piggyBac (PB) transposase* inserted into their *rosa26* locus and kindly provided by Roland Rad (TranslaTUM, Munich). To activate the transgene, the loxP-flanked stop-cassette - inserted in front of it - must be deleted by the Cre-recombinase. To perform a B cell specific transposon screen, LSL-PB mice were crossed to CD19-Cre mice. For the lymphoma screen the PiggyBac system was combined with either E μ CycD1 or LMP1/CD40 mice, to generate the cohorts E μ CycD1//LSL-PB//ATP2//CD19-Cre (cycD1//PB), LMP1/CD40//LSL-PB//ATP2//CD19-Cre (LC40//PB) and LSL-PB//ATP2//CD19-Cre (control//PB).

C57BL/6 or BALB/c

These mice were initially purchased from Charles River and used for breeding and also served as controls.

NSG

NOD scid gamma (NSG) mice are immune deficient mice, lacking B, T and natural killer cells. These mice were only used for transplantation experiments and kindly provided by Irmela Jeremias group (AHS, Helmholtz Zentrum München).

5.2. Molecular biology

5.2.1. Mouse genotyping

The first step to genotype the transgenic mice was to purify genomic DNA. Therefore, tissue from ear clippings was incubated over night at 56°C with 500 μ L lysis buffer (100 mM Tris/HCL pH8, 5 mM EDTA, 0.2% SDS, 200 mM NaCl, 100 μ g/mL Proteinase K) in a shaking Thermo Mixer. If incubation time had to be shortened to 3 h, the concentration of Proteinase K was

adjusted to 150µg/mL. After complete tissue lysis, 170µL of saturated NaCl (min. 5 M) was added to participate proteins. Following centrifugation for 10 mins at 20 000xg at 4°C, the supernatant was collected in a new tube prefilled with 500µL of 100% (v/v) isopropanol. The tube was inverted several times, centrifuged again at the same conditions and the supernatant was discarded. The DNA pellet was washed one time with 70% (v/v) ethanol, centrifuged again and the supernatant was discarded. Afterwards the DNA pellet was dried at 37°C and dissolved in 100µL TrisE (10 mM Tris pH=7.9, 1 mM EDTA) puffer while shaking at 37°C for 2-3 h in a Thermo Mixer.

Table 2 The primer sequences are given for each PCR.

PCR	Oligonucleotide	Sequence (5'-3')
CD19	Cre7	tca gct aca cca gag acg g
	CD19c	aac cag tca aca ccc ttc c
	CD19d	cca gac tag ata cag acc ag
ATP2	ATP R	gcc tta tcg cga ttt tac ca
	ATP F	ctc gtt aat cgc cga gct ac
PB	BpA 5F	gct ggg gat gcg gtg ggc tc
	Rosa 3R	ggc gga tca caa gca ata ata acc tgt agt tt
LMP1/CD40 (CD40)	CD40 PCR3	ctg aga tgc gac tct ctt tgc cat
	LMP1ex1fw1	agg agc cct cct tgt cct cta
Rosa (wildtype locus)	Rosa 60	tac tcc gag gcg gat cac aag c
	Rosa 62	ctc tcc caa agt cgc tct g
RelB	RelB-GT 1	agg ttg atg gta act ttg
	SeqTVRelB1	tcc aaa aaa acc aaa cca
	SeqTVRelB8	gtt ttc cct gct tgg ttc
CycD1	Tg F2	agt gcg tgc aga agg aga tt
	Tg R2	Cac aac ttc tcg gca gtc aa

For the second step, polymerase chain reactions (PCR) were performed to amplify modified or wildtype genes depending on the transgenic mouse strain. In the following tables the primers (Table 2 The primer sequences are given for each PCR. Table 2), program (Table 3) and recipe (Table 4) for each PCR are given. PCRs were run in thermal cyclers (Biometra) and the primers were purchased from metabion. DMSO was received from Carl Roth and all other PCR ingredients from Thermo Fisher.

Table 3 The master mix for each PCR is shown. Each value is given in μL .

Indredient	CD19	ATP2/PB	CD40	rosa	RelB	CycD1
dH ₂ o	18.55	18.35	19.65	18.4	16.85	19.6
10x Taq buffer	2.5	2.5	2.5	2.5	2.5	2.5
MgCl ₂ (50 mM)	1	1	1	1	1.5	1
dNTP (10 mM)	0.5	0.5	0.5	0.5	0.5	0.5
Primer (100 μM)	0.1	0.25	0.1	0.1	0.5	0.125
Taq polymerase (5U/ μL)	0.15	0.15	0.15	0.15	0.15	0.15
DMSO (100%)	-	-	-	0.25	1	-
DNA (5-10 ng)	2	2	1	1.5	2	1

In the last step, the amplified DNA was detected in an agarose gel electrophoresis. The gels were made of 1x TAE (40 mM Tris/HCL, 20 mM acetic acid, 1 mM EDTA pH 8.5), 5 $\mu\text{g}/\text{mL}$ ethidium bromide, and 1.5 – 2 % (w/v) agarose (Biozym). The PCR product was mixed with ready to use 6x loading dye (Thermo Fisher) and loaded on the gels. The electrophoresis was performed in chambers (PEQLAB Biotechnologie GmbH) containing 1x TAE buffer at 70 to 100 V for up to 90 mins. Since the ethidium bromide intercalated with the nucleic acids, amplified PCR products could be visualized using a UV luminescence screen (Quantum ST-4).

Table 4 The time and temperature are indicated for each step of each PCR program.

Phase	CD19	ATP2/PB	CD40	rosa	RelB	CycD1
Start	5' 95°C	30'' 98°C	5' 95°C	3' 95°C	4' 95°C	5' 95°C
Denaturation	45'' 95°C	5'' 98°C	45'' 95°C	45'' 95°C	45'' 95°C	30'' 94°C
Hybridization	45'' 57°C	5'' 58°C	45'' 55°C	45'' 58°C	45'' 58°C	30'' 61°C
Elongation	1.15' 72°C	15'' 72°C	1.15' 72°C	1' 72°C	45'' 72°C	30'' 72°C
Final elongation	10' 72°C	60'' 72°C	10' 72°C	10' 72°C	10' 72°C	10' 72°C
Cycle number	30	30	31	33	34	29

5.2.2. RNA extraction, cDNA synthesis and qPCR

If freshly purified B cells were used, they were allowed to rest for 1h at 37°C in B cell medium. The cells (0.5-1x10⁷) obtained from cell culture or freshly isolated cells were washed one time with PBS, and after centrifugation (10 mins, 4°C, 540 rcf), the supernatant was discarded. The pellet was resuspended in Trizol LS (Thermo Fisher) and vigorously vortexed 3x5 sec. After the sample was snap frozen on dry ice, it was stored at -80°C. Before starting the RNA extraction,

the pipettes and workspace were cleaned with RNA ZAP (Thermo Fisher). The sample was thawed on ice and after a 5 min incubation at RT, 200µL chloroform were added to 1 mL Trizol. The tube was inverted for 15 seconds and then incubated for 2-3 min at RT. To receive a nice phase separation, samples were centrifuged (5 min, 12000 rcf, 4°C). For RNA extraction the aqueous phase was used and processed according to the manufactures protocol of the RNeasy Mini Kit (Qiagen). Purified RNA was stored at -80°C. To obtain cDNA, the QuantiTec Reverse Transcription Kit (QIAGEN) was used according to manufacture protocol. The RNA concentration was determined by NanoDrop (PeqLab) at PeqLab), 1 µg of RNA was used and processed according to the manufacture's manual. RT qPCR was performed using the LightCycler 480 Probes Master (Roche) according to the manufacturers protocol and a LightCycler 480 II (Roche). Primers and probes were designed with the Universal Probe Library Assay Design Center provided by Roche. As reference genes served RNAPol2 and YWHAZ. In the table below the primers and probes are indicated (Table 5).

Table 5 List of primers and Roche probe number used to specifically detect the indicated target.

Target	Primer sequence (5'-3')	Roche probe number
YWHAZ	cgc taa taa tgc agt tac tga gag aga	2
	ttg gaa ggc cgg tta att tt	
RNA POL2	aat ccg cat cat gaa cag tg	69
	tca tca tcc att tta tcc acc a	
CD85k	tggagtctggtgtcattcc	69
	tgtgtttcttcacagaagcatt	
IL9R	ggacagttggcagtaagtcacc	20
	ccactctccaaggcca	
RHBDF1	aatgatcggctctgggtgtgt	63
	ctaggatgaacgggccact	
CXCR7	gcaagagatggccaagagac	68
	cttgaggagagcgaccaagt	
CNR1	gggcaaattcctttagca	79
	ggctcaacgtgactgagaaa	
CYCD1	ttt ctt tcc aga gtc atc aag tgt	72
	tga ctc cag aag ggc ttc aa	

5.2.3. Southern Blot

This method was used to detect monoclonal B cell expansions of RelBKO//LC40, LC40 BALB/c and control mice. In the first step the JH probe spanning the JH₄ and Eµ of the IgH locus was prepared. 10µg (about 10µL) of plasmid DNA (*Bluescript* Vector) containing this probe were digested using 2µL HindIII, 1µL EcoRI and 32µL water and 5µL 10x buffer for 2-3 hours on RT.

After the digestion the sample was loaded on a 1.5% agarose gel and the 1.6 kB fragment cut out after gel electrophoresis. To extract the probe, the Qiax II Gel Extraction Kit (Qiagen) was used according to manufacturer's manual.

Genomic DNA extraction of 1×10^7 splenocytes was performed as the DNA extraction of ear clipping described in 5.2.1. Though the protein lysis was always performed overnight for at least 10h and after the last washing step the supernatant was not discarded, but the DNA pellet was fished with a glass hook. The glass hook was directly placed into a fresh tube and after 30 mins incubation at RT to dry the pellet, the DNA pellet was dissolved in 50 μ L TE overnight at 37 °C. The genomic DNA was digested using EcoRI (50 U/ μ L Fermentas) and 1x digestion mix contained 25 μ L of genomic DNA, 3.5 μ L 10x buffer, 0.35 μ L 100x BSA, 0.1 M Spermidine, 0.15 of 10 mg/mL RNase, 2 μ L of the restriction enzyme and 3.65 μ L water. The digestion was performed for 16 h at 37 °C. The next day the samples as well as a 1kB ladder were directly loaded on a 0.8% agarose gel. The electrophoresis was performed at 50V for ~ 15h. To ensure a sufficient sample separation the gel was photographed using short waved UV-light.

Then the gel was incubated for 20 mins in freshly prepared 0.25 M HCL to depurate the DNA, followed by a washing step with deionized water and a min. 40 min incubation step in transfer buffer (0.4 M NaOH, 0.6 M NaCl) to denature the DNA. For blotting a nylon membrane (Immobilon Ny⁺ membrane, Millipore) was used and the blot was assembled as the following: 5 cm cellulose paper, 5 Whatman paper, membrane, gel, 5 Whatman paper and on top one long Whatman paper as bridge to ensure the flow of the transition buffer. The next day, the membrane was washed in 2x SSC (20x SSC stock solution: 3 M NaCl, 0.3 M NaCitrat, ad 1L water) until the membrane had a neutral pH (measured using pH paper). To fix the DNA to the membrane, the membrane was baked at 80°C for 2h. After baking the membrane was stored in the fridge until used for hybridization.

To receive a radioactively labeled probe, the Amersham Ready-to-go DNA Labeling Beads System and Amersham Rediprime II Random Prime Labelling (GE Healthcare) were used with 150 ng of probe DNA and 50 μ Ci ³²P dCTP (Hartmann Analytic) according to manufacturer's manual. To extract the radioactive fraction, the labeled probe was purified using a Sephadex column (GE Healthcare). The column was calibrated with 2 mL TE, then the sample was loaded and eluted in 1x 400 μ L and 4x 150 μ L TE. The radioactive incorporation of the fractions was

measured with the Bioscan QC 4000 XER and fractions having a value of at least 35 000 000 dpm were used. For denaturation, the radioactive probe was incubated at 95°C for 5 mins and cooled on ice for 2 mins. Afterwards, the probe was added to the membrane which had been already prehybridized in hybridization buffer (1M NaCl, 50 mM Tris (pH 7.6), 10% (w/v) Dextranulfat, 1% (w/v) SDS, 250 g denatured salmon sperm DNA/ml (Sigma Aldrich)) at 65°C overnight. To ensure a sufficient labeling the membrane was incubated at least 12h at 65°C. The next day, the membrane was washed with 0.5-1x SSC/0.1-0.5% SDS buffer at 58°C. Washing was stopped when a radioactivity of ~70 counts was measured. For development the membrane is placed with a radiosensitive film (KODAK) in a Biomax cassette and exposed for up to 1.5 days at -80°C.

5.2.4. BCR and transposon insertion site sequencing

For BCR and TRADIS sequencing a section of the spleen was cut and stored in RNAlater (Sigma) at -20°C. The following steps were performed by our collaborators in AG Rad (TranslaTUM). RNA and DNA were extracted simultaneously using the AllPrep DNA/RNA Micro Kit (Qiagen) according to manufacturer's instructions. The RNA was used to perform BCR repertoire sequencing as previously described in Weber *et al.*, 2019. In brief, cDNA was generated by using 700ng RNA and 5' template switch oligos (TSO) containing unique molecular identifiers. To introduce indexed Nextera sequencing adapters, IGHC-specific and 5'TSO-specific primers were used for the library preparation. The libraries were analyzed by Illumina MiSeq. Bioinformatic analysis of the BCR repertoire was kindly performed by Olga Baranov (TranslaTUM, Munich). The CDR3 region was used to determine clonal clusters (Weber *et al.*, 2019).

The purified DNA was used to sequence the insertion site and direction of the ATP2 transposons. Therefore, a semiquantitative insertion site sequencing (QiSeq) was performed. This method is based on splinkerette PCR. By using transposon and adaptor-specific primers, this allows an amplification of the transposon–genome junction fragments. The amplified products were sequenced and mapped to the murine genome. A very detailed description of this method is provided by Friedrich *et al.*, 2017. To determine common insertion site (CIS), TAPDANCE (Transposon Annotation Poisson Distribution Association Network Connectivity Environment) analysis was performed. To include only relevant insertions only ATP2 insertions with a read coverage ≥ 4 were included.

5.2.5. RNA sequencing

Purified B cells were resuspended in Trizol and snap frozen. RNA extraction and sequencing were performed at the Laboratory of Functional Genome Analysis (LAFUGA, Gene Center Munich). Bioinformatic analysis was performed by Lothar and Daniel Strobl. For further information please contact them.

5.3. Mouse related assays

Generally, young mice were analyzed at an age of 3-4 months and old mice were sacrificed at first signs of disease. All mice were bred and maintained in specific pathogen-free conditions. Experiments were performed in compliance with the German Animal Welfare Law and were approved by the Institutional Committee on Animal Experimentation and the government of Upper Bavaria.

5.3.1. Preparation of murine lymphocytes

Mice were euthanized with CO₂ or sacrificed by cervical dislocation. The spleens were kept in 1% B cell medium (BCM; 1x RPMI 1640 containing 1% (v/v) heat-inactivated fetal calf serum (FCS) (PAA Cell Culture Company), 100 U/mL penicillin, 100 g/mL streptomycin, 1 mM sodium pyruvate, 2 mM L-glutamine, 1x non-essential amino acids, and 52 M-mercaptoethanol (all Gibco)). To receive a single cell suspension, the spleen was mashed through a 70 µm strainer and centrifuged at 1200 rpm for 10 min at 4°C (Rotana 460-R, Hettich centrifuge). Blood was taken by direct heart punctuation of euthanized mice and directly placed into PBS with 0.5M EDTA to prevent it from clogging. To get rid of erythrocytes in splenic and blood samples, red blood cell lysis was performed resuspending the pellet with 1 mL RBC buffer (eBioscience) and incubate it at RT for 3 min. The reaction was stopped with BCM and samples were centrifuged again. For blood samples this step was repeated 3 times. To count the cells for further experiments Neubauer counting chambers and a light microscope with a phase contrast (Zeiss Axio) were used.

5.3.2. Isolation of B cells and T cells

The isolation of murine B and T cells was performed by magnetic associated cell sorting (MACS) or fluorescence associated cell sorting (FACS). To purify naïve B cells, the murine CD43 depletion kit (Miltenyi Biotec) was used. To purify B cells of tumor mice, the pan B cell kit (Miltenyi Biotec) was used and to receive CD4⁺ T cells the murine CD4⁺ T Cell Isolation Kit

(Miltenyi Biotech). All kits were used according to the manufacture's manual. For FACS sorting the FACS Aria III (Beckton Dickson) was used. The surface staining was performed as described in 5.4, except the volume of the staining mix was increased to 500 μ L. Cells were sorted into pure FCS.

5.3.3. Transplantation experiments

For transplantation experiments sterile work conditions were always ensured. For the first transplantation CD21⁻/CD23⁻ B cell population and all remaining B cells of old LC40 mice were sorted by FACS. The donor mice did not have an age-related increase of splenic weight nor did they show any signs of disease. Of each population 3x10⁶ B cells were transplanted intravenously (i.v.) into NSG mice. After 6 months the initial recipient NSG mice were sacrificed. For re-transplantation splenic B cells were purified using the pan B cell kit (Miltenyi Biotech) and 3-4.5 x10⁶ cells were transplanted i.v. into NSG mice. These mice were sacrificed after 6 weeks due to an accelerated lymphoma development.

5.4. Flow cytometry

Flow cytometry analysis was performed with the LSR Fortessa, FACS Calibur or FACS Canto (all Beckton Dickson). The analysis was done using the FlowJo10 software. Depending on the experimental set-up surface or intracellular (IC) staining was done.

5.4.1. Surface staining

For surface staining 5x10⁵-1x10⁶ cells were plated into a FACS plate (Greiner Bio One). Cells were washed with MACS buffer (Miltenyi Biotech) by centrifugation (5 min, 4°C, 1200rpm; Rotana 460, Hettich centrifuge). Afterwards, 25 μ L of the antibody mixes in MACS buffer were used to resuspend the cell pellets and incubated for at least 20 mins on ice in the dark. The used antibodies were coupled to streptavidin or the following fluorochromes: FITC, PE, PerCP, APC, Horizon V450, Brilliant Violet 421, PeCy7, eF660 or Alexa664. The antibodies are indicated in the following list (Table 7). After staining, the cells were washed with MACS buffer and resuspended in 100 μ L MACS and ready to be measured by FACS. If dead cells had to be excluded the LIVE/DEAD fixable dead cell stain (Invitrogen) was used prior to IC-staining or TOPRO-3 (1:40000, Molecular Probes) supplemented to the MACS buffer when resuspending cells for FACS analysis.

Table 6 Table of FACS antibodies indicates the clone company and from which it was purchased. The IL-9R antibody is not commercially available but gifted from Daisuke Kitamura (Tokyo).

Epitope	Clone	Company
AA4.1	AA4.1	eBioscience
B220	RA3-6B2	BD Biosciences
CD4	RM4-5	BD Biosciences
CD5	53-7.3	BD Biosciences
CD19	1D3	BD Biosciences
CD21	7G6	BD Biosciences
CD23	B3B4	BD Biosciences
CD43	S7	BD Biosciences
CD80	16-10A1	BD Biosciences
CD95	Jo2	BD Biosciences
ICAM	3E2	BD Biosciences
ICOS-L	HK5.3	eBioscience
IgM	R6-60.2	BD Biosciences
IgD	R26-46	BD Biosciences
IL9	RM9A6	eBioscience
IL9-R	N.A.	Kindly gifted from Kitamura Lab
Isotype	eBRG1	BD Biosciences
LiLRB4/CD85k	H1.1	BD Biosciences
Human CD19	HIB19	BD Biosciences
Human IL9R	AH9R7	BD Biosciences
Human isotype	27-35	BD Biosciences

5.4.2. Detection of IL-9 by intracellular FACS

For the detection of IL-9, MACS-purified CD4⁺ T cells (1×10^7 cells/mL) were incubated with 1x protein transport inhibitor cocktail (Invitrogen), ionomycin (500ng/mL) and PMA (50 ng/mL) for 4h at 37°C and 5% CO₂. Afterwards cells were washed with PBS and intracellular (IC) FACS staining was performed using the Fixation/Permeabilization Solution Kit (Invitrogen) according to manufacture manual. To exclude dead cells, the LIVE/DEAD fixable dead cell stain (Invitrogen) was used prior to IC-staining.

5.5. Cell culture

Generally, cell culture experiments were performed under a sterile workbench (Bio Flow technique), using sterile tools and expendable/sterile materials. For cell cultivation an incubator (Binder) was used at 37°C, 5% CO₂ and 95% humidity.

5.5.1. Cultivation and stimulation of murine B cells

B cells purified by CD43-depletion MACS were cultivated in flat bottom plates (Nunc). Per well $3-5 \times 10^5$ cells were plated and kept in BCM with 10% FCS. Depending on the assay cells were

stimulated with the following stimuli: anti-CD40 antibody (2,5 µg/mL, HM40-3, eBioscience), IL-4 (10 ng/mL, Sigma-Aldrich), recombinant IL-9 (10 ng/mL, eBioscience). To have cells for FACS compensations some cells were additionally stimulated with LPS (50 µg/mL, Sigma-Aldrich).

5.5.2. Cell proliferation assay

To trace cell proliferation, purified B cells were labeled with CellTrace™ CFSE Cell Proliferation Kit (Molecular Probes) according to manufactures protocol. To stop the labeling process 10% BCM was used and as soon as cells were labeled cells were kept in dark, because CFSE becomes fluorescent as soon as it entered the cell and the two acetate groups are removed (Parrish, 2010). After 24 hours, cells were analyzed by FACS to determine the undivided cell peak. Since the fluorescence intensity is halved with each cell division, cell proliferation can be tracked by FACS analysis.

5.5.3. Establishment of the LMP1/CD40 cell line

Pan B cell purified B cells derived from a re-transplantation experiment (5.3.3) were cultured in BCM containing 70% FCS. First, 1×10^6 cells were plated in 24-well plate. Cells were fed every 4 days by replace 50 % of the medium. After 2 weeks, cells were transferred into a 12 well plate and the FCS concentration was reduced to 50%. The concentration of FCS was reduced every two weeks for 10%, until the final concentration of 20% was reached and cells were split according to their growth behavior. In the end cells had a doubling of 48 hours.

5.5.4. Cultivation of feeder layer cell

A L929 mouse fibroblast cell line, which expresses the human CD40 ligand was kindly gifted from Andreas Moosmann (Helmholtz Zentrum München) and used as stimulator for primary human B cells. In the following it will be called CD40L feeder layer cells. As a control feeder layer fibroblast, which express CD32 were used. Both cell lines were cultivated in RPMI1640 – high glutamine (Gibco/Invitrogen), 10% tested FCS, Streptomycin (100ug/ml) and split 1:25 once a week using Trypsin/EDTA (Gibco).

The feeder layer cells had to be irradiated to prevent them from overgrowing the B cells in experiments. Thus, feeder layer cells were irradiated with 180 Gy. After irradiation, 1×10^6 cells were equally seeded on a 6 well plate and the plates were used the next day to stimulate human B cells.

5.5.5. Cultivation and stimulation of primary human B cells

Human primary B cells were isolated from adenoids biopsies of anonymous donors. The biopsies were a kind gift from the LMU Klinikum (Großhadern, Munich). The tissue was rinsed twice with PBS was mashed through a 100 µm strainer to receive a single cell suspension. The total volume of the suspension was added to 30 mL PBS. To get rid of T cells, 0.5 mL defibrinated sheep blood (Oxoid, Thermo Scientific) was added to the suspension and it was under layered with 15 mL Ficoll Hypaque. After the sample was centrifuged at 500 g for 30 min, the cells were carefully collected from the interphase and transferred to a new tube. For the final step, the cell suspension was washed 3x with PBS and centrifuged with decreasing sedimentation forces (450, 400 and 300 g) for 10 min each.

Purified B cells were directly seeded on fresh and irradiated CD40L feeder layer or CD32 feeder layer cells using B cell medium with 10% of tested FCS. In one 6-well well a total number of 3×10^6 B cells were seeded and harvested after 2 days.

5.6. Immunohistochemistry

A section of the spleen was cut and stored in Formalin (Sigma). The samples were embedded in paraffin, cut, and stained by the research unit Analytical Pathology at the Hemholtz Zentrum München. Staining was performed as in Sperling et al. 2019.

5.7. Western Blot and WES simple protein

To receive whole cell protein lysates, 5×10^6 purified B cells were washed twice with cold PBS and centrifuged (540 rcf, 4°C, 10 mins). Cell lysis was performed with 2x NP-40 buffer (100mM Tris pH 7.4, 300 mM NaCl, 4 mM EDTA, 2% (v/v) NP40) supplemented with a protease inhibitor (1/7, Mini Complete Tabs Roche) and phosphatase inhibitors (1/100, Halt Phosphatase-Inhibitor Cocktail Pierce). The lysis was performed for 30 mins on ice, while the tube was vigorously vortexed for 15 seconds every 5 mins. Afterwards, the samples were centrifuged (15.000 rpm, 4°C, 15 min) in a table centrifuge (Eppendorf). The supernatant which contained the free protein was collected in a new tube and stored at -80°C.

To receive nuclear protein fraction, the NE-PER Kit (Thermo Scientific) was used according to the manufacturer's instructions. Samples were also stored at -80°C.

The protein concentration was determined in a Bradford assay (BioRad-Reagent, DC Protein Assay) according to manufacturer's instructions. The protein samples were thawed on ice, and

1 μ L of sample was mixed with 799 μ L water and 200 μ L reagent and incubated for ~20mins in the dark at RT. To be able to quantify the absorption at 600 nm, samples were filled in cuvettes (Plastikbrand). To be able to calculate the protein concentration a standard curve with a determined BSA concentration had been performed in parallel.

For classic Western Blot SDS pre-casted pages (10% acrylamide, Biorad) were used. 15 μ g of the protein extracts were mixed with 5x Laemmli buffer (300 mM Tris pH = 6.8; 75 % (w/v) SDS; 50 % (v/v) glycine; 0.01 % (v/v) Bromphenolblue; 1% β -Mercaptoethanol) and 1-2 μ L 1 M DTT (Fermentas). For denaturation, the samples were cooked for 10 mins at 70 °C and the samples were loaded on the gels together with a pre-stained protein ladder (Thermo Scientific). Electrophoresis was performed using the Biorad system first at 30V and after 30 mins the voltage was increased to 100V. The running buffer contained 25 mM Tris, 0.2 M glycine, 0.1 % (v/v) SDS. After the proteins were separated, they were transferred on a polyvinylidenflourid (PVDF) membrane (Immobilon P membrane, Millipore) by wet blotting in a transfer buffer (25 mM Tris, 0.2 M glycine, 20 % (v/v) methanol) at 4°C and 60mA overnight. The next day, the membrane was incubated in 5% bovine serum albumin (BSA) diluted in TBST (0.1 M Tris/HCL pH 7.5, 0.1 M NaCL, 0,02 % (v/v) Tween (Carl Roth)) for 1 h at RT to block unspecific antibody binding sites. Then the membrane was incubated with the first antibody diluted in 5% BSA TBST at 4°C overnight. The next day, the membrane was washed 3x with TBST for 5 mins at RT. The incubation with the secondary antibody was performed in 5% milk TBST for 1.5 h at RT. The used antibodies are indicated in the following table. After another 3x washing step with TBST, ECL (Enhanced Chemiluminescence ECLTM, GE Healthcare) was used for detection according to manufacturer's protocol. The chemiluminescence was detected with a Fusion (Vilber) and for quantification ImageJ was used.

Table 7 Antibodies used for Western Blot or WES protein simple. The secondary antibodies are coupled to horse radish peroxidase (HRP).

Epitope	Conjugate	Clone	Company
RelB	-	4922S	Cell Signaling
p100/p52	-	4882S	Cell Signaling
GAPDH	-	6C5	Merck millipore
Tubulin	-	2148S	Cell Signaling
Lamin B2	-	E1S1Q	Cell Signaling
Anti-rabbit	HRP	7074S	Cell Signaling
Anti-mouse	HRP	7076S	Cell Signaling

WES protein simple detection was performed to detect protein in nuclear protein fractions. This is a fully automated, capillary based Western Blot assay. The kits 12-230 kDa Jess/Wes Separation Module (protein simple) and Anti-Rabbit Detection Module (protein simple) were used according to manufacturer's instruction. For analysis the Compass Software (protein simple) was utilized.

5.8. Statistics and data analysis

Generally, GraphPad Prism 9 was used to perform statistical analysis. In the figure description is indicated which statistical test was used. The P values are indicated as ns > 0.05, * \leq 0.05, ** \leq 0.01, *** \leq 0.001, **** \leq 0.0001.

Data analysis of the PiggyBac transposon data was performed using R version 4.0.2 (2020-06-22).

6. References

- Adolfsson, J. *et al.* (2001) 'Upregulation of Flt3 expression within the bone marrow Lin-Sca1+c-kit+ stem cell compartment is accompanied by loss of self-renewal capacity', *Immunity*. Cell Press, 15(4), pp. 659–669. doi: 10.1016/S1074-7613(01)00220-5.
- Aggarwal, P. *et al.* (2009) 'Nuclear accumulation of cyclin D1 during S phase inhibits Cul4-dependent C ... Nuclear accumulation of cyclin D1 during S phase inhibits Cul4- dependent Cdt1 proteolysis and triggers p53-dependent DNA rereplication Nuclear accumulation of cyclin D1 during', 21(22), pp. 1–14. doi: 10.1101/gad.1586007.PMCID.
- Ahuja, A. *et al.* (2020) 'High levels of LINE-1 transposable elements expressed in Kaposi's sarcoma-associated herpesvirus-related primary effusion lymphoma', *Oncogene*. Springer US, 1. doi: 10.1038/s41388-020-01549-9.
- Akçimen, F. *et al.* (2020) 'Transcriptome-wide association study for restless legs syndrome identifies new susceptibility genes', *Communications Biology*. Springer US, 3(1), pp. 1–5. doi: 10.1038/s42003-020-1105-z.
- Allman, D. *et al.* (2001) 'Resolution of Three Nonproliferative Immature Splenic B Cell Subsets Reveals Multiple Selection Points During Peripheral B Cell Maturation', *The Journal of Immunology*. The American Association of Immunologists, 167(12), pp. 6834–6840. doi: 10.4049/jimmunol.167.12.6834.
- Almaden, J. V *et al.* (2016) 'B-cell survival and development controlled by the coordination of NF-κB family members RelB and cRel.', *Blood*. American Society of Hematology, 127(10), pp. 1276–86. doi: 10.1182/blood-2014-10-606988.
- Ametller, E. *et al.* (2010) 'Tumor promoting effects of CD95 signaling in chemoresistant cells', *Molecular Cancer*, 9, pp. 1–12. doi: 10.1186/1476-4598-9-161.
- Andersen, N. S. *et al.* (2000) 'Soluble CD40 ligand induces selective proliferation of lymphoma cells in primary mantle cell lymphoma cell cultures', *Neoplasia (United States)*, 9(6), pp. 2219–2226.
- Anderson, K. J. and Allen, R. L. (2009) 'Regulation of T-cell immunity by leucocyte immunoglobulin-like receptors: Innate immune receptors for self on antigen-presenting cells', *Immunology*, 127(1), pp. 8–17. doi: 10.1111/j.1365-2567.2009.03097.x.
- De Andres, B. *et al.* (1999) 'A regulatory role for Fcγ receptors (CD16 and CD32) in hematopoiesis', *Immunology Letters*, 68(1), pp. 109–113. doi: 10.1016/S0165-2478(99)00038-3.
- Anwar, S. L., Wulaningsih, W. and Lehmann, U. (2017) 'Transposable elements in human cancer: Causes and consequences of deregulation', *International Journal of Molecular Sciences*. MDPI AG, p. 974. doi: 10.3390/ijms18050974.
- Aqil, B. *et al.* (2018) 'Immunophenotypic variations in mantle cell lymphoma and their impact on clinical behavior and outcome', *Archives of Pathology and Laboratory Medicine*, 142(10), pp. 1268–1274. doi: 10.5858/arpa.2017-0368-OA.
- Bauert, J. H. *et al.* (1998) 'Heteromerization of the γ(c) chain with the interleukin-9 receptor subunit leads to STAT activation and prevention of apoptosis', *Journal of Biological Chemistry*. © 1998 ASBMB. Currently published by Elsevier Inc; originally published by American Society for Biochemistry and Molecular Biology., 273(15), pp. 9255–9260. doi: 10.1074/jbc.273.15.9255.
- Benson, R. J., Hostager, B. S. and Bishop, G. A. (2006) 'Rapid CD40-mediated rescue from CD95-induced apoptosis requires TNFR-associated factor-6 and PI3K.', *European journal of immunology*, 36(9), pp. 2535–43. doi: 10.1002/eji.200535483.

- Biram, A., Davidzohn, N. and Shulman, Z. (2019) 'T cell interactions with B cells during germinal center formation, a three-step model', *Immunological Reviews*. Blackwell Publishing Ltd, 288(1), pp. 37–48. doi: 10.1111/imr.12737.
- Bishop, G. A. and Hostager, B. S. (2003) 'The CD40-CD154 interaction in B cell-T cell liaisons', *Cytokine and Growth Factor Reviews*, 14(3–4), pp. 297–309. doi: 10.1016/S1359-6101(03)00024-8.
- Brady, G. *et al.* (2009) 'Downregulation of RUNX1 by RUNX3 requires the RUNX3 VWRPY sequence and is essential for Epstein-Barr virus-driven B-cell proliferation.', *Journal of virology*. American Society for Microbiology Journals, 83(13), pp. 6909–16. doi: 10.1128/JVI.00216-09.
- Burns, K. H. (2017) 'Transposable elements in cancer', *Nature Reviews Cancer*. Nature Publishing Group, 17(7), pp. 415–424. doi: 10.1038/nrc.2017.35.
- Busslinger, M. (2004) 'Transcriptional control of early B cell development', *Annual Review of Immunology*, 22, pp. 55–79. doi: 10.1146/annurev.immunol.22.012703.104807.
- Cai, Q. *et al.* (2017) 'NF- κ B p50 activation associated with immune dysregulation confers poorer survival for diffuse large B-cell lymphoma patients with wild-type p53', *Modern Pathology*. Nature Publishing Group, 30(6), pp. 854–876. doi: 10.1038/modpathol.2017.5.
- Campo, E. *et al.* (2011) 'The 2008 WHO classification of lymphoid neoplasms and beyond: Evolving concepts and practical applications', *Blood*. American Society of Hematology, pp. 5019–5032. doi: 10.1182/blood-2011-01-293050.
- Castigli, E. *et al.* (2005) 'TACI and BAFF-R mediate isotype switching in B cells', *Journal of Experimental Medicine*, 201(1), pp. 35–39. doi: 10.1084/jem.20032000.
- Castillo, R. *et al.* (2000) 'Proliferative response of mantle cell lymphoma cells stimulated by CD40 ligation and IL-4', *Leukemia*. Nature Publishing Group, 14(2), pp. 292–298. doi: 10.1038/sj.leu.2401664.
- Cella, B. M. *et al.* (1997) 'A Novel Inhibitory Receptor (ILT3) Expressed on', 185(10).
- Chapuy, B. *et al.* (2018) 'Molecular subtypes of diffuse large B cell lymphoma are associated with distinct pathogenic mechanisms and outcomes', *Nature Medicine*, 24(5), pp. 679–690. doi: 10.1038/s41591-018-0016-8.
- Chatzigeorgiou, A. *et al.* (2009) 'CD40/CD40L signaling and its implication in health and disease', *BioFactors*, 35(6), pp. 474–483. doi: 10.1002/biof.62.
- Chen, N. *et al.* (2014) 'Overexpression of IL-9 induced by STAT6 activation promotes the pathogenesis of chronic lymphocytic leukemia', *Int J Clin Exp Pathol*, 7(5), pp. 2319–2323. Available at: www.ijcep.com (Accessed: 31 July 2017).
- Chen, Q. *et al.* (2020) 'Structural basis of seamless excision and specific targeting by piggyBac transposase', *Nature Communications*. Springer US, 11(1), pp. 1–14. doi: 10.1038/s41467-020-17128-1.
- Cheng, H. *et al.* (2011) 'Crystal structure of leukocyte Ig-like receptor LILRB4 (ILT3/LIR-5/CD85k): A myeloid inhibitory receptor involved in immune tolerance', *Journal of Biological Chemistry*, 286(20), pp. 18013–18025. doi: 10.1074/jbc.M111.221028.
- Chiu, Y.-K. *et al.* (2014) 'Transcription Factor ABF-1 Suppresses Plasma Cell Differentiation but Facilitates Memory B Cell Formation', *The Journal of Immunology*, 193(5), pp. 2207–2217. doi: 10.4049/jimmunol.1400411.
- Colovai, A. *et al.* (2007) 'Measurement of antigen specific immune responses: 2006 update', *Cytometry Part B: ...*, 85(December 2006), pp. 77–85. doi: 10.1002/cyto.b.

- Colovai, A. I. *et al.* (2007) 'Expression of Inhibitory Receptor ILT3 on Neoplastic B Cells Is Associated with Lymphoid Tissue Involvement in Chronic Lymphocytic Leukemia', *Cytometry Part B: ...*, 85(December 2006), pp. 77–85. doi: 10.1002/cyto.b.
- Cooper, M. D. *et al.* (1966) 'The functions of the thymus system and the bursa system in the chicken.', *The Journal of experimental medicine*. The Rockefeller University Press, 123(1), pp. 75–102. doi: 10.1084/jem.123.1.75.
- Dada, R. (2019) 'Diagnosis and management of follicular lymphoma: A comprehensive review', *European Journal of Haematology*, 103(3), pp. 152–163. doi: 10.1111/ejh.13271.
- Dadgostar, H. *et al.* (2002) 'Cooperation of multiple signaling pathways in CD40-regulated gene expression in B lymphocytes', *Proceedings of the National Academy of Sciences of the United States of America*, 99(3), pp. 1497–1502. doi: 10.1073/pnas.032665099.
- Dalloul, A. (2009) 'CD5: A safeguard against autoimmunity and a shield for cancer cells', *Autoimmunity Reviews*. Elsevier B.V., 8(4), pp. 349–353. doi: 10.1016/j.autrev.2008.11.007.
- Davies, A. *et al.* (2019) 'Gene-expression profiling of bortezomib added to standard chemoimmunotherapy for diffuse large B-cell lymphoma (REMoDL-B): an open-label, randomised, phase 3 trial', *The Lancet Oncology*. Lancet Publishing Group, 20(5), pp. 649–662. doi: 10.1016/S1470-2045(18)30935-5.
- Della-Valle, V. *et al.* (2020) 'Nfkbie-deficiency leads to increased susceptibility to develop B-cell lymphoproliferative disorders in aged mice', *Blood Cancer Journal*. Springer US, 10(3). doi: 10.1038/s41408-020-0305-6.
- Demoulin, J. B. *et al.* (2003) 'MAP kinase activation by interleukin-9 in lymphoid and mast cell lines', *Oncogene*, 22(12), pp. 1763–1770. doi: 10.1038/sj.onc.1206253.
- Deutsch, A. J. A. *et al.* (2013) 'Chemokine receptors in gastric MALT lymphoma: Loss of CXCR4 and upregulation of CXCR7 is associated with progression to diffuse large B-cell lymphoma', *Modern Pathology*. Nature Publishing Group, 26(2), pp. 182–194. doi: 10.1038/modpathol.2012.134.
- Du, Z., Tong, X. and Ye, X. (2013) 'Cyclin D1 promotes cell cycle progression through enhancing NDR1/2 kinase activity independent of cyclin-dependent kinase', *Journal of Biological Chemistry*, 288(37), pp. 26678–26687. doi: 10.1074/jbc.M113.466433.
- Edwards, S. K. E. *et al.* (2014) 'Expression and function of a novel isoform of Sox5 in malignant B cells', *Leukemia Research*. Elsevier Ltd, 38(3), pp. 393–401. doi: 10.1016/j.leukres.2013.12.016.
- Ekua W Brenu, E. W. B. (2014) 'Methylation Profile of CD4+ T Cells in Chronic Fatigue Syndrome/Myalgic Encephalomyelitis', *Journal of Clinical & Cellular Immunology*, 05(03). doi: 10.4172/2155-9899.1000228.
- Farmer, J. R. *et al.* (2019) 'Induction of metabolic quiescence defines the transitional to follicular B cell switch', *Science Signaling*. American Association for the Advancement of Science, 12(604), p. 5573. doi: 10.1126/scisignal.aaw5573.
- Feng, L.-L. *et al.* (2011) 'IL-9 Contributes to Immunosuppression Mediated by Regulatory T Cells and Mast Cells in B-Cell Non-Hodgkin's Lymphoma', *Journal of Clinical Immunology*. Springer US, 31(6), pp. 1084–1094. doi: 10.1007/s10875-011-9584-9.
- Freedman, A. and Jacobsen, E. (2020) 'Follicular lymphoma: 2020 update on diagnosis and management', *American Journal of Hematology*, 95(3), pp. 316–327. doi: 10.1002/ajh.25696.
- Friedrich, M. J. *et al.* (2017) 'Genome-wide transposon screening and quantitative insertion site sequencing for cancer gene discovery in mice', *Nature Protocols*. doi: 10.1038/nprot.2016.164.

- G. Swennen, MD, A. Janssens, MD, PhD, V. Vergote, MD, S. Bailly, MD, C. Bonnet, MD, PhD, E. Van den Neste, MD, PhD, M. Maerevoet, MD, S. Snauwaert, MD, PhD, K. Saevels, MD, C. Jacquy, M. (2020) 'BHS guidelines for the treatment of newly diagnosed diffuse large B-cell lymphoma (DLBCL) anno 2020', *BELG J HEMATOL, Practice Guidelines*, 11.
- Garcia-Carmona, Y. *et al.* (2018) 'TACI isoforms regulate ligand binding and receptor function', *Frontiers in Immunology*, 9(OCT). doi: 10.3389/fimmu.2018.02125.
- Gatto, D. and Brink, R. (2010) 'The germinal center reaction', *Journal of Allergy and Clinical Immunology*. Elsevier Ltd, 126(5), pp. 898–907. doi: 10.1016/j.jaci.2010.09.007.
- Genik, P. C. *et al.* (2014) 'Strain background determines lymphoma incidence in Atm knockout mice', *Neoplasia (United States)*, 16(2), pp. 129–136. doi: 10.1593/neo.131980.
- Goswami, R. and Kaplan, M. H. (2011) 'A Brief History of IL-9', *The Journal of Immunology*, 186(6), pp. 3283–3288. doi: 10.4049/jimmunol.1003049.
- Gu, Z. *et al.* (2020) 'The SUMOylation of TAB2 mediated by TRIM60 inhibits MAPK/NF- κ B activation and the innate immune response', *Cellular and Molecular Immunology*, (April). doi: 10.1038/s41423-020-00564-w.
- Guégan, J. P. and Legembre, P. (2018) 'Nonapoptotic functions of Fas/CD95 in the immune response', *FEBS Journal*, 285(5), pp. 809–827. doi: 10.1111/febs.14292.
- Hammad, H. *et al.* (2017) 'Transitional B cells commit to marginal zone B cell fate by Taok3-mediated surface expression of ADAM10', *Nature Immunology*, 18(3), pp. 313–320. doi: 10.1038/ni.3657.
- Hampel, F. *et al.* (2011) 'CD19-independent instruction of murine marginal zone B-cell development by constitutive Notch2 signaling', *Blood*, 118(24), pp. 6321–6331. doi: 10.1182/blood-2010-12-325944.
- Harnett, M. M. (2004) 'CD40: a growing cytoplasmic tale.', *Science's STKE : signal transduction knowledge environment*, 2004(237), p. pe25. doi: 10.1126/stke.2372004pe25.
- Hayakawa, K. *et al.* (2018) 'Early Generated B-1-Derived B Cells Have the Capacity To Progress To Become Mantle Cell Lymphoma-like Neoplasia in Aged Mice', *The Journal of Immunology*, 201(2), pp. 804–813. doi: 10.4049/jimmunol.1800400.
- Hojer, C. *et al.* (2014) 'B-cell expansion and lymphomagenesis induced by chronic CD40 signaling is strictly dependent on CD19.', *Cancer research*. American Association for Cancer Research, 74(16), pp. 4318–28. doi: 10.1158/0008-5472.CAN-13-3274.
- Hömig-Hölzel, C. *et al.* (2008) 'Constitutive CD40 signaling in B cells selectively activates the noncanonical NF-kappa B pathway and promotes lymphomagenesis', *J. Exp. Med*, 205(6), pp. 1317–1329. doi: 10.1084/jem.20080238.
- Hornakova, T. *et al.* (2009) 'Acute lymphoblastic leukemia-associated JAK1 mutants activate the Janus kinase/STAT pathway via interleukin-9 receptor α homodimers', *Journal of Biological Chemistry*, 284(11), pp. 6773–6781. doi: 10.1074/jbc.M807531200.
- Hu, H. *et al.* (2011) 'Noncanonical NF- κ B regulates inducible costimulator (ICOS) ligand expression and T follicular helper cell development', *Proceedings of the National Academy of Sciences of the United States of America*, 108(31), pp. 12827–12832. doi: 10.1073/pnas.1105774108.
- Humpert, M.-L. *et al.* (2014) 'CXCR7 influences the migration of B cells during maturation', *European Journal of Immunology*. Wiley-VCH Verlag, 44(3), pp. 694–705. doi: 10.1002/eji.201343907.
- Islam, T. C. *et al.* (2003) 'High level cannabinoid receptor 1, resistance of regulator G protein signaling 13 and differential expression of Cyclin D1 in mantle cell lymphoma', *Leukemia*, 17(9), pp. 1880–

1890. doi: 10.1038/sj.leu.2403057.

J. Crombie, and A. L. (2020) 'Treatment of Burkitt lymphoma in adults', *Blood*. doi: 10.1182/blood.2019004099.

Jain, P. and Wang, M. (2019) 'Mantle cell lymphoma: 2019 update on the diagnosis, pathogenesis, prognostication, and management', *American Journal of Hematology*, 94(6), pp. 710–725. doi: 10.1002/ajh.25487.

Jares, P., Colomer, D. and Campo, E. (2007) 'Genetic and molecular pathogenesis of mantle cell lymphoma: perspectives for new targeted therapeutics.', *Nature reviews. Cancer*, 7(10), pp. 750–762. doi: 10.1038/nrc2230.

Jebb, D. *et al.* (2020) 'Six reference-quality genomes reveal evolution of bat adaptations', *Nature*. Springer US, 583(7817), pp. 578–584. doi: 10.1038/s41586-020-2486-3.

Kalisz, K. *et al.* (2019) 'An update on Burkitt lymphoma: a review of pathogenesis and multimodality imaging assessment of disease presentation, treatment response, and recurrence', *Insights into Imaging*. Springer Verlag. doi: 10.1186/s13244-019-0733-7.

Kanayama, A. *et al.* (2004) 'TAB2 and TAB3 activate the NF- κ B pathway through binding to polyubiquitin chains', *Molecular Cell*, 15(4), pp. 535–548. doi: 10.1016/j.molcel.2004.08.008.

Kaplan, B. L. F. (2013) 'The role of CB1 in immune modulation by cannabinoids', *Pharmacology and Therapeutics*. Elsevier Inc., 137(3), pp. 365–374. doi: 10.1016/j.pharmthera.2012.12.004.

Karube, K. *et al.* (2018) 'Integrating genomic alterations in diffuse large B-cell lymphoma identifies new relevant pathways and potential therapeutic targets', *Leukemia*, 32(3), pp. 675–684. doi: 10.1038/leu.2017.251.

Katz, S. G. *et al.* (2014) 'Mantle cell lymphoma in cyclin D1 transgenic mice with Bim -deficient B cells', 123(6), pp. 884–893. doi: 10.1182/blood-2013-04-499079.

Kawakami, K., Largaespada, D. A. and Ivics, Z. (2017) 'Transposons As Tools for Functional Genomics in Vertebrate Models.', *Trends in genetics : TIG*. Elsevier, 33(11), pp. 784–801. doi: 10.1016/j.tig.2017.07.006.

Keane, T. M. *et al.* (2011) 'Mouse genomic variation and its effect on phenotypes and gene regulation', *Nature*, 477(7364), pp. 289–294. doi: 10.1038/nature10413.

Kilger, E. *et al.* (1998) 'Epstein-Barr virus-mediated B-cell proliferation is dependent upon latent membrane protein 1, which simulates an activated CD40 receptor', *EMBO Journal*, 17(6), pp. 1700–1709. doi: 10.1093/emboj/17.6.1700.

Koike, T. *et al.* (2019) 'The quantity of CD40 signaling determines the differentiation of b cells into functionally distinct memory cell subsets', *eLife*. eLife Sciences Publications Ltd, 8. doi: 10.7554/eLife.44245.001.

Koncz, G. and Hueber, A. O. (2012) 'The Fas/CD95 receptor regulates the death of autoreactive B cells and the selection of antigen-specific B cells', *Frontiers in Immunology*, 3(JUL), pp. 1–12. doi: 10.3389/fimmu.2012.00207.

de Koning, A. P. J. *et al.* (2011) 'Repetitive elements may comprise over Two-Thirds of the human genome', *PLoS Genetics*, 7(12). doi: 10.1371/journal.pgen.1002384.

Kurtsdotter, I. *et al.* (2017) 'SOX5/6/21 prevent oncogene-driven transformation of brain stem cells', *Cancer Research*, 77(18), pp. 4985–4997. doi: 10.1158/0008-5472.CAN-17-0704.

Ladha, A. *et al.* (2019) 'Mantle cell lymphoma and its management: Where are we now?'

- Experimental Hematology and Oncology*. BioMed Central, 8(1), pp. 1–9. doi: 10.1186/s40164-019-0126-0.
- Lanier, L. L. *et al.* (1995) 'CD80 (B7) and CD86 (B70) provide similar costimulatory signals for T cell proliferation, cytokine production, and generation of CTL.', *Journal of immunology (Baltimore, Md. : 1950)*, 154(1), pp. 97–105. Available at: <http://www.ncbi.nlm.nih.gov/pubmed/7527824> (Accessed: 17 September 2016).
- Lenz, G. *et al.* (2008) 'Oncogenic CARD11 mutations in human diffuse large B cell lymphoma', *Science*. American Association for the Advancement of Science, 319(5870), pp. 1676–1679. doi: 10.1126/science.1153629.
- Leonard, J. P. *et al.* (2017) 'Randomized Phase II study of R-CHOP with or without bortezomib in previously untreated patients with non-germinal center B-cell-like diffuse large B-cell lymphoma', *Journal of Clinical Oncology*. American Society of Clinical Oncology, 35(31), pp. 3538–3546. doi: 10.1200/JCO.2017.73.2784.
- Li, S., Young, K. H. and Medeiros, L. J. (2018) 'Diffuse large B-cell lymphoma', *Pathology*, 50(1), pp. 74–87. doi: 10.1016/j.pathol.2017.09.006.
- Liebert, M. A. *et al.* (2002) 'the Initiation and Maintenance of CD4 1 T-Cell Proliferation after Activation with Suboptimal Doses of PHA', 21(3), pp. 137–149.
- Liu, D. *et al.* (2015) 'T-B-cell entanglement and ICOSL-driven feed-forward regulation of germinal centre reaction', *Nature*. Nature Publishing Group, 517(7533), pp. 214–218. doi: 10.1038/nature13803.
- Lv, X. *et al.* (2013) 'Overexpression of IL-9 receptor in diffuse large B-cell lymphoma', 6(5), pp. 911–916.
- Lv, X. *et al.* (2016) 'Interleukin-9 promotes cell survival and drug resistance in diffuse large B-cell lymphoma.', *Journal of experimental & clinical cancer research : CR*. Journal of Experimental & Clinical Cancer Research, 35(1), p. 106. doi: 10.1186/s13046-016-0374-3.
- Maier, H. J. *et al.* (2003) 'Critical role of RelB serine 368 for dimerization and p100 stabilization', *Journal of Biological Chemistry*. American Society for Biochemistry and Molecular Biology, 278(40), pp. 39242–39250. doi: 10.1074/jbc.M301521200.
- Martín-García, D. *et al.* (2019) 'CCND2 and CCND3 hijack immunoglobulin light-chain enhancers in cyclin D12 mantle cell lymphoma', *Blood*. American Society of Hematology, 133(9), pp. 940–951. doi: 10.1182/blood-2018-07-862151.
- Martinez-Morales, P. L. *et al.* (2010) 'SOX5 controls cell cycle progression in neural progenitors by interfering with the WNT-B-catenin pathway', *EMBO Reports*. Nature Publishing Group, 11(6), pp. 466–472. doi: 10.1038/embor.2010.61.
- Mathas, S., Hartmann, S. and Küppers, R. (2016) 'Hodgkin lymphoma: Pathology and biology', *Seminars in Hematology*, 53(3), pp. 139–147. doi: 10.1053/j.seminhematol.2016.05.007.
- Mesin, L., Ersching, J. and Victora, G. D. (2016) 'Germinal Center B Cell Dynamics', *Immunity*. Cell Press, pp. 471–482. doi: 10.1016/j.immuni.2016.09.001.
- Mesin, L., Jonatan, E. and Victora, G. D. (2016) 'Germinal Center B Cell Dynamics', *Immunity*. doi: 10.1016/j.immuni.2016.09.001.GERMINAL.
- Miliotou, A. N. and Papadopoulou, L. C. (2018) 'CAR T-cell Therapy: A New Era in Cancer Immunotherapy', *Current Pharmaceutical Biotechnology*. Bentham Science Publishers Ltd., 19(1), pp. 5–18. doi: 10.2174/1389201019666180418095526.

- Montecino-Rodriguez, E. and Dorshkind, K. (2012) 'B-1 B Cell Development in the Fetus and Adult', *Immunity*. Cell Press, pp. 13–21. doi: 10.1016/j.immuni.2011.11.017.
- Moore, C. R. *et al.* (2012) 'Specific deletion of TRAF3 in B lymphocytes leads to B-lymphoma development in mice', *Leukemia*, 26(5), pp. 1122–1127. doi: 10.1038/leu.2011.309.
- Mottok, A. *et al.* (2019) 'Integrative genomic analysis identifies key pathogenic mechanisms in primary mediastinal large B-cell lymphoma', *Blood*, 134(10), pp. 802–813. doi: 10.1182/blood.2019001126.
- Murphy, K. (2012) *Janeway's Immunobiology*. 8th edn. Garland Science.
- Niebuhr, B. *et al.* (2013) 'Runx1 is essential at two stages of early murine B-cell development', *Blood*, 122(3), pp. 413–423. doi: 10.1182/blood-2013-01-480244.
- Noe, S. N. *et al.* (2000) 'Anti-CD40, anti-CD3, and IL-2 stimulation induce contrasting changes in CB1 mRNA expression in mouse splenocytes', *Journal of Neuroimmunology*, 110(1–2), pp. 161–167. doi: 10.1016/S0165-5728(00)00349-0.
- Novak, A. J. *et al.* (2004) 'Expression of BCMA, TACI, and BAFF-R in multiple myeloma: A mechanism for growth and survival', *Blood*, 103(2), pp. 689–694. doi: 10.1182/blood-2003-06-2043.
- Nowosad, C. R., Spillane, K. M. and Tolar, P. (2016) 'Germinal center B cells recognize antigen through a specialized immune synapse architecture', *Nature Immunology*, 17(7), pp. 870–877. doi: 10.1038/ni.3458.
- Odqvist, L. *et al.* (2014) 'NFκB expression is a feature of both activated B-cell-like and germinal center B-cell-like subtypes of diffuse large B-cell lymphoma', *Modern Pathology*, 27(10), pp. 1331–1337. doi: 10.1038/modpathol.2014.34.
- Okayasu, R. *et al.* (2000) 'A deficiency in DNA repair and DNA-PKcs expression in the radiosensitive BALB/c mouse', *Cancer Research*, 60(16), pp. 4342–4345.
- Peng, B. S. L. *et al.* (1996) 'A Tumor-suppressor Function for Fas (CD95) Revealed in T Cell-deficient Mice', *J. Exp. Med.*, 184(September), pp. 6–11.
- Pillai, S. and Cariappa, A. (2009) 'The follicular versus marginal zone B lymphocyte cell fate decision', *Nature Reviews Immunology*. Nature Publishing Group, pp. 767–777. doi: 10.1038/nri2656.
- Pires, B. R. B. *et al.* (2018) 'NF-κB: Two Sides of the Same Coin', *Genes*. doi: 10.3390/genes9010024.
- Pratama, A. *et al.* (2015) 'MicroRNA-146a regulates ICOS-ICOSL signalling to limit accumulation of T follicular helper cells and germinal centres.', *Nature communications*, 6, p. 6436. doi: 10.1038/ncomms7436.
- Puente, X. S., Jares, P. and Campo, E. (2018) 'Chronic lymphocytic leukemia and mantle cell lymphoma: Crossroads of genetic and microenvironment interactions', *Blood*. American Society of Hematology, pp. 2283–2296. doi: 10.1182/blood-2017-10-764373.
- Qu, X. *et al.* (2019) 'Genomic alterations important for the prognosis in patients with follicular lymphoma treated in SWOG study S0016', *Blood*. American Society of Hematology, 133(1), pp. 81–93. doi: 10.1182/blood-2018-07-865428.
- Rad, R. *et al.* (2010) 'PiggyBac transposon mutagenesis: A tool for cancer gene discovery in mice', *Science*, 330(6007), pp. 1104–1107. doi: 10.1126/science.1193004.
- Rad, R. *et al.* (2015) 'A conditional piggyBac transposition system for genetic screening in mice identifies oncogenic networks in pancreatic cancer.', *Nature genetics*, 47(1), pp. 47–56. doi:

10.1038/ng.3164.

Rahrmann, E. P. *et al.* (2019) 'Sleeping beauty screen identifies RREB1 and other genetic drivers in human B-cell lymphoma', *Molecular Cancer Research*, 17(2), pp. 567–582. doi: 10.1158/1541-7786.MCR-18-0582.

Rakhmanov, M. *et al.* (2014) 'High levels of SOX5 decrease proliferative capacity of human B Cells, but permit plasmablast differentiation', *PLoS ONE*, 9(6). doi: 10.1371/journal.pone.0100328.

Rauert-Wunderlich, H. *et al.* (2018a) 'CD40L mediated alternative NFκB-signaling induces resistance to BCR-inhibitors in patients with mantle cell lymphoma', *Cell Death & Disease*. Nature Publishing Group, 9(2), p. 86. doi: 10.1038/s41419-017-0157-6.

Rauert-Wunderlich, H. *et al.* (2018b) 'CD40L mediated alternative NFκB-signaling induces resistance to BCR-inhibitors in patients with mantle cell lymphoma article', *Cell Death and Disease*. Nature Publishing Group, 9(2), pp. 1–9. doi: 10.1038/s41419-017-0157-6.

Razani, B., Reichardt, A. D. and Cheng, G. (2011) 'Non-canonical NF-κB signaling activation and regulation: Principles and perspectives', *Immunological Reviews*, 244(1), pp. 44–54. doi: 10.1111/j.1600-065X.2011.01059.x.

Richard, M. *et al.* (1999) 'Interleukin-9 regulates NF-kappaB activity through BCL3 gene induction.', *Blood*, 93(12), pp. 4318–4327.

Rickert, R. C., Roes, J. and Rajewsky, K. (1997) 'B lymphocyte-specific, Cre-mediated mutagenesis in mice.', *Nucleic acids research*, 25(6), pp. 1317–8. Available at: <http://www.ncbi.nlm.nih.gov/pubmed/9092650> (Accessed: 18 September 2016).

Robinson, J. E. *et al.* (2020) 'Identification of a Splenic Marginal Zone Lymphoma Signature: Preliminary Findings With Diagnostic Potential', *Frontiers in Oncology*. Frontiers Media S.A., 10, p. 640. doi: 10.3389/fonc.2020.00640.

Rodriguez-Terrones, D. and Torres-Padilla, M. E. (2018) 'Nimble and Ready to Mingle: Transposon Outbursts of Early Development', *Trends in Genetics*. Elsevier Ltd, 34(10), pp. 806–820. doi: 10.1016/j.tig.2018.06.006.

Rossi, B. *et al.* (2011) 'Inverse agonism of cannabinoid CB1 receptor blocks the adhesion of encephalitogenic T cells in inflamed brain venules by a protein kinase A-dependent mechanism', *Journal of Neuroimmunology*. Elsevier B.V., 233(1–2), pp. 97–105. doi: 10.1016/j.jneuroim.2010.12.005.

Rossi, D. *et al.* (2011) 'Alteration of BIRC3 and multiple other NF-κB pathway genes in splenic marginal zone lymphoma', *Blood*, 118(18), pp. 4930–4934. doi: 10.1182/blood-2011-06-359166.

Rothlein, R. *et al.* (1986) 'A human intercellular adhesion molecule (ICAM-1) distinct from LFA-1.', *Journal of immunology (Baltimore, Md. : 1950)*, 137(4), pp. 1270–4. Available at: <http://www.ncbi.nlm.nih.gov/pubmed/3525675> (Accessed: 17 September 2016).

Roué, G. and Sola, B. (2020) 'Management of drug resistance in mantle cell lymphoma', *Cancers*, 12(6), pp. 1–26. doi: 10.3390/cancers12061565.

Saba, N. S. *et al.* (2016) 'Pathogenic role of B-cell receptor signaling and canonical NF-κB activation in mantle cell lymphoma', *Blood*. American Society of Hematology, 128(1), pp. 82–92. doi: 10.1182/blood-2015-11-681460.

Saito, T. *et al.* (2003) 'Notch2 is preferentially expressed in mature B cells and indispensable for marginal zone B lineage development', *Immunity*, 18(5), pp. 675–685. doi: 10.1016/S1074-7613(03)00111-0.

- Sanders, V. and Vitetta, E. (1991) 'B cell-associated LFA-1 and T cell-associated ICAM-1 transiently cluster in the area of contact between interacting cells. - PubMed - NCBI', *Cellular Immunology*. Available at: <http://www.ncbi.nlm.nih.gov/pubmed/1676615>.
- Sasaki, Y. *et al.* (2004) 'TNF Family Member B Cell-Activating Factor (BAFF) Receptor-Dependent and -Independent Roles for BAFF in B Cell Physiology', *The Journal of Immunology*. The American Association of Immunologists, 173(4), pp. 2245–2252. doi: 10.4049/jimmunol.173.4.2245.
- Sasaki, Y. *et al.* (2008) 'NIK overexpression amplifies, whereas ablation of its TRAF3-binding domain replaces BAFF:BAFF-R-mediated survival signals in B cells', *Proceedings of the National Academy of Sciences of the United States of America*, 105(31), pp. 10883–10888. doi: 10.1073/pnas.0805186105.
- Seelig, D. M. *et al.* (2017) 'Constitutive activation of alternative nuclear factor kappa B pathway in canine diffuse large B-cell lymphoma contributes to tumor cell survival and is a target of new adjuvant therapies', *Leukemia & Lymphoma*, 58(7), pp. 1702–1710. doi: 10.1080/10428194.2016.1260122.
- De Semir, D. *et al.* (2018) 'PHIP as a therapeutic target for driver-negative subtypes of melanoma, breast, and lung cancer', *Proceedings of the National Academy of Sciences of the United States of America*, 115(25), pp. E5766–E5775. doi: 10.1073/pnas.1804779115.
- Sermer, D. *et al.* (2020) 'Outcomes in patients with DLBCL treated with commercial CAR T cells compared with alternate therapies', *Blood Advances*, 4(19), pp. 4669–4678. doi: 10.1182/bloodadvances.2020002118.
- Shanbhag, S. and Ambinder, R. (2019) 'Hodgkin Lymphoma: a review and update on recent progress', *CA Cancer J Clin.*, 68(2), pp. 116–132. doi: 10.3322/caac.21438.Hodgkin.
- Shi, J. H. and Sun, S. C. (2018) 'Tumor necrosis factor receptor-associated factor regulation of nuclear factor κ B and mitogen-activated protein kinase pathways', *Frontiers in Immunology*, 9(AUG), pp. 1–13. doi: 10.3389/fimmu.2018.01849.
- De Silva, N. S. *et al.* (2016) 'Transcription factors of the alternative NF- κ B pathway are required for germinal center B-cell development', *Proceedings of the National Academy of Sciences of the United States of America*, 113(32), pp. 9063–9068. doi: 10.1073/pnas.1602728113.
- Smith, M. R. *et al.* (2006) 'Murine model for mantle cell lymphoma [7]', *Leukemia*, 20(5), pp. 891–893. doi: 10.1038/sj.leu.2404177.
- Smulski, C. R. *et al.* (2017) 'BAFF- and TACI-Dependent Processing of BAFFR by ADAM Proteases Regulates the Survival of B Cells', *Cell Reports*. ElsevierCompany., 18(9), pp. 2189–2202. doi: 10.1016/j.celrep.2017.02.005.
- Spender, L. C. *et al.* (2005) 'Transcriptional cross-regulation of RUNX1 by RUNX3 in human B cells', *Oncogene*, 24(11), pp. 1873–1881. doi: 10.1038/sj.onc.1208404.
- Spina, V. *et al.* (2016) 'The genetics of nodal marginal zone lymphoma', *Blood*. American Society of Hematology, 128(10), pp. 1362–1373. doi: 10.1182/blood-2016-02-696757.
- Stojanovic, K. (2013) 'Die Rolle des NF- κ B Signalwegs in LMP1/CD40-exprimierenden B-Zellen in vivo', *Dissertation*.
- Suan, D., Sundling, C. and Brink, R. (2017) 'Plasma cell and memory B cell differentiation from the germinal center', *Current Opinion in Immunology*. Elsevier Ltd, 45, pp. 97–102. doi: 10.1016/j.coi.2017.03.006.
- Suciu-Foca, N. *et al.* (2007) 'Soluble Ig-Like Transcript 3 Inhibits Tumor Allograft Rejection in Humanized SCID Mice and T Cell Responses in Cancer Patients', *The Journal of Immunology*, 178(11),

pp. 7432–7441. doi: 10.4049/jimmunol.178.11.7432.

Sugimoto, T. and Watanabe, T. (2016) 'Follicular Lymphoma: The Role of the Tumor Microenvironment in Prognosis', *Journal of Clinical and Experimental Hematopathology : JCEH*. Japanese Society for Lymphoreticular Tissue Research, 56(1), p. 1. doi: 10.3960/JSLRT.5601.

Suzuki, T. *et al.* (2017) 'RUNX1 regulates site specificity of DNA demethylation by recruitment of DNA demethylation machineries in hematopoietic cells', *Blood Advances*, 1(20), pp. 1699–1711. doi: 10.1182/bloodadvances.2017005710.

Swerdlow, S. H. *et al.* (2016) 'The 2016 revision of the World Health Organization classification of lymphoid neoplasms', *Blood*. American Society of Hematology, pp. 2375–2390. doi: 10.1182/blood-2016-01-643569.

Takatsuka, S. *et al.* (2018) 'IL-9 receptor signaling in memory B cells regulates humoral recall responses', *Nature Immunology*. Nature Publishing Group, 19(9), pp. 1025–1034. doi: 10.1038/s41590-018-0177-0.

Tellier, J. and Nutt, S. L. (2017) 'Standing out from the crowd: How to identify plasma cells', *European Journal of Immunology*, 47(8), pp. 1276–1279. doi: 10.1002/eji.201747168.

Trauth, B. C. *et al.* (1989) 'Monoclonal antibody-mediated tumor regression by induction of apoptosis.', *Science (New York, N.Y.)*, 245(4915), pp. 301–5. Available at: <http://www.ncbi.nlm.nih.gov/pubmed/2787530> (Accessed: 17 September 2016).

Vieyra-Garcia, P. A. *et al.* (2016) 'STAT3/5-dependent IL9 overexpression contributes to neoplastic cell survival in mycosis fungoides', *Clinical Cancer Research*. American Association for Cancer Research Inc., 22(13), pp. 3328–3339. doi: 10.1158/1078-0432.CCR-15-1784.

Vincent-Fabert, C. *et al.* (2018) 'Reproducing Transformation of Indolent B-cell Lymphoma by T-cell Immunosuppression of L.CD40 Mice.', *bioRxiv*. Cold Spring Harbor Laboratory, p. 477273. doi: 10.1101/477273.

Vink, A. *et al.* (1999) 'Interleukin 9-induced in vivo expansion of the B-1 lymphocyte population.', *The Journal of experimental medicine*, 189(9), pp. 1413–1423. doi: 10.1084/jem.189.9.1413.

Wang, C. Q. *et al.* (2014) 'Disruption of Runx1 and Runx3 Leads to Bone Marrow Failure and Leukemia Predisposition due to Transcriptional and DNA Repair Defects', *Cell Reports*. Cell Press, 8(3), pp. 767–782. doi: 10.1016/J.CELREP.2014.06.046.

Wang, Y. *et al.* (2017) 'Germinal-center development of memory B cells driven by IL-9 from follicular helper T cells', *Nature Publishing Group*. doi: 10.1038/ni.3788.

Wasik, A. M. *et al.* (2014) 'Perturbations of the endocannabinoid system in mantle cell lymphoma: Correlations to clinical and pathological features', *Oncoscience*, 1(8), pp. 550–557. doi: 10.18632/oncoscience.77.

Weber, J. *et al.* (2019) 'PiggyBac transposon tools for recessive screening identify B-cell lymphoma drivers in mice', *Nature Communications*, 10(1). doi: 10.1038/s41467-019-09180-3.

Weih, F. *et al.* (1995) 'Multiorgan inflammation and hematopoietic abnormalities in mice with a targeted disruption of RelB, a member of the NF- κ B/Rel family', *Cell*. Cell Press, 80(2), pp. 331–340. doi: 10.1016/0092-8674(95)90416-6.

Weinstein, J. S. *et al.* (2014) 'B Cells in T Follicular Helper Cell Development and Function: Separable Roles in Delivery of ICOS Ligand and Antigen', *The Journal of Immunology*, 192(7), pp. 3166–3179. doi: 10.4049/jimmunol.1302617.

Witzig, T. E. and Inwards, D. (2019) 'Acalabrutinib for mantle cell lymphoma', *Blood*, 133(24), pp.

2570–2574. doi: 10.1182/blood.2019852368.

Woolaver, R. A. *et al.* (2018) 'TRAF2 Deficiency in B Cells Impairs CD40-Induced Isotype Switching That Can Be Rescued by Restoring NF- κ B1 Activation', *The Journal of Immunology*. The American Association of Immunologists, 201(11), pp. 3421–3430. doi: 10.4049/jimmunol.1800337.

Wu, Y. *et al.* (2019) 'TAK1 is a druggable kinase for diffuse large B-cell lymphoma', *Cell Biochemistry and Function*, 37(3), pp. 153–160. doi: 10.1002/cbf.3381.

Xu, S. and Lam, K.-P. (2020) '(TACI): Another Potential Target for Immunotherapy of Multiple Myeloma ?', *Cancers*. doi: doi:10.3390/cancers12041045.

Yamamoto, K. *et al.* (2015) 'Early B-cell-specific inactivation of ATM synergizes with ectopic CyclinD1 expression to promote pre-germinal center B-cell lymphomas in mice.', *Leukemia : official journal of the Leukemia Society of America, Leukemia Research Fund, UK*, 29(6), pp. 1414–1424. doi: 10.1038/leu.2015.41.

Zapf, S. (2017) 'Die Rolle des nicht-kanonischen NF- κ B Transkriptionsfaktor RelB in murinen B-Zellen und B- Zelllymphomen Angefertigt am Helmholtz Zentrum München Deutsches Forschungszentrum für Gesundheit und Umwelt', *Dissertation*.

Zaretsky, I. *et al.* (2017) 'ICAMs support B cell interactions with T follicular helper cells and promote clonal selection', *Journal of Experimental Medicine*. Rockefeller University Press, 214(11), pp. 3435–3448. doi: 10.1084/jem.20171129.

Zelenetz, A. D. *et al.* (2015) 'Chronic lymphocytic leukemia/small lymphocytic lymphoma, version 1.2015', *JNCCN Journal of the National Comprehensive Cancer Network*. Harborside Press, pp. 326–362. doi: 10.6004/jnccn.2015.0045.

Zhang, B. *et al.* (2015) 'An Oncogenic Role for Alternative NF- κ B Signaling in DLBCL Revealed upon Deregulated BCL6 Expression', *Cell Reports*, 11(5), pp. 715–726. doi: 10.1016/j.celrep.2015.03.059.

Zhang, Q., Lenardo, M. J. and Baltimore, D. (2017) '30 Years of NF- κ B: A Blossoming of Relevance to Human Pathobiology', *Cell*. Elsevier, 168(1–2), pp. 37–57. doi: 10.1016/j.cell.2016.12.012.

Zhang, T. T. *et al.* (2017) 'Germinal center B cell development has distinctly regulated stages completed by disengagement from T cell help', *eLife*. eLife Sciences Publications Ltd, 6. doi: 10.7554/eLife.19552.

Zhijian J, C. (2005) 'Ubiquitin signals in the NF-kappaB pathway.', *Nat Cell Biol.*, 7(8), pp. 758–65.

Available at:

<http://pubget.com/paper/17956251?institution=%0Apapers3://publication/doi/10.1042/BST0350942>.

Zou, H. *et al.* (2009) 'Human rhomboid family-1 gene RHBDF1 participates in GPCR-mediated transactivation of EGFR growth signals in head and neck squamous cancer cells.', *FASEB journal : official publication of the Federation of American Societies for Experimental Biology*. Federation of American Societies for Experimental Biology, 23(2), pp. 425–32. doi: 10.1096/fj.08-112771.

Zucca, E. *et al.* (2020) 'Marginal zone lymphomas: ESMO Clinical Practice Guidelines for diagnosis, treatment and follow-up', *Annals of Oncology*. Elsevier Ltd., 31(1), pp. 17–29. doi: 10.1016/j.annonc.2019.10.010.

Zucca, E., Bertoni, F. and Rossi, D. (2018) 'Recent advances in understanding the biology of marginal zone lymphoma', *F1000Research*. F1000 Research Ltd, p. 406. doi: 10.12688/f1000research.13826.1.

Zurli, V. *et al.* (2017) 'Ectopic ILT3 controls BCR-dependent activation of Akt in B-cell chronic lymphocytic leukemia', *Blood*. doi: 10.1182/blood-2017-03-775858.

7. Appendix

7.1. Supplement data

Table 8 List samples derived from aged LC40, RelBKO//LC40 and control mice, which were analysed by Southern Blot. If a clonal expansion was detected, it is indicated with TRUE. If no clonality was detected FALSE is indicated. This table combines data of Stefanie Zapf and me. For some individuals no splenic weight data was available (NA).

LC40				RelBKO//LC40				Control			
ID	Age (Days)	SB analysis	SP weight	ID	Age (Days)	SB analysis	SP weight	ID	Age (Days)	SB analysis	SP weight
34	492	TRUE	1.6	917	497	TRUE	0.25	21	483	TRUE	0.15
54	463	TRUE	3	865	481	TRUE	0.3	20	481	TRUE	NA
46	454	FALSE	1.1	921	468	FALSE	NA	803	524	FALSE	NA
2588	445	TRUE	NA	796	429	FALSE	NA	3555	461	FALSE	NA
2666	487	TRUE	NA	792	422	FALSE	NA	2584	450	FALSE	NA
2650	335	TRUE	NA	798	560	FALSE	NA	83	447	FALSE	NA
29	444	TRUE	1	927	458	FALSE	0.4	19	433	FALSE	NA
20	435	TRUE	1.9	794	422	TRUE	NA	3837	356	FALSE	NA
87	411	TRUE	NA	949	510	TRUE	NA	16	350	FALSE	0.15
100	358	TRUE	NA	909	447	FALSE	0.4	96	347	FALSE	0.14
48	330	FALSE	0.9	138	350	FALSE	0.3	3	330	FALSE	0.14
44	324	TRUE	0.8	883	347	FALSE	0.27	58	271	FALSE	0.12
14	310	TRUE	0.7	920	337	FALSE	0.38	15084	364	FALSE	NA
13	303	TRUE	0.8	981	337	TRUE	0.29	18088	319	FALSE	0.115
110	224	TRUE	NA	977	320	FALSE	0.32	8628	570	FALSE	0.136
11922	442	FALSE	0.532	879	317	FALSE	NA	19218	556	FALSE	NA
16377	359	FALSE	1.4	986	260	TRUE	NA	19220	563	FALSE	0.189
18078	327	TRUE	0.98	1060	186	FALSE	NA	19223	563	FALSE	0.145
17031	391	FALSE	1.1	26792	331	TRUE	NA	19956	541	FALSE	0.12
30205	301	FALSE	0.65	19109	343	FALSE	0.49	20310	536	FALSE	0.115
30208	405	TRUE	4	20708	441	FALSE	2	20704	410	FALSE	0.10
				20707	417	FALSE	0.849	19111	343	FALSE	0.094
				16585	318	FALSE	0.86				
				19949	384	FALSE	0.397				
				19112	556	FALSE	NA				
				19120	295	FALSE	0.26				

7.2. Curriculum Vitae

Education

- PhD November 2016 – today
University: Fakultät für Medizin, Ludwig-Maximilians-Universität München, Germany
Supervisor: PD Dr. Ursula Zimmer-Strobl
Employer: Helmholtz Zentrum München, Germany
- Master October 2014 – September 2016
Degree: Master of Science in Biology
University: Fakultät für Biologie, Ludwig-Maximilians-Universität München, Germany
- Bachelor October 2011 – September 2014
Degree: Bachelor of Science in Biology
University: Fakultät für Biologie & vorklinische Medizin, Universität Regensburg,
Germany

Presentations at selected Conferences

- 2018 @ American Society of Haematology, Annual Meeting 2018; San Diego, USA. Poster
2018 @ German National B Cell Conference; Masserberg, Germany. Talk
2018 @ International Symposium Cancer Evolution; Munich, Germany. Poster

Publications

Schäfer N*, Pujol-Lereis LM*, Kuhn LB, Rohrer B, Pauly D. (2016) Interrelation between oxidative stress and complement activation in models of age-related macular degeneration. *Adv. Exp. Med. Biol.* 854, 87–93, IF 1.760

Kuhn LB*, Zapf S*, Djermanovic K, Strobl D, Weih F, Blum H, Weigert O, Strobl L & Zimmer-Strobl U. (2018). The non-canonical NF-kappaB Signaling Pathway Contributes to the Expansion and Lymphomagenesis of CD40-activated B Cells. *Blood*. 132. 1340-1340. 10.1182/blood-2018-99-113793. (Conference Abstract, Full Paper in preparation)

Weber J., [...], Kuhn LB, [...], Zimmer-Strobl U, [...], Bradley A & Rad R et al. (2019) 'PiggyBac transposon tools for recessive screening identify B-cell lymphoma drivers in mice', *Nature Communications*, 10(1). doi: 10.1038/s41467-019-09180-3.

7.3. Eidesstattliche Erklärung

Hiermit versichere ich an Eides Statt, dass die vorgelegte Dissertation von mir selbstständig angefertigt wurde. Ich habe nur die angegebenen Hilfsmittel verwendet und übernommene Erkenntnisse aus dem Schrifttum wurden gekennzeichnet und die Fundstelle wurde nachgewiesen.

München, den 31.01.2022

Laura Kuhn

Laura Bernhardine Kuhn

7.4. Erklärung

Hiermit erkläre ich, dass die hier vorgelegte Dissertation nicht in dieser oder einer ähnlichen Form bei einer anderen Prüfungskommission eingereicht wurde. Außerdem versichere ich, dass die gebundene Ausgabe meiner Dissertation mit der elektronischen Fassung übereinstimmt.

München, den 31.01.2022

Laura Kuhn

Laura Bernhardine Kuhn

7.5. Danksagung

First of all, I want to thank PD Dr. Ursula Zimmer-Strobl for giving me the chance to work on this interesting topic and also giving me the opportunity for my personal growth and development. I am very grateful for these experiences, as I am sure these will help me in my future career.

Moreover, I want to thank my TAC members Prof. Dr. Irmela Jeremias and Prof. Dr. Roland Rad. Thank you for the nice discussions and input. Further, I want to thank you for the great collaborations which arose either for transplantation experiments or the entire PiggyBac project.

Speaking of collaborators, I especially want to thank Anja from AG Rad! I enjoyed working with you and would start collaborations with you any time again!

Special thanks also go to my previous and current lab colleagues of AG Strobl since it is always more fun to work in a team! Especially to Lothar, Tea, Markus, Ursula R., and Yana: Thanks for the discussions, especially concerning methods! “Falla” and “Köszönöm” to Kris, because you elevate the lab work atmosphere by simply noticing little personal details, which can have a huge impact on a workday. Additionally, I want to thank the entire AGV for the nice seminars, borrowing dispensable material in case of delivery delays and nice chats on the hallway!

Further all these mouse experiments would not have been possible without the animal caretakers, Michael, Franzi L., Franzi W. and Martina. Thank you for the mouse maintenance.

A special shout out also goes to Sophie, Kerstin and Christina, because work is the most fun when your colleagues turn into good friends!!

También me gustaría dar las gracias a Diego. Gracias por darme valor y calma cuando me asaltaban las dudas o era demasiado impaciente conmigo misma.

Als letztes möchte ich mich bei meinen Eltern und meinem Bruder Juri bedanken, dafür, dass ihr schon immer für mich da wart und seid! Ohne Euch hätte ich viele Krisen, auf die ich jetzt mit einem Lächeln zurückblicke, nicht so gut überstanden und hätte meine bisherigen Ziele nicht so schnell erreichen können. Daher geht mein größter Dank auch an euch!